

UFAL

INSTITUTO DE QUÍMICA E BIOTECNOLOGIA
PROGRAMA DE PÓS-GRADUAÇÃO
EM QUÍMICA E BIOTECNOLOGIA

Hydroxylated surfactants as growth-driving agents for the synthesis of anisotropic gold nanoparticles

MONIQUE GABRIELLA ANGELO DA SILVA

Universidade Federal de Alagoas

**Campus A. C. Simões
Tabuleiro do Martins
57072-970 - Maceió-AL**

E
École

N
nationale

S
supérieure de

C
chimie de

R
Rennes



THESE / ECOLE NATIONALE SUPERIEURE DE
CHIMIE DE RENNES

sous le sceau de l'Université européenne de Bretagne

pour obtenir le grade de

DOCTEUR DE L'ENSCR

Mention : Chimie

École doctorale Sciences De La Matière

présentée par

Monique Angelo da Silva

Préparée à l'Unité Mixte de Recherche (n° 6226)

Institut des Sciences Chimiques de Rennes

**Tensioactifs hydroxylés
comme agent de croissance
pour la synthèse de
nanoparticules
anisotropes d'or**

Thèse soutenue le 7 Juillet 2014,
devant le jury composé de :

Antonio Euzébio G. SANTANA
Professeur - Université Fédérale d'Alagoas

Fabiane CAXICO de ABREU GALDINO
Professeur - Université Fédérale d'Alagoas

Liane Marcia ROSSI
Professeur - Université de São Paulo

Michel PFEFFER
Directeur de Recherches CNRS – Université de Strasbourg

Mario Roberto MENEGHETTI
Professeur - Université Fédérale d'Alagoas / *Co-Directeur de thèse*

Alain ROUCOUX
Professeur – Ecole Nationale Supérieure de Chimie de Rennes / *Directeur de thèse*

Résumé

Les nanobâtônnetts d'or (AuNRs) suscitent un intérêt considérable en raison de leurs propriétés optiques particulières, fortement dépendantes de leur rapport d'aspect (longueur/épaisseur), et donc de leurs applications potentielles en optique et en médecine. Dans ce contexte, le développement de nouvelles stratégies pour la synthèse de nanobâtônnetts avec des rendements et des sélectivités élevés reste un challenge avec un objectif de contrôle efficace de la taille et de la morphologie. Parmi les différentes voies de préparation, la méthodologie par ensemencement est la plus utilisée, notamment en présence de bromure de cétyltriméthylammonium (CTAB), comme agent de croissance. A notre connaissance, peu de travaux ont été reportés dans la littérature en présence d'autres agents de croissance. Dans ce contexte, nous avons développé une famille originale d'agents de croissance, les sels de *N,N*-diméthyl-*N*-cétyl-*N*-hydroxyalkylammonium (HAAX), produisant des nanobâtônnetts d'or avec des rendements et des sélectivités élevés dans l'eau. Ces tensioactifs présentant une bonne solubilité dans l'eau sont facilement synthétisés avec de bons rendements et différents paramètres structuraux peuvent être modulés tels que: i) la longueur de la chaîne lipophile (C12, C16, C18), ii) la nature des contre-ions par métathèse anionique ($X^- = F^-, Cl^-, Br^-, I^-, BF_4^-$ et HCO_3^-), et plus particulièrement iii) la tête polaire hydroxylée. Les nanoparticules d'or obtenues par la méthode d'ensemencement ont été caractérisées par spectroscopie Uv-vis et par Microscopie Electronique à Transmission, montrant l'influence du tensioactif sur la morphologie et la taille (dimension, rapport d'aspect). Cette famille de sels d'ammonium, de par sa modularité, permet d'accéder à différentes formes et tailles de nanoparticules d'or suivant l'objectif souhaité et ouvre ainsi des perspectives intéressantes en termes d'applications.

Gold nanorods (AuNRs) have attracted great interest owing to their particular optical properties, strongly dependent on the size and aspect ratio (thickness/length), and thus their potential applications in optics and medicine (therapy, cancer diagnosis...). In this context, the development of new strategies for the synthesis of anisotropic nanorods with high yields and selectivities remains a challenge towards an effective control of the size and morphology. Among the different preparation routes, the seed mediated method is most commonly used, especially in the presence of cetyltrimethylammonium bromide (CTAB) as a growth-driving agent. To our knowledge, few works have been reported in the literature in presence of other growth driving agents. In this context, we have developed a novel family of growth driving agents, *N,N*-dimethyl-*N*-cetyl-*N*-hydroxyalkylammonium salts (HAAX), producing gold nanorods with high yields and selectivities in water. These surfactants have good solubility in water and are easily synthesized in good yields and different structural parameters could be modulated such as : i) the length of the lipophilic chain (C12, C16, C18), ii) the nature of the counter ion by anionic metathesis ($X^- = F^-, Cl^-, Br^-, I^-, HCO_3^-$ and BF_4^-), and more particularly iii) the hydroxylated polar head. The gold nanoparticles obtained by the seed mediated method were characterized by Uv-vis spectroscopy and transmission electron microscopy, showing the influence of the surfactant on the morphology and on the size (aspect ratio). Thus, this family of easily tunable ammonium salts allows access to various shapes and sizes of gold nanoparticles according to the desired target and opens interesting perspectives in terms of applications.

Mots-clés

Or
Nanobâtônnetts
Nanoparticules anisotropes
Tensioactifs hydroxylés

Keywords

Gold
Nanorods
Anisotropic nanoparticles
Hydroxylated surfactants



Universidade Federal de Alagoas
Instituto de Química e Biotecnologia

Programa de Pós-Graduação em Química e Biotecnologia
PPGQB



IQB

MONIQUE GABRIELLA ANGELO DA SILVA

*Hydroxylated surfactants as growth-driving agents for
the synthesis of anisotropic gold nanoparticles*

Defesa de doutorado apresentada ao Programa de Pós-Graduação em Química e Biotecnologia da Universidade Federal de Alagoas para obtenção do título de Doutora em Química.

Orientador: Prof. Dr. Mario Roberto Meneghetti

Coorientador: Prof. Dr. Alain Roucoux

Maceió – Alagoas

Julho de 2014

Catálogo na fonte
Universidade Federal de Alagoas
Biblioteca Central
Divisão de Tratamento Técnico

Bibliotecário Responsável: Valter dos Santos Andrade

S586h Silva, Monique Gabriella Angelo da.
Hydroxylated surfactants as growth-dring agents for the synthesis of
Anisotropic gold nanoparticles / Monique Gabriella Angelo da Silva . –
2014.
xix, 125 f. : il., gráfs. e tabs.

Orientador: Mario Roberto Meneghetti.
Co-orientador: Alain Roucoux.
Tese (Doutorado em Química e Biotecnologia) – Universidade
Federal de Alagoas. Instituto de Química e Biotecnologia. Maceió, 2014.

Inclui bibliografia.
Apêndices: f. 104-125
1. Agentes ativos de superfícies. 2. Nanopartículas de ouro.
3. Surfactantes. I. Título.

CDU: 544.77



Universidade Federal de Alagoas
Instituto de Química e Biotecnologia
Programa de Pós-Graduação em Química e Biotecnologia
PPGQB

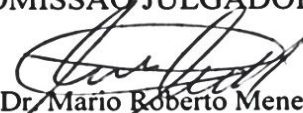


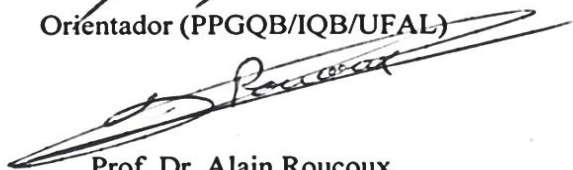
IQB

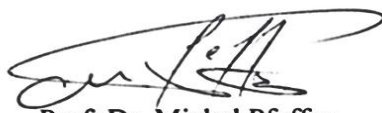
FOLHA DE APROVAÇÃO

Membros da Comissão Julgadora da Defesa de Tese da doutoranda **Monique Gabriella Angelo da Silva**, intitulada: “**SURFACTANTES HIDROXILADOS PARA SÍNTESE DE NANOPARTÍCULAS ANISOTRÓPICAS**”, apresentada ao Programa de Pós-Graduação em Química e Biotecnologia da Universidade Federal de Alagoas em 07 de julho de 2014, às 14 h, no Auditório da Biblioteca Central da UFAL.

COMISSÃO JULGADORA


Prof. Dr. Mario Roberto Meneghetti
Orientador (PPGQB/IQB/UFAL)


Prof. Dr. Alain Roucoux
Coorientador (ENSCR, Rennes, França).


Prof. Dr. Michel Pfeffer
(UNISTRA, Estrasburgo, França)


Prof.ª Dr.ª Liane Marcia Rossi
(USP, São Paulo)


Prof. Dr. Antonio Euzébio Goulart Sant'Ana
(PPGQB/IQB/UFAL)


Prof.ª Dr.ª Fabiane Caxico de Abreu Galdino
(PPGQB/IQB/UFAL)

I do dedicate this thesis to my mother!

ACKNOWLEDGEMENTS

Foremost, I would like to express my sincere gratitude to God, the Lord of my life for all paternal care, guidance, complaints and unconditional love.

I would never have been able to finish my thesis without the guidance of my advisers, help from friends, and support from my family, my mother and husband.

I would like to express my deepest gratitude to my Brazilian adviser, Prof. Dr. Mario Roberto Meneghetti, for his excellent guidance, knowledge which inspired and motivated me.

I would like to thank my French adviser, Prof. Dr. Alain Roucoux who gave me the opportunity of taking part in his research group in France, for his excellent guidance and good discussions. I would also like to thank Dr. Audrey Denicourt-Nowicki for her patience, guidance, discussions and articles corrections.

I would like to thank the committee member Prof. Dr. Antonio Euzébio G. Santana (IQB-UFAL/PPGQB), Prof. Dr. Fabiane Caxico de Abreu Galdino (IQB-UFAL/PPGQB), Prof. Dr. Liane Marcia Rossi (USP, São Paulo) and Prof. Dr. Michel Pfeffer (UNISTRA, Strasbourg, France) for the presence, corrections and suggestions to improve my work.

I would like to thank the CNPq for the financing support (my fellowship) in Brazil and CAPES/Cofecub for the financing support in France; the Group of Catalysis and Chemical Reactivity for all supporting research, the Institute of Chemistry and Biotechnology at Federal University of Alagoas for providing my academic development.

I would also like to thank Ábner Nunes, who, as a good friend, was always willing to help me. Many thanks to Luis Carlos and Eid Cavalcante, It would have been a lonely lab without them; Sara Figueirêdo, who is a great science colleague and friend, and others also so important. My research would not have been possible without their helps. I can't forget Carl-Hugo for his company and good discussions on the Organometallic, Materials and Catalysis Group.

I would also like to thank my mother, Marluce Angelo. She was always supporting me and encouraging me with her best wishes and prayers. She was always there cheering me up and stood by me through the good times and bad ones.

Finally, I would like to thank my husband Wanderson Reis, for his love and patience.

Resumo

Os nanobastões de ouro (AuNRs) têm atraído grande interesse devido às suas propriedades ópticas diferenciadas, fortemente dependentes do tamanho e da taxa de proporção (comprimento/largura) e, às suas potenciais aplicações em óptica e medicina (termoterapias, diagnósticos imediatos, diagnóstico de câncer etc.). Neste contexto, o desenvolvimento de novas estratégias para a síntese de nanobastões anisotrópicos com elevados rendimentos e seletividades contínuas a ser um desafio para a obtenção do controle efetivo da morfologia e do tamanho. Entre as diversas metodologias de preparação, o método mediado por semente é o mais utilizado, especialmente na presença de brometo de cetiltrimetilamônio (CTABr) como um agente direcionador de crescimento. Para nosso conhecimento, poucos trabalhos foram relatados na literatura referentes a esse sistema em presença de outros agentes direcionadores de crescimento. Neste contexto, foi desenvolvida uma nova família de agentes direcionadores de crescimento: os sais de amônio *N,N*-dimetil-*N*-cetil-*N*-hidroxialquilamônio (HAAX), produzindo nanobastões de ouro com alto grau de rendimento e seletividade em meio aquoso. Esses surfactantes possuem uma boa solubilidade em água e são facilmente sintetizados com bons rendimentos e com diferentes parâmetros estruturais que podem ser modificados, tais como: i) o comprimento da cadeia lipofílica (C12, C16, C18), ii) a natureza do contra-íon trocado por metátese aniônica ($X = F^-$, Cl^- , Br^- , I^- , HCO_3^- e BF_4^-), e de forma original, iii) a região polar hidroxilada. As nanopartículas de ouro obtidas pelo método mediado por semente foram caracterizadas por espectroscopia de UV-vis e por microscopia eletrônica de transmissão, que mostram a influência do surfactante sobre a morfologia e o tamanho (taxa de proporção) das nanopartículas de ouro. Assim, a modificação da estrutura dos sais de amônio dessa família permite um acesso a diferentes formatos e tamanhos de nanopartículas de ouro de acordo com a aplicação almejada. O controle do processo de crescimento gerado pela região do grupo polar permite a modificação dos parâmetros estruturais dos nanobastões de ouro e abre interessantes perspectivas em termos de aplicações.

Palavras-chave:
Nanopartículas anisotrópicas
Nanopartículas de ouro
Nanobastões de ouro
Surfactantes hidroxilados

Résumé

Les nanobâtonnets d'or (AuNRs) suscitent un intérêt considérable en raison de leurs propriétés optiques particulières, fortement dépendantes de leur rapport d'aspect (longueur/épaisseur), et donc de leurs applications potentielles en optique et en médecine. Dans ce contexte, le développement de nouvelles stratégies pour la synthèse de nanobâtonnets avec des rendements et des sélectivités élevés reste un challenge avec un objectif de contrôle efficace de la taille et de la morphologie. Parmi les différentes voies de préparation, la méthodologie par ensemencement est la plus utilisée, notamment en présence de bromure de cetyltriméthylammonium (CTABr), comme agent de croissance. A notre connaissance, peu de travaux ont été reportés dans la littérature en présence d'autres agents de croissance. Dans ce contexte, nous avons développé une famille originale d'agents de croissance, les sels de *N,N*-diméthyl-*N*-cétyle-*N*-hydroxyalkylammonium (HAAX), produisant des nanobâtonnets d'or avec des rendements et des sélectivités élevés dans l'eau. Ces tensioactifs présentant une bonne solubilité dans l'eau sont facilement synthétisés avec de bons rendements, et différents paramètres structuraux peuvent être modulés tels que: i) la longueur de la chaîne lipophile (C12, C16, C18), ii) la nature des contre-ions par métathèse anionique ($X = F^-$, Cl^- , Br^- , I^- , HCO_3^- et BF_4^-), et plus particulièrement; iii) la tête polaire hydroxylée. Les nanoparticules d'or obtenues par la méthode d'ensemencement ont été caractérisées par spectroscopie Uv-vis et par Microscopie Electronique à Transmission, montrant l'influence du tensioactif sur la morphologie et la taille (dimension, rapport d'aspect) des nanoparticules d'or. Ainsi, cette famille de sels d'ammonium, de par sa modularité, permet d'accéder à différentes formes et tailles de nanoparticules d'or suivant l'application souhaitée et ouvre ainsi des perspectives intéressantes en termes d'applications.

Mots-clés :
Nanoparticules anisotropes
Nanoparticules d'or
Nanobâtonnets d'or
Tensioactif hydroxylé

Abstract

The gold nanorods (AuNRs) have attracted considerable interest due to their special optical properties, strongly dependent on the size and aspect ratio (thickness/length), and thus, their potential applications in optics and medicine (therapy, cancer diagnosis...). In this context, the development of new strategies for the synthesis of anisotropic nanorods with high yields and selectivities remains a challenge towards an effective control of the size and morphology. Among the different preparation routes, the seed mediated method is most commonly used, especially in the presence of cetyltrimethylammonium bromide (CTABr) as a growth-driving agent. To our knowledge, few works have reported in the literature this system in presence of other growth driving agents. In this context, we have developed a novel family of growth driving agents, *N,N*-dimethyl-*N*-cetyl-*N*-hydroxyalkylammonium salts (HAAX), producing gold nanorods with high yields and selectivities in water. These surfactants have good solubility in water and are easily synthesized in good yields in presence of different structural parameters that can be modulated such as: i) the length of the lipophilic chain (C12 , C16 , C18), ii) the nature of the counter ions by metathesis ($X = F^-$, Cl^- , Br^- , I^- , HCO_3^- e BF_4^-), and an original way, iii) hydroxylated polar head. The gold nanoparticles obtained by the seed mediated method were characterized by UV -vis spectroscopy and transmission electron microscopy, showing the influence of the surfactant on the morphology and on the size (aspect ratio) of the gold nanoparticles. Thus, the modulation of this family of ammonium salts allows the access to different shapes and sizes of gold nanoparticles according to the desired application. The growth process control generated by the polar head groups allows the modulation of the structural parameters of gold nanorods and opens interesting perspectives in terms of applications.

Keywords:

Anisotropic nanoparticles
Gold nanoparticles
Gold nanorods
Hydroxylated Surfactants

MOTIVATION AND OBJECTIVES

The interest in inorganic nanomaterials such as nanoparticles, nanowires, and nanotubes, comes from the fact that different and singular properties are reached in nanosized dimensions. The natural, predominant forces in the macroscopic scale such as combustion, gravity and friction lose importance in reduced scales to others as Brownian movement, electrostatic forces and quantum mechanics rules. This phenomenon promotes two important consequences: a surface and an electronic effect on the material surfaces that are responsible for all the unusual properties. However, the expression of these intermediate and unusual properties at this length scale is not just due to scaling factors, but it also depends on the morphology, size and shape distribution, and environment in which these particles are present. Therefore, these singular properties are normally assembled in a set of features that are dependent of a "*nano effect*". Furthermore, due to their dimensions, normally in the range of 1 to 100 nm, several nanostructures are studied, evaluated, and applied in the fields like catalysis, optics, electronic systems, and as similar biological structures (e.g., membrane cell genes, proteins, and viruses). Nowadays, the volume of studies dealing with these topics represents one of the most impressive phenomena in all scientific history.

Despite the advances in the preparation and application of nanomaterials, it is well known that nanoparticles are thermodynamically unstable and have a natural tendency to agglomerate or even grow. Thus, the preparation of high quality nanostructured materials via homogeneous and reproducible methodologies remains a challenge, particularly with a high control of the morphology, allowing to tune the material properties and their applications.

Among the anisotropic particles that can be obtained, some attention is given to the preparation of metal nanowires and nanorods. Ultimately, these materials are widely used because of their optical properties: they exhibit two plasmon absorption bands, longitudinal and transversal, in the visible region of the spectrum, making them promising candidates for detecting and displaying information.

As we already know, for the syntheses of gold nanorods (AuNRs), cetyltrimethylammonium bromide (CTABr) acts as a classical growth-driving agent. This type of ammonium salt is crucial to obtain a well-controlled growth process, blocking the long axis crystal faces {100} and/or {110} through the surfactant bilayer structure and thus promoting metal growth on the short-axis faces {111} to produce AuNRs. The cationic site of the surfactant interacts preferentially with lateral faces of the metal crystal structure that are less stable than the ends of the faces of the extremities due to the number of defects.

Some works have been published with the aim to tune the aspect ratio of AuNRs, adding or modifying some synthetic parameters, such as the amount of the driving agent, the size of the seeds used, the effect of additives etc., According to previous works carried out by the group of Murphy, the nature of the growth-driving agents or even a mixture of these agents is essential in the AuNRs elongation. Thus, several studies have been done in order to improve reaction yields and selectivity. To our knowledge, only the cetylpyridinium chloride (CPyCl), possessing a larger and more anisotropic head group, has been proposed as a potential growth-driving agent to produce AuNRs, but multi-shaped nanoparticles, such as nanospheres, triangles, pentagons, were observed. Also, binary mixtures, such as CTABr/BDACl (benzyltrimethyl ammonium chloride), and CTABr/OTABr (octyltrimethylammonium bromide) were tested, but only modest improvements have been obtained.

Considering this lack of options, we have envisaged new growth-driving agents for the preparation of anisotropic AuNPs in high yields and selectivity. A series of an original library of easily prepared *N,N*-dimethyl-*N*-cetyl-*N*-(hydroxyalkyl)ammonium salts (HAAX) were tested as growth-driving agents, instead of the usual CTABr. These growth-driving agents, bearing hydroxyl groups, possess high water-solubility, as well as a good stability in a large pH range.

Moreover, we have initiated catalytic and manipulation studies with the nanoparticles prepared in order to evaluate the potential application of these nanostructured systems.

LIST OF FIGURES

Figure 1 - Light surface interaction on metal nanosphere. The electromagnetic field of the light induces a dipole oscillation of the conducting electrons along the particle surface.	02
Figure 2 - Illustration of the two main approaches to provide nanomaterials.	04
Figure 3 - Scheme illustrating a supersaturation condition to begin the nucleation process as a function the solute concentration in the system.	06
Figure 4 - Free global energy ΔG as function of particles radius.	07
Figure 5 - Illustration of the nanoparticles sequence formation in solution.	08
Figure 6 - Examples of particles stabilization mechanisms in colloidal solutions by (a) repel phenomenon among electric charges, (b) steric effects, (c) electrostatic and steric effects. Adapted from reference 15.	10
Figure 7 - Representative examples of anisotropic particles. A) Spheres, B), rods, C) branched and D) polyhedral shapes.	10
Figure 8 - Illustrative graph showing the relationship between the cluster size with its potential, b) cluster containing magic number of atoms (13, 55, 147, 309, 561...). Figure adapted from reference 38.	11
Figure 9 - Possibilities of the growth of nanocrystals as function of the monomer concentration in the system. Figure adapted from reference 38.	12
Figure 10 - Three growth stages in elongated nanocrystals formation as function of different monomers concentrations. Figure adapted from ref. 38.	13
Figure 11 - (a) Schematic representation and (b) photograph of set up used for polyol synthesis.	14
Figure 12 - An illustration of the cage-shaped protein apoferritin without iron core and ferritin with iron core (Adapted from Iwahori and Yamashita, 2007).	15
Figure 13 - An illustration of hydro/solvothermal instrumentation.	16
Figure 14 - Mechanistic studies on the formation of nanobowls by galvanic replacement reactions.	16
Figure 15 - Formation of Gold Nanoparticles by photochemical reaction.	17

Figure 16 - Schematic diagram showing formation of electrochemically produced PVP-stabilized silver clusters.	18
Figure 17 - (a and b) FEG–SEM images of an alumina membrane. (c) Schematic representation of the successive stages during formation of gold nanorods via the template method. (d) TEM micrographs of gold nanorods obtained by the template method.	19
Figure 18 - Schematic illustration of the seed solution, growth solution and the beginning of the growth process.	26
Figure 19 - Schematic illustration of the dissymmetric growth of gold nanorod from a seed particle and Au (I) ion species that are reduced to Au(0) on the surface of the metal particle.	27
Figure 20 - Illustration of gold nanorod preparation via seed mediated method.	48
Figure 21 - Scheme illustrating the generation of AuNRs from seed particles.	50
Figure 22 - AuNRs obtained in presence of CTABr, TEM and UV-vis spectrum.	50
Figure 23 - Structure of surfactants HAAX.	51
Figure 24 - Transmission Electron Microscopy images of gold nanoparticles obtained face to surfactants with different counter-ions. Spectrum de UV-vis for each one. a) AuNP@HEA16F (8.5 nm) and b) AuNP@HEA16Cl (10 nm).	53
Figure 25 - Uv-vis spectrum of AuNP@HEA16Cl in different levels of surfactant concentrations: a) 0.096 mol/L and b) 0.128 mol/L.	53
Figure 26 - Transmission Electron Microscopy images of gold nanoparticles obtained face to surfactants with different counter-ions. Spectrum de UV-vis for each one: a) AuNR@HEA16Br (30 nm x 10 nm; aspect ratio: 3.0) and b) AuNR@HCO ₃ (29 nm x 7 nm; aspect ratio: 4.2).	55
Figure 27 - Transmission Electron Microscopy images, histograms and Uv-vis spectra of gold nanoparticles obtained face an iodide counter-ion.	56
Figure 28 - Transmission Electron Microscopy images and Uv-vis spectra of the AuNRs obtained using growth-driving agents with different long alkyl chains. a) AuNR@HEA12Br and b), AuNR@HEA18Br.	58
Figure 29 - Transmission Electron Microscopy images and Uv-vis spectrum of a) AuNR@HPA16Br, and b) AuNR@HBA16Br.	60

Figure 30 - Chemical structures of the surfactants a) H2PA16Br, b) H1,2PA16Br, c) HDA16Br, d) DHEA16Br, e) DHA16Br, f) THEA16Br, g) NOx16, h) NMeEPh16Br, i) EA16Br, j) PA16Br, and k) BA16Br.	61
Figure 31 - Uv-vis spectrum and TEM images of AuNR@H2PA16Br.	61
Figure 32 - Uv-vis spectrum and TEM images of AuNR@H1,2PA16Br.	62
Figure 33 - Uv-vis spectrum and TEM images of AuNR@HDA16Br.	62
Figure 34 - TEM images and the Uv-vis spectrum of a) AuNP@DHEA16Br, b) AuNP@DHA16Br and c) AuNP@THEA16Br.	63
Figure 35 - Uv-vis spectrum of AuNP@NOx16 at a) 0.064 mol/L, and b) 0.016 mol/L; and AuNP@NMeEPh16Br at c) 0.016 mol/L, and d) 0.0064 mol/L, respectively.	64
Figure 36 - Spectra of Uv-vis and TEM images of a) AuNP@EA16Br, b) AuNP@PA16Br and c) AuNP@BA16Br.	66
Figure 37 - Three steps to prepare high aspect ratios AuNRs	67
Figure 38 - TEM images of the solutions A, B, and C in absence of silver ions, using HBA16Br driving agent.	68
Figure 39 - TEM images of the solution B in presence of a) HEA16Br, b) HPA16Br, and c) HBA16Br.	69
Figure 40 - TEM images of the solution B in absence of silver ions obtained from solution A in presence of silver ions .	69
Figure 41 - TEM images of the solution B obtained in presence of silver ions from solution A in presence of silver ions, too.	70
Figure 42 - Absorption spectra of the colloids containing gold nanorods prepared with different amounts of seed particles in the reaction medium.	71
Figure 43 - UV-vis spectra of the colloids obtained from various growth-driving agents, collected during the very first 3 hours of the NPs formation.	72
Figure 44 - Intensity of the second absorption band in function of time from 0 to 60 min, using four of the various growth-driving agents.	73
Figure 45 - TEM images showing the selective interaction between AuNRs via end-to-end fashion.	77
Figure 46 - Schematic representation of AuNRs transverse and longitudinal plasmon absorbance in spherical and rod gold nanoparticles.	79

Figure 47 - A) Calculated energy along the minimum-energy reaction path for H ₂ dissociation on the (111) surface of Ni, Cu, Pt and Au; (B) optimized geometry for adsorbed H ₂ (I), transition state (II) and dissociated H ₂ (III) at the edge of a monoatomic row on a defective Au (111) surface: adapted from reference 27.	81
Figure 48 - Image of the reactor employed to the hydrogenation reaction.	83
Figure 49 - TEM images of AuNR@HEA16Br (30 x 10 nm) and spherical AuNP@HEA16Br (3 nm).	84
Figure 50 - Toluene hydrogenation reaction product using gold nanoparticles as catalysts	84
Figure 51 - Anisole hydrogenation reaction products using gold nanoparticles as catalysts	85
Figure 52 - Styrene hydrogenation reaction products using gold nanoparticles as catalysts	85
Figure 53 - Acetophenone hydrogenation reaction products using gold nanoparticles as catalysts	86
Figure 54 - Nitrobenzene hydrogenation reaction products using gold nanoparticles as catalysts	86
Figure 55 - TEM images of AuNRs before and after the first hydrogenation reaction of toluene.	87
Figure 56 - UV-vis spectra of AuNRs in water and in presence of acetonitrile: water (4:1)	89
Figure 57 - Scheme of homo-organization using the TIOB.	90
Figura 58 - UV-vis spectrum of gold nanorods treated with TIOB and the values of dynamic light scattering of the sample.	90

LIST OF TABLES

Table 1	Predominant effects by scale reduction from meters to angstroms dimensions.	20
Table 2	Principal techniques used in the characterization of nanoparticles.	23
Table 3	Reagents and solvents used in this work.	38
Table 4	Characteristics of the AuNRs obtained in presence of surfactants with different nature of counter ions.	57
Table 5	Characteristics of the AuNRs obtained in presence of surfactants with different length of alkyl chain.	59
Table 6	Characteristics of the AuNRs obtained in presence of surfactants with different hydroxylated polar head.	60
Table 7	Characteristics of the AuNRs obtained in presence of surfactants with different polar head groups.	64
Table 8	Characteristics of the AuNRs obtained in presence of non-hydroxylated head groups.	66
Table 9	Characteristics of the AuNRs obtained with high aspect ratio.	69
Table 10	Reaction conditions for toluene hydrogenation reaction using gold nanoparticles as catalysts (AuNRs: gold nanorods; AuNPs: gold nanospheres).	84
Table 11	Reaction conditions for anisole hydrogenation reaction using gold nanoparticles as catalysts (AuNRs: gold nanorods; AuNPs: gold nanospheres; and A: Methoxy-cyclohexane; B: Cyclohexanone)	85
Table 12	Reaction conditions for styrene hydrogenation using gold nanoparticles as catalysts (AuNRs: gold nanorods; AuNPs: gold nanospheres; and A: Ethyl-benzene; B: Ethyl-Cyclohexane)	85
Table 13	Reaction conditions for acetophenone hydrogenation using gold nanoparticles as catalysts (AuNRs: gold nanorods; AuNPs: gold nanospheres; and A: Phenylethanol; B: Cyclohexylethanone; C: Cyclohexylethanol)	86

Table 14 Reaction conditions for nitrobenzene hydrogenation using gold nanoparticles as catalysts (AuNRs: gold nanorods; AuNPs: gold nanospheres; and A: Aniline; B: Cyclohexylamine) 86

LIST OF ABBREVIATIONS

AFM	Atomic Force Microscopy
AuNPs	Gold Nanoparticles
AuNRs	Gold Nanorods
BA16Br	<i>N,N</i> - dimethyl- <i>N</i> -cetyl- <i>N</i> -butylammonium Bromide
BDACl	Benzyltrimethylammonium Chloride
BET	Brunauer, Emmet and Teller
CMC	Critical Micellar Concentration
CPyCl	Cetylpyridinium Chloride
CTABr	Cetyltrimethylammonium Bromide
DHA16Br	<i>N</i> -cetyl- <i>N,N</i> -(DiHydroxyEthyl)ammonium Bromide
DHEA16Br	<i>N</i> -methyl- <i>N</i> -cetyl- <i>N,N</i> -(DiHydroxyEthyl)ammonium Bromide
DLS	Dynamic Light Scattering
DRX	X-Ray Diffraction
EA16Br	<i>N,N</i> - dimethyl- <i>N</i> -cetyl- <i>N</i> -ethylammonium Bromide
EDX	X-ray Spectroscopy of disperse energy
ENSCR	École Nationale Supérieure de Chimie de Rennes
FEG-SEM	Field Emission Gun-Scanning Electron Microscope
GCaR	Group of Catalysis and Chemical Reactivity
H2PA16Br	<i>N,N</i> - dimethyl- <i>N</i> -cetyl- <i>N</i> -(2-hydroxypropyl)ammonium Bromide
HAAX	<i>N,N</i> -dimethyl- <i>N</i> -cetyl- <i>N</i> -(hydroxyalkyl)ammonium salts
HBA16Br	<i>N,N</i> - dimethyl- <i>N</i> -cetyl- <i>N</i> -(2-hydroxybutyl)ammonium Bromide
HDA16Br	<i>N,N</i> - diethyl- <i>N</i> -cetyl- <i>N</i> -(2-hydroxyethyl)ammonium Bromide
HEA12Br	<i>N,N</i> - dimethyl- <i>N</i> -dodecyl- <i>N</i> -(hydroxyethyl)ammonium Bromide
HEA16BF₄	<i>N,N</i> - dimethyl- <i>N</i> -cetyl- <i>N</i> -(2-hydroxyethyl)ammonium Tetrafluoroborate
HEA16Br	<i>N,N</i> - dimethyl- <i>N</i> -cetyl- <i>N</i> -(2-hydroxypropyl)ammonium Bromide
HEA16Cl	<i>N,N</i> - dimethyl- <i>N</i> -cetyl- <i>N</i> -(2-hydroxyethyl)ammonium Fluoride
HEA16Cl	<i>N,N</i> - dimethyl- <i>N</i> -cetyl- <i>N</i> -(2-hydroxyethyl)ammonium Chloride
HEA16HCO₃	<i>N,N</i> - dimethyl- <i>N</i> -cetyl- <i>N</i> -(2-hydroxyethyl)ammonium Hydrogen carbonate

HEA16I	<i>N,N</i> - dimethyl– <i>N</i> -cetyl– <i>N</i> -(2-hydroxyethyl) ammonium Iodide
HEA18Br	<i>N,N</i> - dimethyl– <i>N</i> -octadecyl– <i>N</i> -(2-hydroxyethyl)ammonium Bromide
HPA16Br	<i>N,N</i> - dimethyl– <i>N</i> -cetyl– <i>N</i> -(2-hydroxypropyl)ammonium Bromide
IQB	Institute of Chemistry and Biotechnology
MUA	Mercaptoundecanoic acid
NIR	Near Infrared
N-	<i>N,N</i> - dimethyl– <i>N</i> -cetyl– <i>N</i> -methylephidrium Bromide
MeEph16Br	
NMR	Nuclear Magnetic Resonance
NOx16	<i>N,N</i> - dimethyl– <i>N</i> -cetyl– <i>N</i> –Oxide Bromide
NPs	Nanoparticles
NRs	Nanorods
OMC	Organométalliques: Matériaux et Catalyse
OTABr	Octyltrimethylammonium Bromide
PA16Br	<i>N,N</i> - dimethyl– <i>N</i> -cetyl– <i>N</i> -propylammonium Bromide
SAXS	Small-angle X-ray scattering
SEM	Scanning Electron Microscopy
SPR	Surface Plasmon Resonance
TEM	Transmission Electron Microscopy
THEA16Br	<i>N</i> -cetyl– <i>N,N,N</i> –(TrisHydroxyEthyl)ammonium Bromide
TIOB	4,4 - Thiobisbenzenethiol
TMS	Tetramethylsilane
TOABr	Tetraoctylammonium Bromide
UFAL	Federal University of Alagoas
UV-vis	Ultraviolet visible Spectroscopy
XPS	X-ray Photoelectron spectroscopy

SUMMARY

1 – Metallic Nanoparticles – Bibliographic Review

1.0	Introduction	01
1.1	Methods of preparation	03
1.1.2	Nucleation Process	06
1.1.3	Growth Process	08
1.2	Nanoparticles stabilization	09
1.3	Synthesis of anisotropic nanoparticles	10
1.3.1	Seed-mediated synthesis	14
1.3.2	Polyol synthesis	14
1.3.3	Biological synthesis	15
1.3.4	Hydro/solvothermal synthesis	15
1.3.5	Galvanic replacement reactions	16
1.3.6	Photochemical synthesis	17
1.3.7	Electrochemical synthesis	17
1.3.8	Template-mediated synthesis	18
1.4	General aspects of physicochemical properties, applications, and main characterization techniques of anisotropic nanoparticles	19
1.5	Gold Nanorods	23
1.5.1	The seed-mediated growth to gold nanorods: general concepts	24

2– Experimental Part

2.0	Initial considerations	38
2.1	Materials, reagents, and solvents	38
2.1.1	Preparation of the Reagent Solutions	40
2.2	Characterization techniques	40
2.3	Synthesis of surfactants	41
2.3.1	Synthesis of surfactants HEA16X	41
2.3.2	General procedure for preparation of N,N-dimethyl-N-	42

	cetyl-N-(2-hydroxyethyl) ammonium X salts with X= F ⁻ , I ⁻ , HCO ₃ ⁻ , BF ₄ ⁻	
2.3.3	Synthesis of surfactants with different length of the alkyl chain	43
2.3.4	Synthesis of surfactants with different polar head group	44
2.3.5	<i>N-cetyl-N,N,N-(TrisHydroxyEthyl)ammonium Bromide</i> <i>salt: THEA16Br</i>	46
2.3.6	<i>N,N</i> - dimethyl-N-cetyl-N -Oxide Amine - NOx16	47
2.4	Synthesis of gold nanoparticles in aqueous system	47

3 – Results and Discussions

3.0	Introduction	49
3.1	Influence of counter-ions	51
3.2	Influence of the alkyl chain length	57
3.3	Influence of the hydroxylated polar head length	59
3.4	Influence of the polar head group	60
3.5	Influence of the hydroxyl group	65
3.6	Synthesis of high aspect ratio AuNRs	66
3.7	Effect of the number of seeds	70
3.8	Stability study of gold nanorods formation	72

4 – Applications on catalysis and self-assembly studies

4.0.	Introduction	77
4.0.1.	Optical properties of gold nanoparticles	78
4.0.2	Catalytic properties	79
4.0.3	Catalytic Hydrogenation reactions	80
4.1	Gold colloidal for catalytic hydrogenation of unsaturated compounds	82
4.1.1	Experimental description	82

4.1.2	Results and discussions	83
4.1.2.1	Catalytic Hydrogenation Reaction	83
4.1.2.2	Reuse of Colloidal Dispersion of AuNRs	87
4.2	Interaction among gold nanoparticles	88
4.2.1	Experimental description	88
4.2.2	Results and discussions	89
4.2.2.1	Homo-organization	90

5 – Final considerations

Appendix		100
----------	--	-----

Metallic Nanoparticles – Bibliographic Review

1.0. Introduction

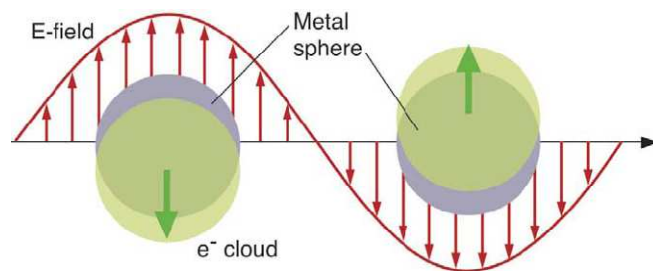
The interest in inorganic nanomaterials such as nanoparticles, nanowires and nanotubes comes from the fact that different and singular properties are reached in nanosized dimensions. The natural forces predominant in the macroscopic scale such as combustion, gravity and friction lose importance in reduced scales to others as Brownian movement, electrostatic forces and quantum mechanics rules. This phenomenon promotes two important consequences: a surface and an electronic effect on the material surfaces that are responsible for all the unusual properties. However, the expression of these intermediate and unusual properties at this length scale is not just due to scaling factors, but it also depends on the morphology, size and shape distribution, and environment in which these particles are present. Therefore, these singular properties are normally assembled in a set of features that are dependent of a "*nano effect*". Furthermore, due to their dimensions, normally in the range of 1 to 100 nm, several nanostructures are applied as great candidates in catalysis, optics, electronic systems and as similar biological structures (e.g., membrane cell genes, proteins and viruses), the nanoparticles have been proposed for investigating biological process as well as for sensing and treating diseases. Nowadays, the volume of studies dealing with these topics represents one of the most impressive phenomena in all scientific history.¹

Despite the advances in the preparation and application of nanomaterials, it is well known that nanoparticles are thermodynamically unstable and have a natural tendency to agglomerate or even grow. Thus, the preparation of high quality nanostructured materials via homogeneous and reproducible methodologies remains a challenge, particularly with a high control of the morphology, allowing to tune the material properties and their applications.

In particular, metal and semiconductor nanomaterials have attracted the interest of several research groups. They exhibit unique optical and electronic properties which most of them are dependent of rules of the quantum

mechanics to be explained and understood; differently when these same materials are in bulk form. In the case of noble metals, when reduced to nanoscale, they present optical properties that are resultant from the collective oscillation of the electrons of the conduction band on particle surface due to the light-surface interaction (Figure 1). For noble metals, a resonant oscillation is achieved by absorption of specific photons of the visible region of the spectrum, leading to systems with distinct colors. This is called the “*surface plasmon resonance*” absorption. When the frequency of the incident electromagnetic wave is the same of the electrons on the surface, there is a strong absorption of the respective photon^{2,6}

Figure 1 - Light surface interaction on metal nanosphere. The electromagnetic field of the light induces a dipole oscillation of the conducting electrons along the particle surface.³



In 1908, Mie⁴ explained the origin of this phenomenon to a particle with radius R , which $2R$ is smaller than the light wavelength (λ), the extinction coefficient of a metallic nanoparticle can be expressed by the equation

$$C_{ext} = \frac{24\pi^2 R^3 \epsilon_m^{3/2}}{\lambda} \frac{\epsilon''}{(\epsilon' + 2\epsilon_m)^2 + \epsilon''^2} \quad \text{eq. 1.1,}$$

Where ϵ is the constant dielectric of nanoparticulated materials, which in this case is dependent on the incident light wavelength, $\epsilon = \epsilon'(\lambda) + i\epsilon''(\lambda)$, and ϵ_m is the constant dielectric of the medium. This equation predicts the wavelength where the maximum extinction will occur, in other words, when $\epsilon = -2\epsilon_m$. When this condition is reached, the electromagnetic field of the light induces a dipole coherent resonant oscillation for the free electrons along the particle.³ The gold particles, for example, may present colors from blue to red, and this

characteristic has been used for centuries like in stained glass windows of cathedrals, vases and other ornaments.⁵

On nanostructured materials, one aspect is quite important: the decrease in the particle size increases the surface ratio. This aspect is one of the main reasons of the particular physical and chemical properties of nanomaterials, and it makes them highly useful in the field of catalysis.⁶

Small nanoparticles have an unstable surface due to the high energy and large curvature. When these nanoparticles are used, not only the surface structure and shape can change, but also their chemical nature and surface. Thus, it is clear that using these nanoparticles fully and effectively will depend, on our understanding, of their general properties and also of their surface properties and stability.⁶

Significant progresses have been also achieved in the last fifteen years focused on novel synthetic routes for anisotropic nanoparticles synthesis. Nowadays, deliberate nanoparticle morphological control, with high yields, and low dispersity is possible. Nevertheless, the understanding of the mechanisms involved in their formation is still unclear.

Also, interactions among nanoparticles are an important subject of research. Different approaches have been proposed to reach nanostructures generated by nanoparticles self-assembly. *Bottom-up* (chemical assembly) or *Top-down* techniques (physical assembly) make the manufacture process of these nanomaterials a great point for the improvement of many future applications of self-assembled nanoparticles (sensors, medical diagnostics, catalysis, nanoelectronics, optoelectronics, photonics etc).^{6,7}

Furthermore, to tune new properties on to nanomaterials, a fine control of the particle surface characteristics is necessary. Usually, the nanoparticle surface (crystal faces exposed, kind of chemical species that surround the particle, quality of the crystal lattice, etc.) plays an essential role in describing the properties of a nanoparticle system.

1.1. Methods of preparation

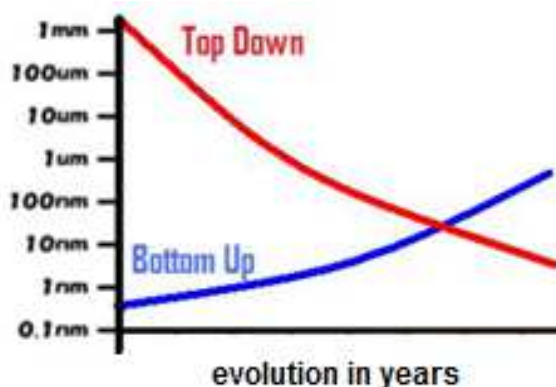
The science of nanomaterials has been characterized by a huge amount of research activities and published studies in characterization and manipulation of nanostructures. The formation of nanoparticles from molecular or ionic

structures named crystallization is well known. The main challenge of nanoparticles preparation is to control the size, shape, and dispersity of the particles as well, in some cases, the control of the nanoparticle coating.⁸

Nanoparticles can be prepared from physical or chemical methods according to two main approaches: i) *bottom-up* or ii) *top-down*, as illustrated in Figure 2. *Top-down* methodologies generate nanoparticles from larger particles. Sonolysis and nanolithography techniques are typical examples of this approach^{9, 10} *Bottom-up* techniques are usually based on wet chemical processes. In such cases, the nanoparticles are prepared from atomic or molecular precursors that interact chemically until they reach the nanometric desired size (and form). The obtained nanoparticles remain dispersed forming a homogeneous solution (colloidal dispersion).^{11,12} In fact, many different methods of metallic nanoparticle synthesis are described in the literature from complexes or metal salts. The reduction of these metals in solution typically occurs in the presence of sodium borohydride, sodium citrate, carbon monoxide, hydrogen and various alcohols.¹³

It is worth to mentioning that this last approach can also include the formation of nanostructures from nanoparticles, i.e. nanoparticles can be arranged together; for example, by a self-assembly process, until they reach nanosuperstructures.¹⁴ In this case, the nanoparticles are considered as versatile "building blocks".⁹

Figure2 - Illustration of the two main approaches to provide nanomaterials.¹⁵



The formation of bulk or nanometer-sized materials from solutions inevitably involves a precipitation/crystallization process*. Despite being a very common issue, the wide understanding of the precipitation process is not a trivial matter. Its knowledge helps to improve the control of the nanoparticles growth until they reach the expected size and shape. There are numerous books^{16,17} and scientific publications^{18,19,20,21,22} that show in detail all theory about precipitation. Some characteristics are observed on nanoparticle formation from solutions:²³

- a. The products of precipitation reactions are generally not very soluble species which results in precipitation and formation of nanoparticles under *sine qua non* conditions of supersaturation by directly dissolving the solute at higher temperature and then cooling to low temperatures or by adding the necessary reactants to produce a supersaturated solution during the reaction.^{24, 25}
- b. The formation of the first and smallest nanoparticles in the middle (nucleation process), followed by the particle growth step, are the two key steps in the formation of nanoparticles in a controlled way.^{26,27}
- c. Secondary processes such as Ostwald ripening (crystal particles dissolve and redeposit onto larger crystals) and aggregation drastically affect the control of the size and shape of the particles obtained.

Although the nanoparticles formation can be induced through various routes such as sonolysis and nanolithography, methods based on chemical reactions are the most common. Generally, these reactions are chosen to stimulate the formation of poorly soluble products to reach, rapidly, the maximum degree of saturation of the substance.²³ Just inducing the compound precipitation does not guarantee that the final product is nanoparticulated and monodispersed. The nucleation and growth procedure also govern the particle size and shape in the precipitation process. When the precipitation starts, many small crystallites are formed through a nucleation process, but rapidly, the

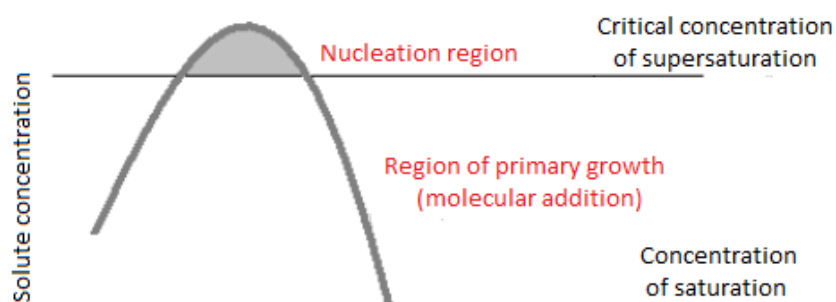
* Here, it is worth mentioning that the precipitation phenomenon is the formation of particles in solution that can be in suspension (colloidal solution) or at the bottom of the flask.

system tends to form larger and thermodynamically stable particles or aggregates.²³

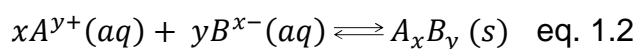
1.1.2 Nucleation Process

Nucleation constitutes an important and critical phase in the dynamic formation of nanostructures because this first step in the process of crystallization gives rise to the first nucleated particles which start to grow. It is essential to create the critical conditions for the molecules in the system come closer and give rise to these first nuclei. These conditions direct the reaction to a critical concentration of supersaturation, where the solute conditions in the reaction is higher than the saturation concentration (limit solubility), are essential to be achieved. This state is naturally very unstable, thus inducing nucleation (Figure 3).

Figure 3 - Scheme illustrating a supersaturation condition to begin the nucleation process as a function the solute concentration in the system.



Considering a hypothetical chemical reaction:



As already commented, the key step to initiate the precipitation of $A_x B_y$ is its degree of supersaturation (S) in the solution, given by

$$S = \frac{a_A a_B}{K_{ps}} \quad \text{eq. 1.3,}$$

Where a_A and a_B are the reactant activities of A and B, and K_{ps} is the product of solubility of the product A_xB_y which can be alternatively expressed as

$$S = \frac{C}{C_{Eq}} \quad \text{eq. 1.4,}$$

Where C and C_{eq} are the concentrations of saturation and equilibrium of the product reaction, respectively. In fact, the literature often considers the difference of C and C_{eq} , $\Delta C = C - C_{eq}$, as the "driving force" of the precipitation, due to the instability of the supersaturated solution.²⁸

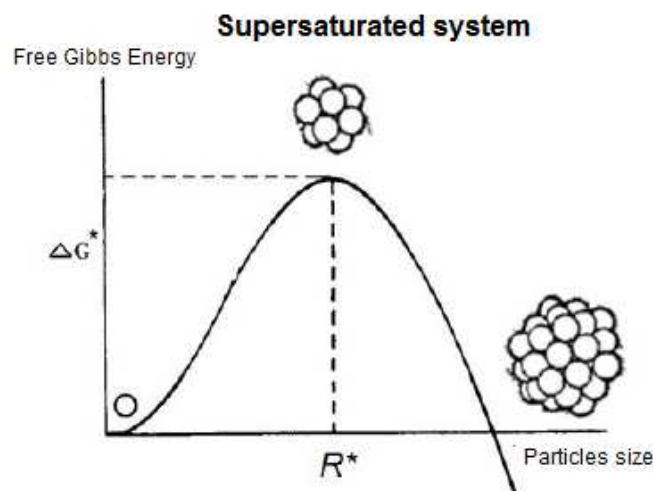
When the nucleation process begins under supersaturated conditions, there is a critical radius, R^* , to particle formation. In this case, nucleated particles with $R > R^*$ will grow, on the other hand, nuclei particles with $R < R^*$ will solubilize.^{6,23} (Figure 4)

The activation energy for the nucleation process of particles is expressed by²²

$$\Delta G^* = \frac{4\pi\sigma_{SL}R^{*2}}{3} = \frac{16\pi\sigma_{SL}^3v^2}{3k^2T^2\ln^2S} \quad \text{eq. 1.5,}$$

Where the term σ_{SL} is the surface tension in the solid-liquid interface, v is the atomic volume of solute, k is Boltzmann's constant, T is temperature, and S is the degree of supersaturation as defined in eq. 1.4.

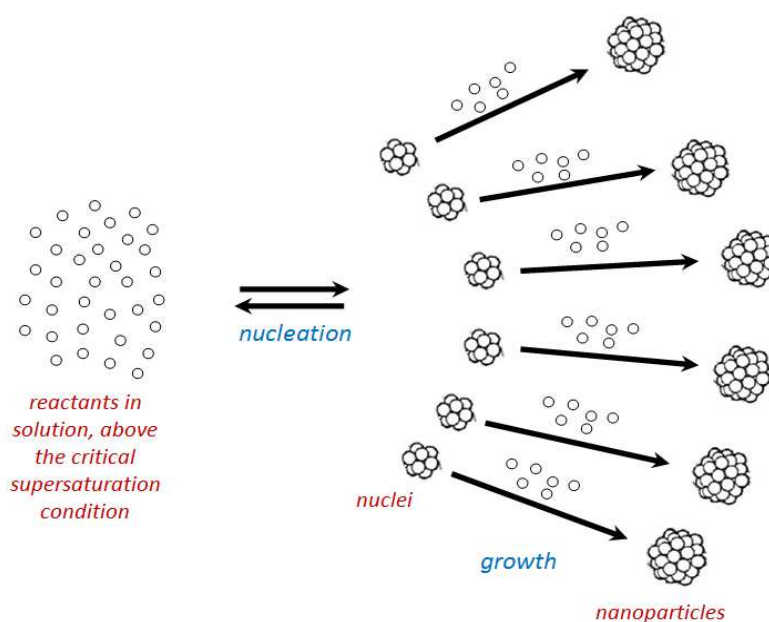
Figure 4 -Free global energy ΔG as function of particle radius.



1.1.3. Growth Process

The growth of the nanoparticles from nuclei is also a complex event. In solution, after the nuclei are formed, they start to grow via atomic/ion/molecular addition which is basically governed by a diffusion process. When the reactant concentration decreases, below the critical level of supersaturation, due to the fast formation of the nuclei, the nucleation process stops, i.e. no new particles are formed. However, the particles continue to grow by molecular addition (Figure 5) until they reach the equilibrium concentration of the species in solution and the particles formed. The uniformity of size is achieved when a short nucleation period occurs and the nuclei formed grow simultaneously. A monodispersed size distribution can be obtained at this stage by a relative fast depletion of the reaction. Furthermore, during and after particle growth it is predicted that smaller particles grow faster than the larger ones, since the free energy driving force is greater for smaller particles.⁶

Figure 5 -Illustration of the nanoparticles sequence formation in solution.



On the other hand, when the concentration of the reactants decreases (depletion) due to the particle growth, other growth process, denominated as Ostwald ripening, could happen. In this case, it is observed that larger particles continue growing and small particles become even smaller, until the point that

they dissolve by themselves. This phenomenon occurs due to the decrease in supersaturation degree (S) and decrease in the critical size of the nuclei (R^*) which, according to Equation 1.5, each particle smaller than the critical size dissolves by itself. In any formation process of nanoparticles when this stage is reached, the particles formed will have a wide size distribution centered on two schemes, larger and smaller particles. On the other hand, when the growth process reaches this stage, monodispersed particles can be obtained if the reaction is extended for a sufficient time, depleting the supersaturation and smaller nuclei. In this case, the particle size is relatively large and could extend to the micrometer size.⁶

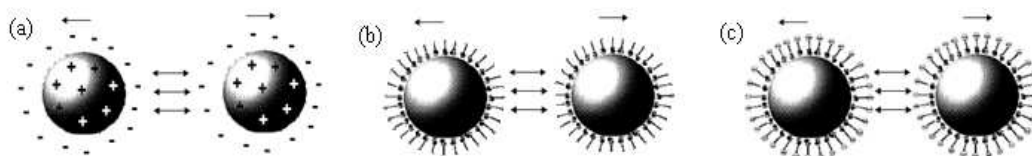
Besides the growth by molecular addition that consists in a deposit of soluble species on the solid surface, the particles could be grown by aggregation among each other. After the particles reach a stable size, they continue to grow and combine with unstable small nuclei.⁶

Indeed, good methods of nanoparticle production must have a good control of all steps discussed above; high quality nanoparticles can be obtained. This is, in fact, an important subject of research in nanoscience and nanotechnology.

1.2. Nanoparticles stabilization

Nanoparticles possess a high surface energy; they are thermodynamically unstable and have a natural tendency to agglomerate and grow which lowers the total energy of the system. To avoid this uncontrolled growth of particles, two mechanisms of particle stabilization are normally required: (i) electrostatic repulsion interactions by equal electric charges between the particles and/or (ii) steric repulsion interactions by impediment effects and (iii) electrostatic and steric effects (Figure 6). Usually these conditions are achieved by addition of a stabilizing agent. In both cases, the nanoparticles do not aggregate due the presence of the stabilizing agent on the particle surface. Among these materials used as protecting agents, there are ionic salts, surfactants, polymers and organic molecules able to interact and to coat the nanoparticle surface.^{11,12}

Figure 6 - Examples of stabilization mechanisms of particles in colloidal solutions stabilized by (a) repel phenomenon among electric charges, (b) by steric effects, (c) electrostatic and steric effects. Adapted from reference 15.

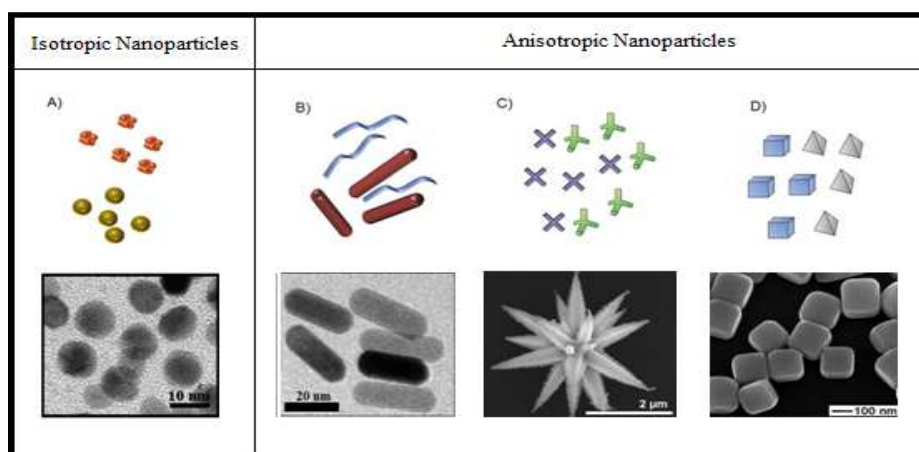


Depending on the nature of the stabilizing agent used, it is possible to precipitate, filter, dry, and re-disperse the colloidal particles without losing their particular characteristics. Furthermore, the protective layer plays other important functions which could influence individual characteristics (solubility, size, structure and distribution)^{11,12} and could induce specific applications of the particles as transport agent of them in biological organisms which is a feature very important to the development of nanostructured *drug delivery* systems.

1.3. Synthesis of anisotropic nanoparticles

In the last 10 years, a huge number of synthetic procedures were developed to produce original nanoparticles with different shapes, sizes, compositions, patterns of distribution, applications etc. (Figure 7). Many research groups reported the synthesis of metal nanoparticles in shapes like tetrahedrons^{29,30}, cubes³¹, prisms³², cylinders³³, stars³⁴, hollows³⁵ etc. To reach each kind of particle, a particular method of preparation has been developed.³⁶

Figure 7 - Representative examples of anisotropic particles. A) spheres, B), rods, C) branched and D) polyhedral shapes.

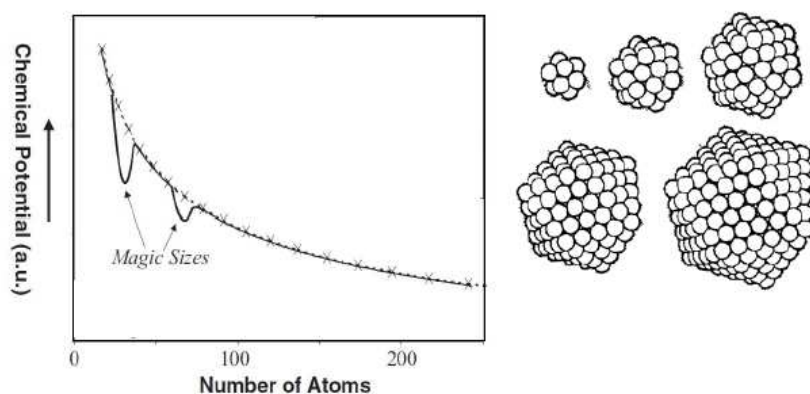


The crystal growth mechanism is one of the main objects of theoretical study in nanoparticle formation and crystallization processes.³⁷ The classic model of the crystal shape control is based on the Gibbs-Curie-Wulff theorem which suggests that the size of a crystal is determined by the surface energy on each side or facet.³⁸ However, it has been observed that purely thermodynamic arguments are not sufficient to explain the variety of nanoparticles recently obtained.³⁹ Currently, two new factors are strongly considered to understand the mechanism of crystal growth: i) the “monomers” concentration, for example, metal species in the solution, and ii) the presence of growth driving agents.

Among the possible shapes for nanoparticles, the spherical ones are the most thermodynamically stable forms. However, depending on the concentration of monomers in solution, and the crystal lattice of the nuclei different forms could be achieved. For example, CdSe particles with the form of spheres, rods and stars could be obtained according to the increasing “monomer” species concentration in the solution.³⁸

Several types of nanoclusters with a defined morphology and number of atoms (magic numbers) are normally detected at the nucleation step. These clusters have minimum chemical potentials, because they have a complete close shell configuration (Figure 8.) These “magical” nanocrystalline structures, formed during the nucleation step, play a fundamental role in the growth of anisotropic structures.

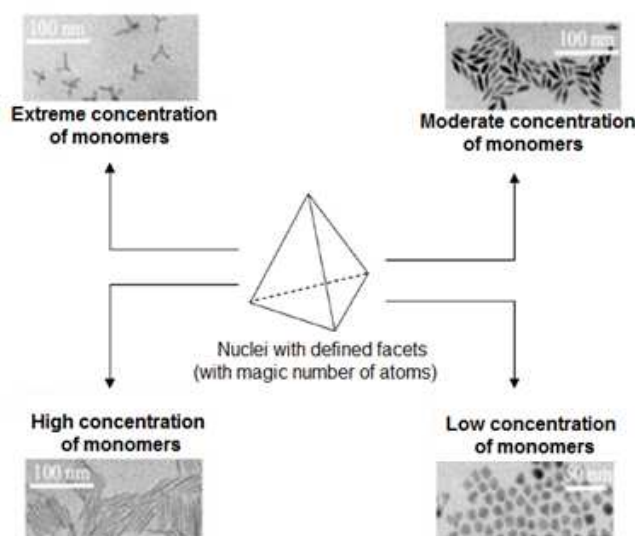
Figure 8 - Illustrative graph showing the relationship between the cluster size with its potential, b) cluster containing magic number of atoms (13, 55, 147, 309, 561 ...). Figure adapted from reference 38.



It has been established that the morphology of final nanoparticles is mainly determined by the number of twin defects present in the initial nuclei (seed particles).⁴⁰ In the next step, the atoms generated from the reduction of the precursor get diffused to the surface of the nuclei and will deposit at active surface sites, forming metallic/covalent bonds with their neighbors. Adjusting the molar ratio between the stabilizer and precursor it is possible to modify the crystal planes and as consequence of this modification, each facet will grow by molecular addition and lead to the formation of nanostructures with distinct shapes.^{41,42,43}

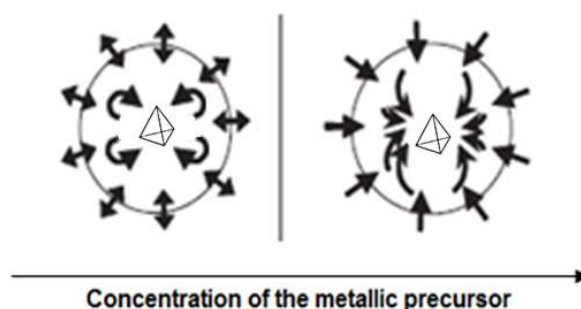
As cited above, the monomers concentration has a strong influence in the dynamic crystal formation. It was reported in Peng's works that nuclei of CdSe with well-defined facets and an extremely high monomer concentration induce the growing process by each facet independently, producing star structures. Moderate and high concentrations of the monomers in the system have a great contribution to lead the growth of only one facet preferred, producing elongated structures. Finally, at low concentrations, the low chemical potential of the system decreases the high potential of the particles surface, responsible for a more homogeneous crystal growth, producing similar spherical particles (Figure 9).

Figure 9 -Possibilities of the growth of nanocrystals as function of the monomer concentration in the system. Figure adapted from reference 38



Two steps are required for the formation of nanoparticles. The first one is the nucleation process and the second one is the growth process by molecular addition (monomer addition) or Brownian motion (aggregation of nanocrystals). Additionally, after that is known a third stage denominated Ostwald ripening, and at this stage, after ceasing the growth of the particles by monomers depletion, it starts a process of atomic rearrangements which depends much of the time, tending to the formation of more energetically stable structures with low surface potential, for example, spherical nanoparticles.³⁸ In understanding this dynamic process, one can understand also the conditions required for the formation of the anisotropic nanoparticles depicted on Figure 9, see scheme presented on Figure 10.

Figure 10 - Growth stages in a defined nanocrystal as function of different concentrations of monomers. Monomer addition and Ostwald ripening under a low monomer concentration. Mainly monomer addition on the facets under high concentration. Figure adapted from reference 38.



In addition to the factors mentioned above (such as reagent concentration, time, reducing agents and metal precursors), it is possible to control the shape and size of nanoparticles, using growth driving agents. These agents preferentially interact with certain planes (facets), blocking or compromising their growth, thus leading to the formation of anisotropic particle.

To conclude this topic, we can mention that the formation and growth of nanocrystals is a highly kinetic process and due to this factor, any nanocrystal could have its growth process driven or stopped by changes in reaction conditions⁴⁴ frequently requiring a systematic study of the conditions of the synthesis.

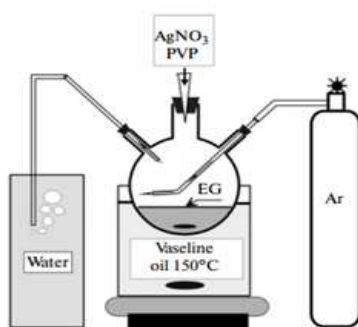
1.3.1. Seed-mediated synthesis

Over the last 20 years, several reliable methods have been developed to prepare anisotropic nanostructure in good yields and size, and shape control. Among these methods, the seed-mediated synthesis of anisotropic nanoparticles is widely and commonly used in the preparation of nanoparticles with rod, wire, triangle, star, flower shapes, and so on. This method, indeed, separates the two steps required for the formation of nanoparticles (nucleation and growth). In other words, in one solution, only the nucleation step occurs, i.e. only small particles are formed, called “seeds”. These particles are added in another solution containing “monomers” in condition to promote the growth process. Indeed, the “seed-mediated” method is the most current method adopted.

1.3.2. Polyol synthesis

Polyol synthesis is a simple method to obtain metal nanoparticles (or alloys) of a range of shapes and sizes. This method is based on the reduction of soluble metal complexes or inorganic salt precursors by polyols (ethylene glycol, propylene glycol, pentane diols, glycerol etc.) at high temperatures. The relation between the reducing power and reaction temperature (polyols display relatively high boiling points) makes polyols appropriate solvents to prepare different size and shape metal nanoparticles. For example, after heating in presence of air, ethylene glycol is converted into glycolaldehyde which works as a reducing agent of Ag(I) precursors, leading to Ag(0) nanostructures in the presence of polyvinyl pyrrolidone (PVP).

Figure 11 - (a) Schematic representation of setup used for polyol synthesis.⁴⁵

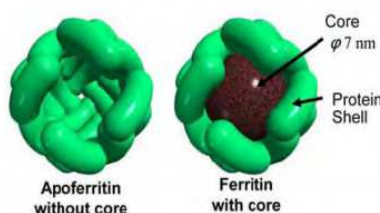


1.3.3. Biological synthesis

Biological systems are able to prepare metallic nanoparticles and functional superstructures of inorganic nanomaterials such as amorphous silica, magnetite (magnetotactic bacteria), and calcite⁴⁶. The shape control of nanomaterials in biological systems has been achieved either by growth in constrained environments such as membranes vesicles or through functional molecules such as polypeptides that bind specifically to inorganic crystal facets.

Furthermore, some proteins such as ferritin, ferritin-like-protein, chaperonin and viruses such as cowpea chlorotic mottle virus which have cavities in the center have been used as template to synthesize various types of nanoparticles most especially that of metals.⁴⁷ These routes, however, do not adequately address the issue of particle monodispersity and uniformity which is very crucial in the applications of these nanoparticles.⁴⁸

Figure 12 - An illustration of the cage-shaped protein apoferritin without iron core and ferritin with iron core (Adapted from Iwahori and Yamashita, 2007).⁴⁸



1.3.4. Hydro/solvothermal synthesis

In hydro/solvothermal synthesis, nanoparticles are synthesized in hot water/solvent in an autoclave under high pressure. The water acts as a catalyst and occasionally as a component of solid phases. However, this method can be considered as solvothermal synthesis due to the possibility of using different solvents.⁴⁹ Moreover, some additives could be associated to modify the initial properties of pure hydrothermal water (e.g. polymers, surfactants, acids or bases to equilibrate the pH, etc.).^{50,51,52,53,54}

Figure 13 - An illustration of hydro/solvothermal instrumentation.

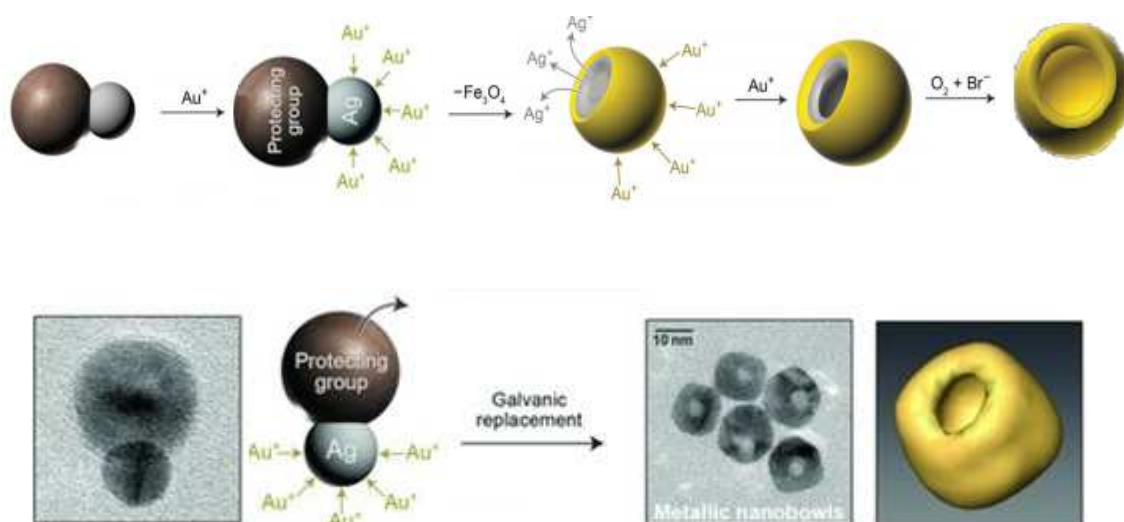


1.3.5. Galvanic replacement reactions

Galvanic replacement reactions are based on a simple method to synthesize nanostructured materials. Indeed, a large number of different metal nanostructures can be prepared based on the variation in the standard electrode potentials of the elements, leading to deposition of the more noble element and dissolution of the less noble component. This methodology is frequently used to prepare bimetallic nanoparticles.⁵⁵

For example, in a bimetallic interaction between Ag and Fe_3O_4 , a thin shell of Au can be deposited on Ag and the Fe_3O_4 domain spontaneously dissociates. Additional Au preferentially deposits on the convex side of the NP while Ag dissolves preferentially from the original site of attachment to Fe_3O_4 , thus, creating a void. When exposed to a mixture of O_2 and Br^- , the bowls increase their cavity size while their diameter does not change.⁵⁶

Figure 14 - Mechanistic studies on the formation of nanobowls by Galvanic replacement reactions.

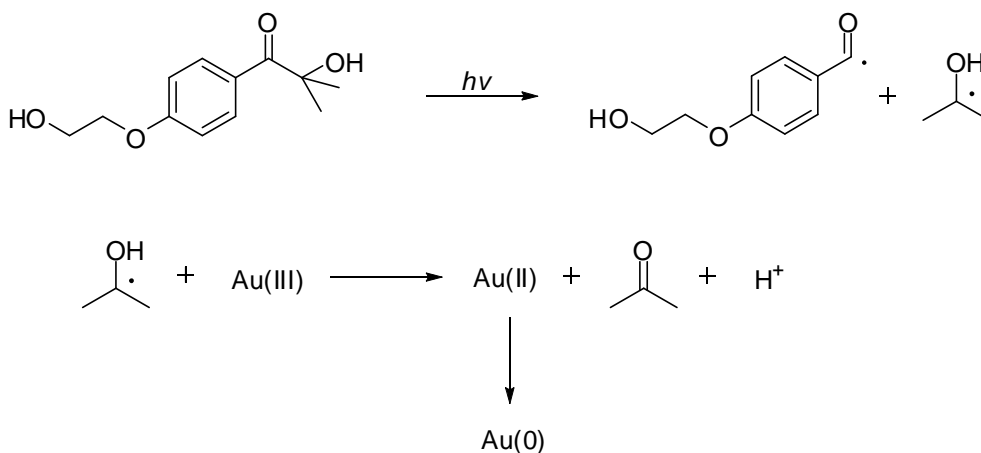


1.3.6. Photochemical synthesis

The reduction of metal salt precursors can also be performed by photochemical methods through photo-irradiation. The major advantage of this technique includes the reduction of the metallic precursor without using an excess of reducing agents. In this case, the radiation is absorbed independently of light-absorbing solutes and products. Thus, photochemical synthesis does not require a specific and costly instrument. This method is similar to the electrochemical method and used concepts from template-assisted synthesis.⁵⁷

For example, gold nanoparticles can be synthesized by preparing a solution containing HAuCl_4 and 1.0 mM Irgacure-2959 (1-[4-(2-hydroxyethoxy)phenyl]-2-hydroxy-2-methyl-1-propane-1-one) I-2959 in water. The HAuCl_4 /I-2959 samples were typically irradiated in a photoreactor with 40 W/m^2 UVA light. Samples were irradiated for a few minutes.

Figure 15 - Formation of Gold Nanoparticles by photochemical reaction



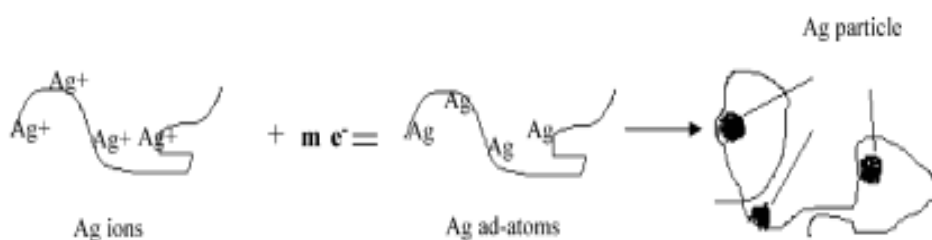
1.3.7. Electrochemical synthesis

Electrochemical reduction methods are broadly used for preparing a great range of different and high size-selective nanoparticles, especially of noble metals by adjusting the current density.⁵⁸ The significant advantage of this technique is the possibility to work at low temperatures, and the preparation of high-quality products. In general, experimentally, metal cations migrate to the

cathode in which the reduction takes place, that in the presence of suitable stabilizing agents, isotropic or anisotropic metal nanoparticles can be obtained.

For example, silver nanoparticles can be produced by electrochemical process in a simple two-electrode cell by using an EG&G M173 potentiostat/galvanostat in presence of poly(*N*-vinylpyrrolidone) – PVP as main stabilizer agent.⁶⁰

Figure 16 - Schematic diagram showing formation of electrochemically produced PVP-stabilized silver clusters.⁵⁹

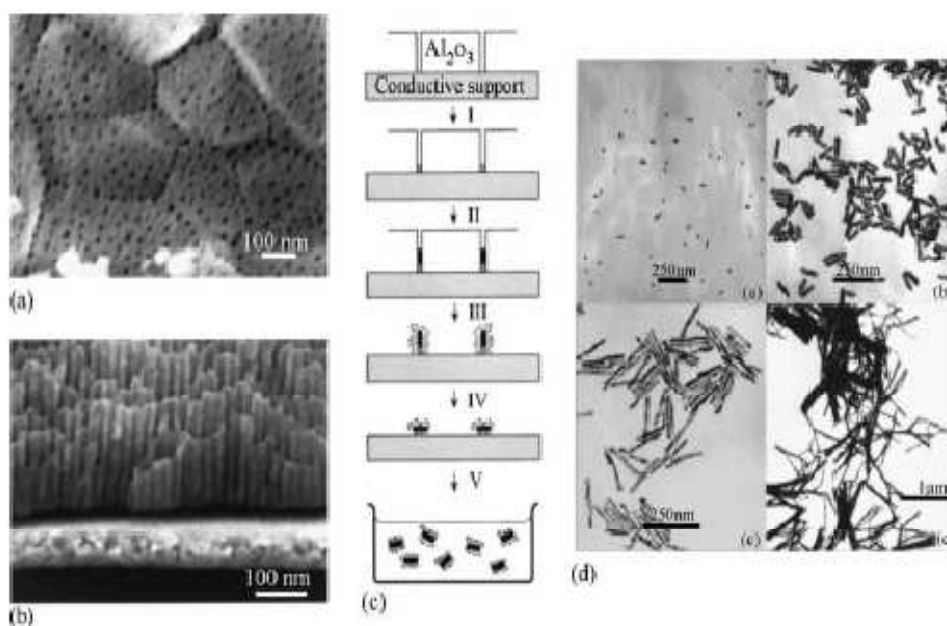


1.3.8. Template-mediated synthesis

The template method is one of the most popular methods to produce 1D nanostructures with controllable size and architecture. The main advantage of this technique is the easy fabrication (possibility to work in normal atmosphere), low cost, high yield, and adaptability to various types of materials.^{60,61,62,63} In this method, nanoporous materials, like polycarbonate or alumina, are used as templates.^{64,65}

For example, the template method for the synthesis of the gold nanorods was first introduced by Martin and co-workers. This method is based on the electrochemical deposition of Au in the pores of nanoporous polycarbonate or alumina template membranes.

Figure 17 - (a and b) FEG–SEM images of an alumina membrane. (c) Schematic representation of the successive stages during formation of gold nanorods via the template method. (d) TEM micrographs of gold nanorods obtained by the template method.¹⁵



1.4. General aspects of physicochemical properties, applications, and main characterization techniques of anisotropic nanoparticles

As we have already discussed, it is well recognized that physical and chemical properties of materials can change dramatically at nanoscale. Indeed, nanomaterials exhibit unusual properties that are different from their bulk form counterpart. Thus, the properties of a specific material are characterized from their scale size; a critical size that are usually on the nanometer range. If the physical size of the material is reduced from this limit, its properties change and become sensitive to its architecture.⁶⁶ These changes on the properties are not due only the size reduction, but for new aspects that are normally manifested on nanoscale, and are normally neglected on macroscopic scale.^{67,68,69,70}

In human being's world, the gravitational and friction forces are the most predominated effects. Whereas, as the dimensions of the bodies decrease, the electrostatic force, vander Waals, Brownian movement and quantum mechanical aspects receive important attention. In a subatomic scale, the electrostatic attraction force between two protons is 10^{36} times greater than gravitational force. The gravitational force begins to dominate the bodies and

particles universe when exist a significant quantity of the matter that means a wide scale.^{71,72} Table 1 presents the predominant effects on materials at macro, micro and nanosize scales.

Table 1 - Predominant effects by scale reduction from meters to angstroms dimensions.⁶⁷

Unit of measure	Size similar to	Predominant effects
Meter (m) 1 m	Child, bike etc	gravity, friction, combustion
Centimeter (cm) 10^{-2} m	Human thumb, coins etc.	gravity, friction, combustion
Millimeter (mm) 10^{-3} m	Sugar grains etc	gravity, friction, combustion, electrostatic force
Micrometer (μ m) 10^{-6} m	1/40 of an hair diameter	Electrostatic force, Van der Waals, Brownian Movement
Nanometer (nm) 10^{-9} m	A line with 5 to 10 atoms	Electrostatic force, Van der Waals, Brownian Movement, Quantum mechanics
Angstrom (\AA) 10^{-10} m	1 atom, 10 times the wavelength of the electron	Quantum mechanics

Two relevant aspects of electrostatic forces which are predominant in nanotechnology are the van der Waals forces and the Brownian movement. Most molecules are rarely symmetrical, thus, a non-uniform distribution of charges generates asymmetric electric fields, allowing attraction or repulsion among other molecules. The Brownian movement occurs in small molecules or particles where the gravity influence is negligible. This movement does not allow the molecules to remain in the same position in which they are folded, due to this behavior; it is a challenge, for example, the nanomanipulation. On the other hand, this phenomenon is one way which the nanodevices could be moved. Furthermore, other effects appear from the materials reduction to nanometric scale. The two main effects are:

Size effects: quantum effects on the size where the normal electronic structure is substituted by a series of discrete electronic levels. For example, when magnetic nanoparticles are reduced to small dimensions, their atomic

structure with discrete electronic levels gives rise to new phenomena such as superparamagnetism, changes in optical properties, etc.

Induced effects by the increased surface area: the increasing surface area of nanomaterials causes a significant increase in the reactivity, hardness, as well as magnetic, catalytic, and optoelectronic properties. This phenomenon could provide a decrease up to few tens of degrees Celsius on process temperature of some dispersed materials thereby reducing energy costs.

While the size effects describe the physical properties of nanostructured materials, the induced effects by the increased surface area play an eminent role in chemical processes, especially in heterogeneous catalysis and sensors.

The size effects could be observed using measurements of physical properties such as mechanical, optical, electrical and magnetic properties. While the induced effects could be observed by measuring the thermodynamic properties such as vapor pressure, specific heat, conductivity, thermal stability and melting point.⁶⁷

Anisotropic particles offer features and functions that are not easily obtained by size-tuning of spherical nanoparticles. For example, a slight change in particle geometry can produce great changes in the surface plasmon peak position of a metallic nanoparticle which can hardly be achieved in the spherical nanosystems through a similar change in diameter. In addition, the optical properties of anisotropic gold or silver nanorods (NRs) or prisms are tunable in the visible, near infrared (NIR), and infrared regions of the spectrum, as a function of their aspect ratios. Even though isotropic gold nanoparticles show intense surface of plasmon resonance (SPR) absorption with good absorption coefficient, it is weakly dependent on particle size which limits its application in sensing.

When anisotropy feature is added to the nanoparticles such as NRs or prisms, the SPR is not only enhanced, but also becomes strongly tunable as a function of aspect ratio. One reason for this is that these structures, well-controlled in size and shape, possess different surface areas and crystallographic facets. Introducing anisotropy into the nanoparticles can also make a substantial change in their magnetic properties. The coercive field of ferromagnetic particles can be increased considerably by introducing shape anisotropy⁷³.

Biocompatibility^{74,75} large extinction, optical absorption in the near-infrared region (blood and tissues are relatively transparent to the radiation in this wavelength region)^{76,77} and photothermal heating capacity^{78,79,80,81,82,83} enable gold NRs, for example, to be good candidates for diagnosis, and therapeutic medical applications.^{84,85,86.}

The utility of anisotropic nanomaterials in treatment of tumor cells and photothermal therapies to cancer diagnosis is well reported in the literature.^{76,84,85,86, 87 , 88 .} Localized electric fields, originated near these nanoparticles, have been investigated for the chemical and biological detection of molecules^{89,90,91,92,93} and surface-enhanced Raman spectroscopy.^{94,95,96,97} The strong electromagnetic fields at the anisotropic surfaces of metallic nanoparticles make them useful for non-linear optical applications in photonics^{98,99,100,101} as well chemical and biological detection.¹⁰²

The anisotropy feature could be enhanced by the incorporation of lower dimensional nanostructures into the same or higher dimensional nanosystems. These systems show different properties due to the effective interaction of unequal domains. Another way to improve the properties and performance of anisotropic nanoparticles is by self-assembly process.^{103, 104} This controlled organization brings unusual properties that cannot be observed in an individual particle system, neither through the bulk form material.^{105,106} It is important to mention that the properties of assembled nanomaterials in 2 or 3D lattices strongly depend on their shape, surface features, charge, polarizability, magnetic dipole moment, mass, and other factors. The additional advantage of assembled nanomaterials is the interaction between the same or different building blocks in the system, promoting different properties, depending on the dimensionality as well as the nature of interaction between the building blocks. These systems can be called as 'anisotropic superstructures'.

Characterization Methods

The adequate characterization of these nanomaterials is essential, since its properties can change dramatically with the variation of some physical and chemical properties. In this characterization, some parameters such as the particle size, area and chemical composition surface are critical. The Table 2 summarizes the principal techniques used to determine the size, surface area,

and composition of the nanoparticles, as well as their morphological characteristics.

Table 2 - Principal techniques used in the characterization of nanoparticles

Technique	Applications/Characteristics	Ref
X-ray diffraction (DRX)	Crystal structure, particle size	107
Dynamic light scattering (DLS)	Particle size (suspension), size distribution	108
Sedimentation by centrifugation	Distribution of the particle sizes / complex	108
Size exclusion chromatography	Good resolution, small sample volume / slow	109
Atomic force microscopy (AFM)	Good Resolution / 3D images, only scans the surface	109
Specific surface area (BET)	Particle size, surface area / simple, the particles are considered as monodispersed spheres	109
Scanning electron microscopy (SEM)	Surface morphology, particle size / good resolution	108
Transmission electron microscopy (TEM)	Local structure and morphology	109
X-ray Spectroscopy of disperse energy (EDX)	Surface composition and elemental mapping	109
X-ray Photoelectron spectroscopy (XPS)	Chemical analysis of the surface	109

1.5. Gold Nanorods

Among all the anisotropic metal nanoparticles that have been synthesized, gold nanorods (AuNRs) have attracted great attention due to the fact that these kind of nanoparticles can be obtain with a good morphologic control and different aspect ratios, allowing different properties for the same material.¹¹⁰

The synthesis of gold nanorods can be accomplished in many ways. The main process to prepare gold nanorods relies on wet methods. These methods involve typical processes of growth nanoparticles. In general, the first step is the reduction of a metal precursor in solution, typically $[\text{AuCl}_4^-]$, that forms very small clusters in an undernanometric dimension (nucleation). Soon after, others Au reduced atoms join these particles, leading larger particles

(growth process). The agglomeration of particles and the growth control are prevented by the addition of stabilizing agents and driving agents that could be the same in many cases. The concentration of reactants, temperature, and pH, influence the kinetics of nucleation and growth process.

Initially, gold nanorods were prepared by using electrochemical deposition, with shape control provided by alumina porous or polycarbonate membrane templates, in the presence of cetyltrimethylammonium bromide, CTABr. After that, other methods emerged as a simple, viable technique such as the Seed Mediated Method that consists basically on two steps: nucleation and growth process used to prepare AuNRs.

One of the most interesting features of the AuNRs is the absorption spectrum in the Uv-vis-NIR region that presents multiple plasmon bands (one band for the transverse plasmon [short axis] and one band for the longitudinal plasmon [long axis]). The longitudinal plasmon is strongly influenced by the aspect ratio of the gold nanorods. These dependent properties of shape have frequently been taken advantage to allow sensing applications, plasmon enhanced spectroscopies, biomedical imaging, and photothermal therapy for cancer.

Improving AuNRs performance in these applications requires AuNRs with specific physicochemical properties. Due to this factor, the control of the shape and dimensions is a focus of intense interest in nanomaterial chemistry. The development of the first seed-mediated growth provided, for the first time, a convenient, versatile, wet, chemical approach to the synthesis of gold nanorods (which was subsequently extended to other anisotropic shapes). Indeed, AuNRs based on this method can now be purchased from major chemical vendors.

1.5.1. The seed-mediated growth to gold nanorods: general concepts

Murphy et al., and other groups have developed a seed mediated method, a multi-step controlled redox reaction that is performed in room temperature aqueous solution. This seeded growth approach has become the model for almost all subsequent AuNRs syntheses. The seed-growth methodology involves the nucleation and the growth process, where small seed particles (~1.5 – 5 nm diameter) are first synthesized from gold salt reduction (HAuCl_4)

by action of strong reducing agent to promote the reduction of Au(III) to Au (0). After, these seed particles are added to a growth solution that contains additional gold salts that are reduced from Au(III) to Au(I) by an action of a weak reducing agent as ascorbic acid, and a “growth driving agent” controls the final particle shape.^{111,112} The ascorbic acid is a too weak reducing agent to reduce the additional gold salts from Au(III) to Au(I) alone, in the growth solution and in a commonly reaction conditions (Figure 18). The growth driving agent classically used is cetyltrimethylammonium bromide (CTABr), a cationic surfactant well-known to form rodlike micelles in water. The CTABr acts as a soft template to direct nanorods formation as the gold seeds grew upon further metal ion addition.^{111, 113} The CTABr has a preferentially higher packing density on the {110} and {100} surfaces, forming a more compact layer with respect to that on the {111} surfaces. All chemical features of CTABr molecule, from its alkyl chain length to its counter ion, are also critical to retain the ability to synthesized rods (Figure 19).^{114,115}

The gold nanorods obtained are supported by a bilayer of CTABr on their surfaces^{116,117,118} that like a primary function are adsorbed to promote the growth of seed particles in a specific direction along certain faces. After the first addition of seed particles in the growth solution, depending on the aspect ratio desired, a re-addition process continues in subsequent solutions. After, shortly aliquot of this growth solution was added to a new growth solution, and if necessary, an aliquot of this second solution was added to a third growth solution. This three-step seeded growth approach provides gold nanorods with aspect ratios between 10 and 25 if stopped along the way, with average gold nanorods dimensions up to 1800 x 25 nm.^{2,111} Although some papers discuss the absence of additives, the majority of the scientific studies reported the use of organic solvents and silver nitrate to influence the micellar packing of CTABr.^{110,113}

Critical control over the reactions conditions such as growth steps used in the synthesis, composition of the surfactant or cosurfactants^{112,119} the seed solution¹²⁰, the concentration and the nature of the additives¹²¹ in the growth solution provides gold nanorods with different aspect ratios, good yields, reproducibility and specific morphologies.^{122,123}

A new seeded growth procedure utilizes smaller AuNPs seeds (1.5 nm) stabilized with CTABr, rather than citrate, and a small amount of silver nitrate is added to the growth solution. The addition of silver nitrate provides short nanorods with low aspect ratios (2-5) AuNRs (~ 45 x 15 nm in dimension) in better than 90% of selectivity relative to other shapes.^{110,118,124}

Other growth-driving agents for AuNRs preparation such as a binary mixture usually in presence of CTABr as CTABr/BDACl (benzyltrimethylammonium chloride),¹²⁵ cetylpyridinium chloride,¹¹⁹ or CTABr/OTABr (octyltrimethylammonium bromide),¹²⁶ have been used with not always good results in terms of selectivity and yield on nanorods formation.

Herein, this work propose as good alternative and an original family of surfactants easily based on hydroxylated ammonium salts as growth-driving agents to prepare AuNRs by the seed-mediated method in aqueous media with high yields and selectivity, instead of the usual CTABr.

Figure 18 -Schematic illustration of the seed solution, growth solution and the beginning of the growth process.

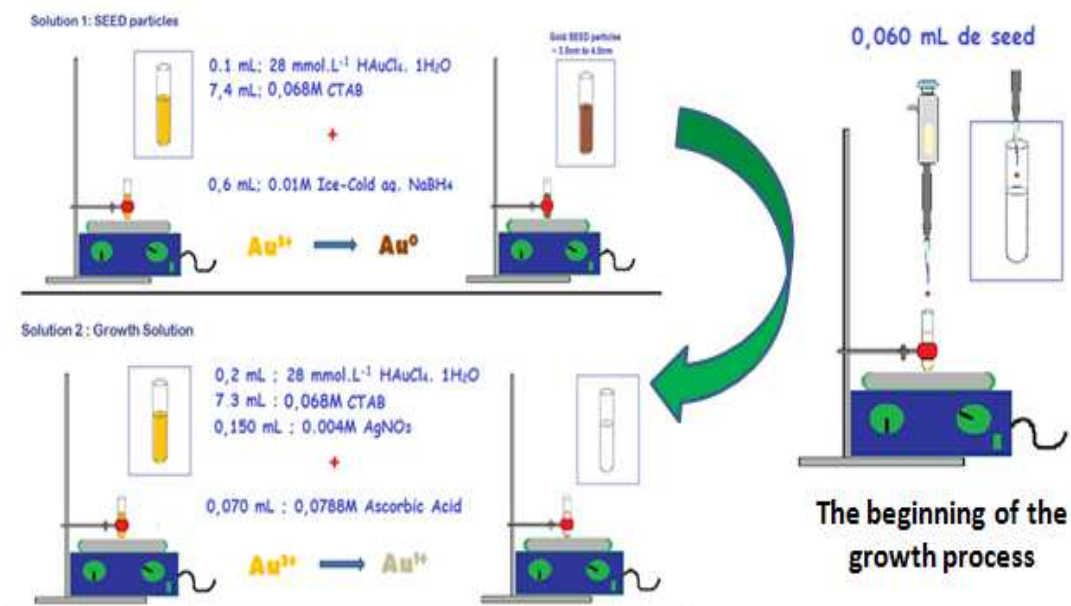
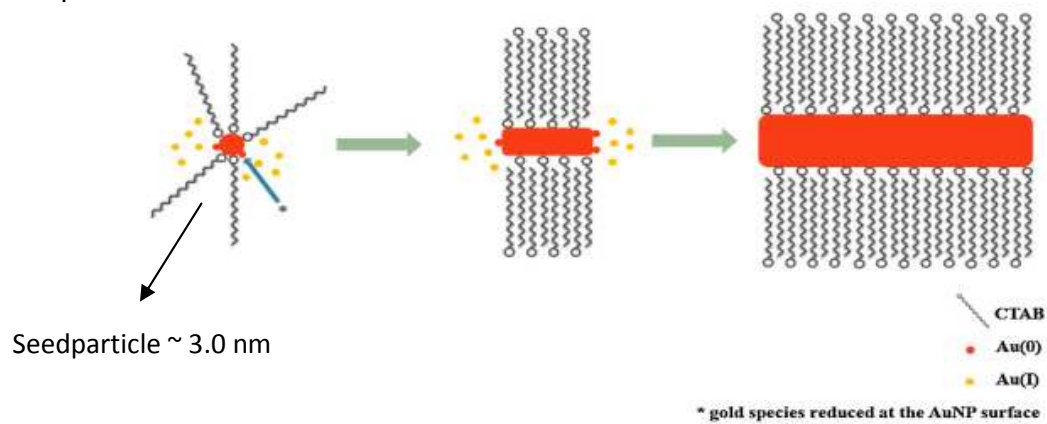


Figure 19 - Schematic illustration of the dissymmetric growth of gold nanorod from a seed particle and Au (I) ion species that are reduced to Au(0) on the surface of the metal particle.¹²⁷



REFERENCES

- ¹C. Altavilla, E. Ciliberto, *Inorganic nanoparticles: Synthesis, applications, and Perspectives*.CRC Press, Taylor & Francis Group 2011.
- ²H. E, Toma, L. S. Bonifácio,.F. J. Anaissi. *Da cor à cor inexistente: Uma reflexão sobre os espectros eletrônicos e efeitos cromáticos*. Quim.Nova 2005, 28, 897.
- ³P. K.Jain, I. H. El-Sayed, M. A. El-Sayed. *Au nanoparticles target câncer*. Nano Today 2007, 2, 18.
- ⁴U.Kreibig, M.Vollmer, *Optical properties of Metal clusters*, Springer – VerlagBerlin Heidelberg New York, 1995.
- ⁵C. J. Murphy. *Nanocubes and Nanoboxes*.Science 2002, 289, 2139.
- ⁶C. Burda, X. Chen, R. Narayanan, M. A. El-Sayed. *Chemistry and Properties of Nanocrystals of Different Shapes*.Chemical Reviews 2005,105, 1025
- ⁷G.Schmid, *Nanoparticles: From Theory to Application*, Wiley, Weinheim 2004.
- ⁸V.J.Mohanraj,Y.Chen, *Nanoparticles - A review*. Trop J Pharm Res 2006, 5, 561.
- ⁹N. Durán, P. D. Marcato, Z. Teixeira, *Nanotecnologia e nanobiotecnologia: Conceitos básicos*. Universidade de Mogi das Cruzes, Mogi das Cruzes, SP, Brasil 2007.
- ¹⁰G. A. Ozin. *Nanochemistry: Synthesis in diminishing dimensions*. Adv. Mater. 1992, 4, 612.
- ¹¹D. Zanchet,B. D. Hall, D. Ugarte, *Structure Population in Thiol-Passivated Gold Nanoparticles*.J. Phys. Chem. B 2000, 104, 11013.
- ¹²D. Zanchet, M. S. Moreno, , D. Ugarte. *Anomalous Packing in Thin Nanoparticle Supercrystals*.Phys. Review.Letters 1999, 82, 5277.
- ¹³H. Xiaoge, D. Shaojun. *Metal nanomaterials and carbon nanotubes— synthesis, functionalization and potential applications towards electrochemistry*.J. Mater. Chem. 2008, 18, 1279.
- ¹⁴S. Zhang, X. Kou, Z. Yang, Q.Shi, G. D. Stucky, L. Sun, J. Wang, C. Yan. *Nanonecklaces assembled from gold rods, spheres, and bipyramids*.Chem. Commun. 2007, 18, 1816.
- ¹⁵M. G., Angelo da Silva.*Síntese, dinâmica de formação, caracterização e propriedades ópticas de nanobastões de ouro dispersos em meio aquoso e matrizes orgânicas*.Master Dissertation, Institute of Chemistry and Biotechnology from Federal University of Alagoas, 2010.
- ¹⁶Ring T. A., *Fundamentals of Ceramic Powder Processing and Synthesis*; Academic Press: San Diego, CA 1996.

-
- ¹⁷ A. E. Nielsen, *Kinetics of Precipitation*; Pergamon Press: Oxford 1964.
- ¹⁸ J. A. Dirksen, T. A. Ring. *Fundamentals of crystallization: Kinetic effects on particle size distributions and morphology*. Chem. Eng. Sci. 1991, 46, 2389.
- ¹⁹ R. M. Tromp, J. B. Hannon. *Thermodynamics of nucleation and growth*. Surf. Rev. Lett. 2002, 9, 1565.
- ²⁰ P. H. Karpinski, J. S. Wey, A. S. Myerson, *In Handbook of Industrial Crystallization*, 2nd ed., Ed.; Butterworth-Heinemann: Stoneham, MA, 2001
- ²¹ D. A. Blackadder. *Nucleation and Crystal Growth Including Precipitation*. Chem. Eng. 1964.
- ²² H. Füredi-Milhofer. *Spontaneous precipitation from electrolyte solutions* Pure Appl. Chem. 1981, 53, 2041.
- ²³ B. L. Cushing, V. L. Kolesnichenko, C. J. O'Connor. *Recent Advances in the Liquid-Phase Syntheses of Inorganic Nanoparticles*. Chem. Rev. 2004, 104, 3893.
- ²⁴ X. Peng, J. Wickham, A. P. Alivisatos. *Kinetics of II-VI and III-V Colloidal Semiconductor Nanocrystal Growth: "Focusing" of Size Distributions* J. Am. Chem. Soc. 1998, 120, 5343.
- ²⁵ C. B. Murray, D. J. Norris, M. G. Bawendi. *Synthesis and Characterization of monodispersed nanocrystals and close-packed nanocrystal assemblies*. Annu. Rev. Mater. Sci. 2000, 30, 545.
- ²⁶ B. R. Pamplin, *Crystal Growth*, Pergamon Press: New York, 1975.
- ²⁷ Y. Jiang, *Forced Hydrolysis and Chemical Co-Precipitation*. In Handbook of Nanophase and Nanostructured Materials; Z. L., Wang, Y. Liu, Z. Zhang, Eds.; Kluwer Academic: New York, 2003, 59.
- ²⁸ P. H. Karpinski, J. S. Wey. *In Handbook of Industrial Crystallization*, 2nd ed., Myerson, A. S., Ed.; Butterworth-Heinemann: Stoneham, MA, 2001.
- ²⁹ Y. Sun, Y. Xia. *Shape-Controlled Synthesis of Gold and Silver Nanoparticles*. Science 2002, 298, 2176.
- ³⁰ D. J. Milliron, S. M. Highes, Y. Cui, L. Manna, J. Li, L. Wang, Alivisatos AP. *Colloidal nanocrystal heterostructures with linear and branched topology*. Nature 2004, 430, 190.

-
- ³¹ T. S. Ahmadi, Z.L. Wang, T. C. Green, A. Henglein, M. A. El-Sayed. *Shape-controlled synthesis of colloidal platinum nanoparticles*. *Science* 1996, 272, 1924.
- ³² R. Jin, Y. Cao, E. Hao, G. S. Metraux, G. C. Schartz, C. A. Mirkin. *Controlling anisotropic nanoparticle growth through plasmon excitation*. *Nature* 2003, 425, 487.
- ³³ (a) X. C. Jiang, A. Brioude, M. P. Pileni. *Gold nanorods: Limitations on their synthesis and optical properties*. *Colloids Surf A, Physicochem Eng. Asp* 2006, 277, 201 (b) Y. Niidome, K. Nishioka, H. Kawasaki, S. Yamada. *Effects of ammonium salts and anionic amphiphiles on the photochemical formation of gold nanorods*. *Colloids Surf A Eng Asp* 2005, 161, 257.
- ³⁴ J. L. Burt, J. L. Elechiguerra, J. G. Reyes, J. M. C. Montejano, M. J. Jose-Yacaman. *Beyond Archimedean solids: Star polyhedral gold nanocrystals*. *Cryst Growth* 2005; 285, 681.
- ³⁵ Y. Yin, R. M. Rioux, C. K. Erdonmez, S. Hughes, G. A. Somorjai. *Formation of Hollow Nanocrystals Through the Nanoscale Kirkendall Effect*. *Alivisatos AP. Science* 2004, 304, 711.
- ³⁶ R. B. Grubbs. *Nanoparticle assembly: Solvent-tuned structure*. *Nature materials*, VOL 6 08/2007 <http://www.nature.com/naturematerials>
- ³⁷ J. W. Mullin. *Crystallization*, 4^a ed.; Butterworth-Heinemann, Linacre House, Jordan Hill, Oxford OX2 8DP, Woburn, MA 2001.
- ³⁸ X. Peng. *Mechanisms for the Shape-Control and Shape-Evolution of Colloidal Semiconductor Nanocrystals*. *Adv. Mater.* 2003, 15, 459.
- ³⁹ X. Peng. *Green Chemical Approaches toward High-Quality Semiconductor Nanocrystals*. *Chem. Eur. J.* 2002, 8, 334.
- ⁴⁰ H. Hofmeister. *Shape variations and anisotropic growth of multiply twinned nanoparticles*. *Z. Kristallogr*, 2009, 224, 528.
- ⁴¹ Y. Sun, Y. Yin, B. T. Mayers, T. Herricks, Y. Xia. *Uniform Silver Nanowires Synthesis by Reducing AgNO₃ with Ethylene Glycol in the Presence of Seeds and Poly(Vinyl Pyrrolidone)*. *Chem Mater* 2002, 14, 4736.
- ⁴² B. Wiley, Y. Sun, B. Mayers, Y. Xia. *Shape-Controlled Synthesis of Metal Nanostructures: The Case of Silver*. *Chem. EurJ* 2005, 1, 454.

-
- ⁴³ X. Lu, M. Rycenga, S. E. Skrabalak, B. Wiley, Y. Xia. Chemical Synthesis of Novel Plasmonic Nanoparticles. *Annu. Rev. Phys. Chem.* 2009, 60, 167.
- ⁴⁴ Z. L. Wang. *Transmission Electron Microscopy of Shape-Controlled Nanocrystals and Their Assemblies.* *J. Phys. Chem. B* 2000, 104, 1153.
- ⁴⁵ Panfilova et al. *Study of polyol synthesis reaction parameters controlling high yield of silver nanocubes.* *Colloid Journal*, 74, 1, 2012.
- ⁴⁶ S. H Yu. *Bio-inspired Crystal Growth by Synthetic Templates.* *Top. Curr. Chem.* 2007, 271, 79, 118.
- ⁴⁷ N. Gálvez, B. Fernandez, E. Valero, P. Sánchez, R. Cuesta, J. Dominguez-Vera. *Apoferitin as a nanoreactor for preparing metallic nanoparticles.* *Comptes Rendus Chimie* 11, 1207, 2008.
- ⁴⁸ A. T. Sennuga. *Biological synthesis of metallic nanoparticles and their interactions with various biomedical targets*; A thesis submitted in fulfillment of the requirements for the degree of Doctor of Philosophy of Rhodes University. 12/2011.
- ⁴⁹ C. Lu, L. Qi, J. Yang, L. Tang, D. Zhang, J. Ma. *Hydrothermal growth of large-scale micro patterned arrays of ultralong ZnO nanowires and nanobelts on zinc substrate.* *Chem. Commun* 2006, 3, 3551.
- ⁵⁰ J. Yuan, W. N. Li, S. Gomez, S. L. Suib. *Shape-Controlled Synthesis of Manganese Oxide Octahedral Molecular Sieve Three-Dimensional Nanostructures.* *J Am Chem Soc* 2005, 127, 5, 14184.
- ⁵¹ G. Shen, D. Chen. *Self-Coiling of Ag₂V₄O₁₁ Nanobelts into Perfect Nanorings and Microloops.* *J. Am. Chem. Soc.* 2006, 128, 11762.
- ⁵² L. Tian, H. Y. Tan, J. Vittal. *Morphology-Controlled Synthesis of Bi₂S₃ Nanomaterials via Single- and Multiple-Source Approaches.* *J. Cryst Growth Des* 2008; 8, 734.
- ⁵³ C. C. Chang, H. L. Wu, C. H. Kuo, M. H. Huang. *Hydrothermal Synthesis of Monodispersed Octahedral Gold Nanocrystals with Five Different Size Ranges and Their Self-Assembled Structures.* *Chemistry of Materials* 2008, 20, 7570.
- ⁵⁴ Q. Lu, F. Gao, S. Komarneni. *Biomolecule-Assisted Reduction in the Synthesis of Single-Crystalline Tellurium Nanowires.* *Adv. Mater* 2004, 16, 1629.
- ⁵⁵ A. Brenner, G. E. Riddell. *Nickel plating on steel by chemical reduction.* *J Res Natl Bur Stand (US)* 1946; 37: 31_4.
- ⁵⁶ Y. Ridelman, G. Singh, R. Popovitz-Biro, S.G. Wolf, S. Das, R. Klajn. *Metallic Nanobowls by Galvanic Replacement Reaction on Heterodimeric Nanoparticles.* *Small* 2012, 8, 654.
- ⁵⁷ K. Esumi, K. Matsuhisa, K. Toriue. *Preparation of Rodlike Gold Particles by*

-
- UV Irradiation Using Cationic Micelles as a Template*. Langmuir 1995, 11, 3285.
- ⁵⁸M. T. Reetz, W. Helbig; *Size-Selective Synthesis of Nanostructured Transition Metal Clusters*. J. Am. Chem. Soc. 1994; 116: 7401_2.
- ⁵⁹ B. Yin, H. Ma, S. Wang, S. Chen. *Electrochemical Synthesis of Silver Nanoparticles under Protection of Poly(N-vinylpyrrolidone)*. J. Phys. Chem. B 2003, 107, 34.
- ⁶⁰ H. W. Liang, S. Liu, S. H. Yu. *Controlled Synthesis of One-Dimensional Inorganic Nanostructures Using Pre-Existing One-Dimensional Nanostructures as Templates*. Adv. Mater 2010, 22, 3925.
- ⁶¹ G. W. Meng, F. M. Han, X L. Zhao, B. S. Chen, D. C. Yang, J. X. Liu, Q. L. Xu, M. G. Kong, X. G. Zhu, Y. J. Jung, Angew. Chem. Int Ed 2009, 48, 166.
- ⁶² C. A. Foss, G. L. Hornyak; J. A. Stockert; C. R. Martin. *Optical properties of composite membranes containing arrays of nanoscopic gold cylinders*. J Phys. Chem 1992; 96, 7497
- ⁶³ C. R. Martin. *Sol-gel template synthesis of semiconductor nanostructures*. Science 1994, 266, 1961.
- ⁶⁴ J. C. Hulteen, C. R. Martin. *A general template-based method for the preparation of nanomaterials*. J Mater Chem 1997, 7, 1075.
- ⁶⁵ B. V. der Zande, M. R. Bohmer, L. G. J. Fokkink, C. Schonenberger. *Colloidal Dispersions of Gold Rods: Synthesis and Optical Properties*. Langmuir 2000, 16, 451.
- ⁶⁶ M. Eddaoudi, D. B. Moler, H. Li, B. Chen, T. M. Reineke, M. O'keeffe, O. M. Yaghi. *Modular Chemistry: Secondary Building Units as a Basis for the Design of Highly Porous and Robust Metal–Organic Carboxylate Frameworks*. Accounts of Chemical Research 2001, 34, 319.
- ⁶⁷ G. Fishbine, *The investor's guide to nanotechnology & micromachines*. John Wiley & Sons, Inc.: New York 2002.
- ⁶⁸ D. E. Nicolau, J. Phillimore, R. Cross, D. V. Nicolau. *Nanotechnology at the crossroads: the hard or the soft way?*. Microelectronics Journal 2000, 31, 611.
- ⁶⁹ M. Rieth. *Nano-engineering in science and technology: an introduction to the world of nanodesign*. Series on the foundation of Natural Science and technology, V.6, World Scientific, New Jersey, 2003.
- ⁷⁰ F. Galembeck. *Polímeros e Nanotecnologia*. Polímeros: Ciência e Tecnologia, 2003, 13, 1.
- ⁷¹ M. C. Roco, W. S. Bainbridge, Eds. *Societal implications of nanoscience and nanotechnology*. NSET Workshop Report. Edited by National Science Foundation, March 2001.

-
- ⁷² N. Duran, L. H. C. Mattoso, P.C. Morais. *Nanotecnologia: introdução, preparação e caracterização de nanomateriais e exemplos de aplicação*. Artliber: São Paulo 2006.
- ⁷³ R. C. O'Handley, *Modern magnetic materials, principles and applications*. New York: Wiley-Interscience Publication 2000.
- ⁷⁴ C. M. Goodman, C. D. McCusker, T. Yilmaz, V. M. Rotello. *Toxicity of Gold Nanoparticles Functionalized with Cationic and Anionic Side Chains*. Chem 2004,15, 897.
- ⁷⁵ K. J Lee, P. D. Nallathamby, L . M. Browning, C. J. Osgood, X. H. N. Xu. *In Vivo Imaging of Transport and Biocompatibility of Single Silver Nanoparticles in Early Development of Zebrafish Embryos*. ACS Nano 2007, 1, 133.
- ⁷⁶ L. R. Hirsch, R. J. Stafford, J. A. Bankson, S. R. Sershen, B. Rivera, R. E. Price et al. *Nanoshell-mediated near-infrared thermal therapy of tumors under magnetic resonance guidance*. Proc. Natl. Acad. Sci. USA 2003, 100, 13549.
- ⁷⁷ S. Link, A. Furube, M. B. Mohamed, T. Asahi, H. Masuhara, M . A. El-Sayed. *Hot Electron Relaxation Dynamics of Gold Nanoparticles Embedded in MgSO₄ Powder Compared To Solution: The Effect of the Surrounding Medium*. J Phys. Chem. B 2002, 106, 945.
- ⁷⁸ S Link, M. A. El-Sayed. *Optical properties and ultrafast dynamics of metallic nanocrystals*. Annu. Rev. Phys. Chem. 2003, 54, 331.
- ⁷⁹ A. K. Salem, P. C. Searson, K. W. Leong. *Multifunctional nanorods for gene delivery*. Nat Mater 2003, 2, 668.
- ⁸⁰ A. K Salem., C. F. Hung, T. W. Kim, T. C. Wu, P. C. Searson, K. W. Leong. *Multi-component nanorods for vaccination applications*. Nanotechnology 2005; 16, 484.
- ⁸¹ M. Hu, J. Chen, Z. Y. Li, L. Au, G. V. Hartland, X. Li et al. *Gold nanostructures: engineering their plasmonic properties for biomedical applications*. Chem. Soc. Rev. 2006, 35, 1084.
- ⁸² P. K. Jain, S. Eustis, M. A. El-Sayed. *Plasmon Coupling in Nanorod Assemblies: Optical Absorption, Discrete Dipole Approximation Simulation, and Exciton-Coupling Model*. J. Phys. Chem. B 2006, 110, 18243.
- ⁸³ A. R. Lowery, A. M. Gobin, E. S. Day, N. Halas. *Immunonanoshells for targeted photothermal ablation of tumor cells*. J. Int. J. Nanomed 2006, 1,1.
- ⁸⁴ C. Loo, A. Lin, L. Hirsch, M. H. Lee, J. Barton, N. Halas et al. *Nanoshell-Enabled Photonics-Based Imaging and Therapy of Cancer*. Technol. Cancer Res. Treat. 2004, 3, 33.

-
- ⁸⁵ M. B. Mohamed, S. A. Temer, S. Link, M. Braun, M. A. El-Sayed. *Hot electron and phonon dynamics of gold nanoparticles embedded in a gel matrix*. Chem. Phys. Lett 2001, 343, 55.
- ⁸⁶ C. J. Murphy, A. M. Gole, J. W. Stone, P. N. Sisco, A. M. Alkilany, E. C. Goldsmith et al. *Gold Nanoparticles in Biology: Beyond Toxicity to Cellular Imaging*. Acc. Chem. Res 2008, 41, 1721.
- ⁸⁷ W. Arap, R. Pasqualini, E. Ruoslahti. *Cancer Treatment by Targeted Drug Delivery to Tumor Vasculature in a Mouse Model*. Science 1998, 279, 377.
- ⁸⁸ W. D. James, L. R. Hirsch, J. L. West, P. D. O'Neal, J. D. Payne, Application of INAA to the build-up and clearance of gold nanoshells in clinical studies in mice. J Radioanal Nucl. Chem 2007, 271, 455.
- ⁸⁹ R. Elghanian, J. J. Storhoff, R. C. Mucic, R. L. Letsinger, C. A. Mirkin. *Selective Colorimetric Detection of Polynucleotides Based on the Distance-Dependent Optical Properties of Gold Nanoparticles*. Science 1997, 277, 1078.
- ⁹⁰ J. M. Nam, C. C. Thaxton, C. A. Mirkin. *Nanoparticle-Based Bio-Bar Codes for the Ultrasensitive Detection of Proteins*. Science 2003, 301, 1884.
- ⁹¹ E. Katz, I. Willner. *Integrated Nanoparticle–Biomolecule Hybrid Systems: Synthesis, Properties, and Applications* Angew. Chem. Int Ed 2004, 43, 6042.
- ⁹² X. Huang, P. K. Jain, I. H. El-Sayed, M. A. El-Sayed, *Special Focus: Nanoparticles for Cancer Diagnosis & Therapeutics – Review*. Nanomedicine 2007, 2, 681.
- ⁹³ K. A. Willets, D. R. P. Van. *Localized Surface Plasmon Resonance Spectroscopy and Sensing*. Annu Rev Phys. Chem 2007, 58, 267.
- ⁹⁴ K. Kneipp, M. Moskovits, H. Kneipp, H. *Surface-enhanced Raman scattering: physics and applications*. Berlin, New York: Springer, 2006.
- ⁹⁵ K. Kneipp, H. Kneipp, I. Itzkan, R. R. Dasari, M. S. Feld. *Ultrasensitive Chemical Analysis by Raman Spectroscopy*. Chem. Rev. 1999; 99, 2957.
- ⁹⁶ C. J. Orendorff, A. Gole, T. K. Sau, C. J. Murphy. *Surface-Enhanced Raman Spectroscopy of Self-Assembled Monolayers: Sandwich Architecture and Nanoparticle Shape Dependence*. Anal Chem 2005, 77, 3261.
- ⁹⁷ A. Campion, P. Kambhampati. *Surface-enhanced Raman scattering*. Chem. Soc. Rev. 1998, 27, 241.

-
- ⁹⁸ D. Segets, L. M. Tomalino, J. Gradl, W. J. Peukert. *Real-Time Monitoring of the Nucleation and Growth of ZnO Nanoparticles Using an Optical Hyper-Rayleigh Scattering Method*. *J Phys. Chem C* 2009, 113, 11995.
- ⁹⁹ A. Neely, C. Perry, B. Varisli, A. Singh, T. Arbneshi, D. Senapati et al. *Ultrasensitive and Highly Selective Detection of Alzheimer's Disease Biomarker Using Two-Photon Rayleigh Scattering Properties of Gold Nanoparticle*. *ACS Nano* 2009, 3, 2834.
- ¹⁰⁰ G. Wang, W. J. Sun, *Optical Limiting of Gold Nanoparticle Aggregates Induced by Electrolytes*. *J PhysChem B* 2006, 110, 20901.
- ¹⁰¹ J. Kneipp, H. Kneipp, B. Wittig, K. Kneipp. *One- and Two-Photon Excited Optical pH Probing for Cells Using Surface-Enhanced Raman and Hyper-Raman Nanosensors*. *Nano Lett* 2007, 7, 2819.
- ¹⁰² P. C. Ray. *Size and Shape Dependent Second Order Nonlinear Optical Properties of Nanomaterials and Their Application in Biological and Chemical Sensing*. *Chem Rev* 2010, 110, 5332.
- ¹⁰³ C. N. R., Rao, G. U. Kulkarni, P. J. Thomas, P. P. Edwards. *Metal nanoparticles and their assemblies*. *ChemSoc Rev* 2000, 29, 35.
- ¹⁰⁴ A. R. Tao, J. Huang, P. Yang. *Langmuir-Blodgett of Nanocrystals and Nanowires*. *AccChem Res* 2008, 41, 1662.
- ¹⁰⁵ M. P. Pileni. *Nanocrystal Self-Assemblies: Fabrication and Collective Properties*. *JPhysChem B* 2001, 105, 3358.
- ¹⁰⁶ S. A. Harfenist, Z. L. Wang, M. M. Alvarez, I. Vezmar, R. L. Whetten. *Highly Oriented Molecular Ag Nanocrystal Arrays*. *J PhysChem* 1996, 100, 13904.
- ¹⁰⁷ L. K. Limbach, Y. Li, R. N. Grass, T. J. Brunner, M. A. Hintermann, M. Muller, D. Gunther, W. J. Stark. *Oxide Nanoparticle Uptake in Human Lung Fibroblasts: Effects of Particle Size, Agglomeration, and Diffusion at Low Concentrations*. *Environ. Sci. Technol.* 2005, 39, 9370.
- ¹⁰⁸ A. Bootz, V. Vogel, D. Schubert, J. Kreuter. *Comparison of scanning electron microscopy, dynamic light scattering and analytical ultracentrifugation for the sizing of poly(butyl cyanoacrylate) nanoparticles*. *Eur. J. Pharm. Biopharm.* 2004, 57, 369.

-
- ¹⁰⁹ K. W. Powers, S. C. Brown, V. B. Krishna, S. C. Wasdo, B. M. Moudgil, S. M. Roberts. *Research Strategies for Safety Evaluation of Nanomaterials. Part VI. Characterization of Nanoscale Particles for Toxicological Evaluation.* *Toxicol. Sci.* 2006, 90, 296.
- ¹¹⁰ S. E. Lohse, C. J. Murphy. *The Quest for Shape Control: A History of Gold Nanorod Synthesis.* *Chem. Mater.* 2013, 25, 1250.
- ¹¹¹ N. R. Jana, L. Gearheart, C. J. Murphy. *Seed-mediated growth approach for shape-controlled synthesis of spheroidal and rod-like gold nanoparticles using a surfactant template.* *Adv. Mater.* 2001, 13, 1389.
- ¹¹² B. Nikoobakht, M. A. El-Sayed. *Preparation and Growth Mechanism of Gold Nanorods (NRs) Using Seed-Mediated Growth Method.* *Chem. Mater.* 2003, 15, 1957.
- ¹¹³ C. J. Murphy et al. *Gold nanorod crystal growth: From seed-mediated synthesis to nanoscale sculpting.* *Current Opinion in Colloid & Interface Science* 2011, 16, 128.
- ¹¹⁴ N. Garg, C. Scholl, A. Mohanty, R. Jin. *The Role of Bromide Ions in Seeding Growth of Au Nanorods.* *Langmuir* 2010, 26, 10271.
- ¹¹⁵ D. K. Smith, N. R. Miller, B. A. Korgel. *Iodide in CTAB Prevents Gold Nanorod Formation.* *Langmuir* 2009, 25, 9518.
- ¹¹⁶ B. Nikoobakht, M. A. El-Sayed. *Evidence for Bilayer Assembly of Cationic Surfactants on the Surface of Gold Nanorods.* *Langmuir* 2001, 17, 6368.
- ¹¹⁷ T. K. Sal, C. J. Murphy. *Self-Assembly Patterns Formed upon Solvent Evaporation of Aqueous Cetyltrimethylammonium Bromide-Coated Gold Nanoparticles of Various Shapes.* *Langmuir* 2005, 21, 2923.
- ¹¹⁸ J. C. Murphy, L. B. Thompson, A. M. Alkilany, P. N. Sisco, S. P. Boulos, S. T. Sivapalan, J. A. Yang, D. J. Chernak, J. Huang. *The Many Faces of Gold Nanorods.* *J. Phys. Chem. Lett.* 2010, 1, 2867.
- ¹¹⁹ J. Gao, C. M. Bender, C. J. Murphy. *Dependence of the Gold Nanorod Aspect Ratio on the Nature of the Directing Surfactant in Aqueous Solution.* *Langmuir* 2003, 19, 9065.
- ¹²⁰ A. Gole, C. J. Murphy. *Seed-Mediated Synthesis of Gold Nanorods: Role of the Size and Nature of the Seed.* *Chem. Mater.* 2004, 16, 3633.
- ¹²¹ T. Sau, C. J. Murphy. *Room Temperature, High-Yield Synthesis of Multiple Shapes of Gold Nanoparticles in Aqueous Solution.* *J. Am. Chem. Soc.* 2004, 126, 8648.

-
- ¹²² O. R. Miranda, N. R. Dollahon, T. S. Ahmadi. *Critical Concentrations and Role of Ascorbic Acid (Vitamin C) in the Crystallization of Gold Nanorods within Hexadecyltrimethyl Ammonium Bromide (CTAB)/Tetraoctyl Ammonium Bromide (TOAB) Micelles*. *Crystal Growth & design* 2006, 6, 12.
- ¹²³ T. H. Ha, H. J. Koo, B. H. Chung. *Shape-Controlled Syntheses of Gold Nanoprisms and Nanorods Influenced by Specific Adsorption of Halide Ions*. *J. Phys. Chem. C* 2007, 111, 1123.
- ¹²⁴ M. G. Angelo da Silva, M. R. Meneghetti, A. Denicourt-Nowicki, A. Roucoux. *New and tunable hydroxylated driving agents for the production of tailor-made gold nanorods*. *RSC Adv.* 2013, 3, 18292.
- ¹²⁵ B. Nikoobakht, M. A. El-Sayed. *Preparation and Growth Mechanism of Gold Nanorods (NRs) Using Seed-Mediated Growth Method*. *Chem. Mater.* 2003, 15, 1957.
- ¹²⁶ Y. Takenaka, H. Kitahata. *High-aspect-ratio gold nanorods synthesized in a surfactant gel phase*. *Chemical Physics Letters* 2009, 467, 327.
- ¹²⁷ M. G. Angelo da Silva, A. M. Nunes, S. M. P. Meneghetti, M. R. Meneghetti. *Tunable hydroxylated surfactants: An efficient toolbox towards anisotropic gold nanoparticles*. *C. R. Chimie* 2013, 16, 640.

Experimental Part

2.0. Initial considerations

Five groups of experiments were conducted during this thesis work : i) synthesis of gold nanorods in aqueous medium; ii) synthesis of hydroxylated surfactants; iii) study of the influence of the hydroxylated surfactants as growth-driving agents of gold nanoparticles; iv) evaluation of the gold nanorods in catalysis; and v) tests in self-assembly mechanisms with the gold nanospheres and nanorods. A huge part of the experiments were performed in the group Nanocatalysis and Molecular Catalysis to Fine Chemistry (Organométalliques: Matériaux et Catalyse team), École Nationale Supérieure de Chimie de Rennes. The tests in self-assembly mechanisms were performed in the Group of Catalysis and Chemical Reactivity of the Institute of Chemistry and Biotechnology, Federal University of Alagoas (GCaR/IQB/UFAL). The characterization of the surfactants and colloidal systems were performed in the laboratory OMC/ENSCR. Transmission Electron Microscopy images were obtained in the Université Pierre et Marie Curie.

2.1. Materials, reagents, and solvents

The glassware were treated with aqua regia and washed with water and detergent before use. In this work the following reagents were used, see Table 3.

Table 3- Reagents and solvents used in this work.

Reagents/Solvents	Origin
H ₂ AuCl ₄ .3H ₂ O, 99.9%	SIGMA - ALDRICH
NaBH ₄ , > 98%	ACROS ORGANICS
L(+)-Ascorbic acid, P.A. 99+%	VETEC
Cetyltrimethylammonium Bromide (CTABr), 99+%	ACROS ORGANICS
AgNO ₃ , > 99%	REAGEN

<i>N,N</i> -dimethyl- <i>N</i> -cetyl- <i>N</i> -(2-hydroxypropyl)ammonium Bromide (HEA16Br)	OMC/ENSCR ^a
<i>N,N</i> -dimethyl- <i>N</i> -cetyl- <i>N</i> -(2-hydroxyethyl)ammonium Chloride(HEA16Cl)	OMC/ENSCR ^a
<i>N,N</i> -dimethyl- <i>N</i> -cetyl- <i>N</i> -(2-hydroxyethyl)ammonium Fluoride (HEA16F)	OMC/ENSCR ^a
<i>N,N</i> -dimethyl- <i>N</i> -cetyl- <i>N</i> -(2-hydroxyethyl)ammonium Iodide (HEA16I)	OMC/ENSCR ^a
<i>N,N</i> -dimethyl- <i>N</i> -cetyl- <i>N</i> -(2-hydroxyethyl)ammonium Hydrogencarbonate (HEA16HCO ₃)	OMC/ENSCR ^a
<i>N,N</i> -dimethyl- <i>N</i> -cetyl- <i>N</i> -(2-hydroxyethyl)ammonium Tetrafluoroborate (HEA16BF ₄)	OMC/ENSCR ^a
<i>N,N</i> -dimethyl- <i>N</i> -octadecyl- <i>N</i> -(2-hydroxybutyl)ammonium Bromide (HEA18Br)	OMC/ENSCR ^a
<i>N,N</i> -dimethyl- <i>N</i> -dodecyl- <i>N</i> -(hydroxyethyl)ammonium Bromide (HEA12Br)	OMC/ENSCR ^a
<i>N,N</i> -dimethyl- <i>N</i> -cetyl- <i>N</i> -(2-hydroxypropyl)ammonium Bromide- (HPA16Br)	OMC/ENSCR ^a
<i>N,N</i> -dimethyl- <i>N</i> -cetyl- <i>N</i> -(2-hydroxybutyl)ammonium Bromide(HBA16Br)	OMC/ENSCR ^a
<i>N,N</i> -dimethyl- <i>N</i> -cetyl- <i>N</i> -(2-hydroxypropyl)ammonium Bromide (H2PA16Br)	OMC/ENSCR ^a
<i>N,N</i> -diethyl- <i>N</i> -cetyl- <i>N</i> -(2-hydroxyethyl)ammonium Bromide (HDA16Br)	OMC/ENSCR ^a
<i>N</i> -methyl- <i>N</i> -cetyl- <i>N,N</i> -(DiHydroxyEthyl)ammonium Bromide (DHEA16Br)	OMC/ENSCR ^a
<i>N</i> -cetyl- <i>N,N</i> -(DiHydroxyEthyl)ammonium Bromide (DHA16Br)	OMC/ENSCR ^a
<i>N</i> -cetyl- <i>N,N,N</i> -(TrisHydroxyEthyl)ammonium Bromide(THEA16Br)	OMC/ENSCR ^a
<i>N,N</i> -dimethyl- <i>N</i> -cetyl- <i>N</i> -Oxide Amine (NOx16)	OMC/ENSCR ^a
<i>N,N</i> -dimethyl- <i>N</i> -cetyl- <i>N</i> -methylephidrine Bromide (<i>N</i> -MeEPh12Br)	OMC/ENSCR ^a
<i>N,N</i> -dimethyl- <i>N</i> -cetyl- <i>N</i> -ethylammonium Bromide - (EA16Br)	OMC/ENSCR ^a
<i>N,N</i> -dimethyl- <i>N</i> -cetyl- <i>N</i> -propylammonium Bromide - (PA16Br)	OMC/ENSCR ^a

<i>N,N</i> - dimethyl- <i>N</i> -cetyl- <i>N</i> -butylammonium Bromide – (BA16Br)	OMC/ENSCR ^a
Ethanol,96%	SIGMA-ALDRICH
Toluene, 98%	SIGMA - ALDRICH
Deionized water	DEIONIZER DIRECT – Q3 MILLIPORE

^asynthesized in OMC/ENSCR

2.1.1 Preparation of the Reagent Solutions

The solution of the metal precursor $\text{HAuCl}_4 \cdot 3\text{H}_2\text{O}$, tetrachloroauric acid trihydrate is prepared by dissolving 1.0 g of acid in 99 mL of deionized water (25.0 mM). The solution is submitted to a high vacuum for degassing and stocked in a Schlenck under inert atmosphere (argon) and under the absence of light.

The solution of the reducing agent sodium borohydride, NaBH_4 , is prepared immediately before the use and left at low temperature ($\sim 10^\circ\text{C}$).

The surfactants were prepared as described in the literature or after adapted modification. A solution of all surfactants is prepared at 0.20M concentration, in exception of the surfactants low water-soluble (HEA16I, HEA16BF₄, THEA16Br, NMeEph16Br...) those need a heating process to get solubilized.

For all other reagents, it takes the necessary care to avoid contamination during preparation.

2.2.Characterization techniques

The colloidal dispersions prepared in aqueous solution were analyzed by ultraviolet visible spectroscopy (UV-vis), and transmission electron microscopy (TEM).The Uv-vis analyses are performed on a Shimadzu UV-vis 1800 spectrophotometer configured for baseline correction with deionized water absorption band from $\lambda 400$ to 1000 nm, using optical glass cuvettes with an optical path of 1.0 cm. The analyses by transmission electron microscopy were performed on a Microscope JEOL TEM 100CXII operating at 100kV. Samples were prepared by placing a film of the colloidal dispersion in a film

coated with carbon copper grid (200 mesh), at least 24 hours before analysis kept in a desiccator. When necessary, the images obtained by transmission electron microscopy were treated with the Sigma Scan program to obtain a histogram of particle size, with an average of 300 to 500 counts.

The surfactants prepared were characterized by Nuclear Magnetic Resonance (NMR), using a BRUCKER Avance III 400 spectrometer at 400.13 MHz for ^1H and 100.61 MHz for ^{13}C . All magnetic resonance spectra were quoted in parts per million (ppm) measured from tetramethylsilane (TMS) as external reference. The following abbreviations were used to describe peak splitting patterns when appropriate: s= singlet, t= triplet, m= multiplet. Coupling constants, J , were reported in hertz unit (Hz). All melting points were measured, using a Stuart melting point apparatus SMP3. The sample was added in a capillary tube that was accommodated in a heating block. Then, the melting process was observed with the help of bright illumination and a powerful magnifying glass. The CMC measurements were performed, using an automatic tensiometer (Krüss K100) and the DuNoüy Ring Method for air-water interface at 298 K. Before each experiment, the platinum ring was cleaned in a water/ethanol mixture and then in a blue color flame. A concentrated solution 1mg/mL (5 mL) was put in a conic vessel (165.7 mL) and was reduced by the addition of small amounts of ultrapure water. After each addition, the solution is stirred for 120 s. The immersion depth of the ring is 1 mm. Equilibrium surface tension was measured three times at 25°C for each concentration with Harkins and Jordan correction method.

2.3. Synthesis of surfactants

2.3.1. Synthesis of surfactants HEA16X

N,N-dimethyl-*N*-cetyl-*N*-(2-hydroxypropyl)ammonium Bromide - HEA16Br

Bromohexadecane (1.2 eq.) and *N,N*-dimethylethanolamine (1 eq.) were refluxed in absolute ethanol for 48h. Then, the solvent was removed under reduced pressure. The obtained solid was washed twice with diethyl ether afford a white solid with a good yield (92%), m.p. 207°C, ^1H NMR (400MHz, CDCl_3 , 25°C, TMS): δ = 0.85 (t, J = 7 Hz, 3H),

1.23 (m, 24H, H-15), 1.32 (m, 2H), 1.73 (m, 2H), 3.36 (s, 6H), 3.56 (m, 2H), 3.74 (m, 2H); 4.10 (m, 2H); 5.0 (t, $J = 5.3$ Hz, 1H). ^{13}C NMR (100MHz, CDCl_3 , 25°C, TMS): $\delta = 14.1, 22.6-31.9, 52.1, 55.8, 65.6, 66.0$ ppm.

N,N-dimethyl-*N*-cetyl-*N*-(2-hydroxyethyl)ammonium chloride - HEA16Cl

Chlorohexadecane (1.2 eq.) and *N,N*-dimethylethanolamine (1 eq.) were refluxed in absolute ethanol for 48h. Then, the solvent was removed under reduced pressure. The obtained solid was washed twice with diethyl ether afford a white solid with a good yield (92%), m.p.: 204 °C, ^1H NMR (400MHz, CDCl_3 , 25°C, TMS): $\delta = 0.81$ (t, $J = 7.1$ Hz, 3H), 1.18 (m, 24H), 1.27 (m, 2H), 1.67 (m, 2H), 3.30 (s, 6H), 3.48 (m, 2H), 3.48 (m, 2H), 3.65 (m, 2H), 4.03 (m, 2H), 4.61 (m, 1H) ppm. ^{13}C NMR (400MHz, CDCl_3 , 25°C, TMS): $\delta = 14.09, 22.7 - 31.09, 52.0, 55.9, 65.7, 66.0$ ppm. ^1H NMR (400MHz, D_2O , 25°C, TMS): $\delta = 0.80$ (t, $J = 6.8$ Hz, 3H), 1.21-1.28 (m, 2H), 1.70 (m, 2H), 3.09 (s, 6H), 3.34 (m, 2H), 3.44 (m, 2H), 3.94 (m, 2H) ppm. ^{13}C NMR (100MHz, D_2O , 25°C, TMS): $\delta = 13.87, 22.45-32.03, 51.55, 55.41, 65.04, 65.7, 66$ ppm.

2.3.2. General procedure for preparation of *N,N*-dimethyl-*N*-cetyl-*N*-(2-hydroxyethyl) ammonium X salts with $X = \text{F}, \text{I}, \text{HCO}_3^-, \text{BF}_4^-$

The surfactants HEA16X were prepared by ion exchange reactions in acetone or methanol with HEA16Cl and the appropriate alkaline (KF, KI, NaHCO_3 , NaBF_4) salt in a molar ratio of 1:1 under refluxing conditions. After reaction, the resulting mixture was filtered through celite and the solvent was removed to afford a white solid (exception to HEA16I that has a light yellow color) that did not need further purification before using for gold colloidal suspension synthesis.

N,N-dimethyl-*N*-cetyl-*N*-(2-hydroxyethyl)ammonium fluoride - HEA16F: yield 97%, m.p.: 75-80°C, ^1H NMR (400MHz, CDCl_3 , 25°C, TMS): $\delta = 0.81$ (t, $J = 7.1$ Hz, 3H), 1.18 (m, 24H), 1.27 (m, 2H), 1.67 (m, 2H), 3.30 (s, 6H), 3.48 (m, 2H), 3.48 (m, 2H), 3.65 (m, 2H), 4.03 (m, 2H), 4.61 (m, 1H) ppm. ^{13}C NMR (100MHz, CDCl_3 , 25°C, TMS): $\delta = 13.85, 22.35-31.97, 51.48, 55.35, 65.06$ ppm. RMN F^{19} (D_2O), $\delta = 122.23$ ppm.

N,N- dimethyl-*N*-cetyl-*N*-(2-hydroxyethyl)ammonium iodide - HEA16I: yield 84%, m.p.: 176-178 °C, ¹H NMR (400MHz, CDCl₃, 25°C, TMS): δ=0.85 (t, *J*=7.1 Hz, 3H), 1.23 (m, 24H), 1.34 (m, 2H), 1.75 (m, 2H), 3.36 (s, 6H), 3.55 (m, 2H), 3.76 (m, 2H), 4.16 (m, 2H) ppm. ¹³C NMR (100MHz, CDCl₃, 25°C, TMS): 14.2, 22.7 – 31.09, 52.5, 55.8, 65.6, 66.4 ppm.

N,N- dimethyl-*N*-cetyl-*N*-(2-hydroxyethyl)ammonium hydrogen carbonate - HEA16HCO₃: Yield 60%, m.p.: 210-215°C. ¹H NMR (400MHz, CDCl₃, 25°C, TMS): δ= 0.81 (t, *J*=7.1 Hz, 3H), 1.18 (m, 24H), 1.27 (m, 2H), 1.67 (m, 2H), 3.30 (s, 6H), 3.48 (m, 2H), 3.65 (m, 2H), 4.03 (m, 2H), 4.61 (m, 1H) ppm. ¹³C NMR (100MHz, CDCl₃, 25°C, TMS): δ= 14.09, 22.7 – 31.09, 52.0, 55.9, 65.7, 66.0 ppm

N,N- dimethyl-*N*-cetyl-*N*-(2-hydroxyethyl)ammonium tetrafluoroborate - HEA16BF₄: yield 94%, m.p.: 114°C. ¹H NMR (400MHz, CDCl₃, 25°C, TMS): δ= 0.81 (t, *J*=7.1 Hz, 3H), 1.18 (m, 24H), 1.27 (m, 2H), 1.67 (m, 2H), 3.30 (s, 6H), 3.48 (m, 2H), 3.65 (m, 2H), 4.03 (m, 2H), 4.61 (m, 1H) ppm. ¹³C NMR (100MHz, CDCl₃, 25°C, TMS): δ= 14.09, 22.7 – 31.09, 52.0, 55.9, 65.7, 66.0 ppm

2.3.3. Synthesis of surfactants with different length of the chain alkyl

Bromododecane (for HEA12Br) or Bromooctadecane (for HEA18Br) (1.2 eq.) and *N,N*-dimethylethanolamine (1 eq.) were refluxed in absolute ethanol for 48h. Then, the solvent was removed under reduced pressure. The obtained solid was washed twice with diethyl ether afford a white solid.

N,N- dimethyl-*N*-octadecyl-*N*-(2-hydroxybutyl)ammonium Bromide - HEA18Br: yield 95%, ¹H NMR (400MHz, CDCl₃, 25°C, TMS): δ = 0.86 (t, *J* = 7 Hz, 3H), 1.23 (m, 28H), 1.33 (m, 2H), 1.73 (m, 2H), 3.24 (m, 2H), 3.30 (s, 6H), 3.54 (m, 2H); 3.97 (m, 2H); 5.0 (t, *J* = 5.3 Hz, 1H). ¹³C NMR (100MHz, CDCl₃, 25°C, TMS): δ = 14.1, 22.8 - 31.9, 52.5, 64.8, 65.0, 67.7 ppm.

N,N- dimethyl-*N*-dodecyl-*N*-(hydroxyethyl)ammoniumBromide - HEA12Br: yield 95%. ¹H NMR (400MHz, CDCl₃, 25°C, TMS): δ = 0.86 (t, *J* = 7 Hz, 3H), 1.29 (m, 20H), 1.33 (m, 2H), 1.73 (m, 2H), 3.26 (m, 2H), 3.31 (s, 6H), 3.43 (m, 2H); 3.97 (m, 2H); 5.0 (t, *J* = 5.3 Hz, 1H) ¹³C NMR (100MHz, CDCl₃, 25°C, TMS): δ = 14.1, 22.8 - 31.9, 52.5, 64.8, 65.0, 67.7 ppm.

2.3.4. Synthesis of surfactants with different polar head group

Bromohexadecane or Bromododecane (1.2 eq.), *N,N*-dimethylpropanolamine (for HPA16Br), *N,N*-dimethylbutanolamine (for HBA16Br), 1-dimethylamino-2-propanol(for H2PA16Br), 3-dimethylamino-1,2-propanediol (for H1,2PA16Br), 2-dimethylaminoethanol (for HDA16Br), *N*-methyldiethanolamine (for HDEA16Br), *N*-diethanolamine (for DHA16Br), (for 1*R*,2*S*-*N*-methylephedrine (for *N*-MeEph12Br), *N,N*-dimethylethylamine (for EA16Br), *N,N*- dimethylhexadecylamine (for PA16Br), *N,N*-dimethylbutylamine (for BA16Br)(all of them 1eq.) were refluxed in absolute ethanol for 48h. Then, the solvent was removed under reduced pressure. The obtained solid was washed twice with diethyl ether (ethylacetate for *N*-MeEph12Br) afford a white solid.

N,N- dimethyl-*N*-cetyl-*N*-(2-hydroxypropyl)ammoniumBromide - HPA16Br: yield 92%, ¹H NMR (400MHz, CDCl₃, 25°C, TMS): δ= 0.80 (t, *J*=7 Hz, 3H, H-16'), 1.22 (m, 24H, H-14'-H-3'), 1.29 (m, 2H- H-15'), 1.70 (m, 2H, H-2'), 1.94 (m, 2H), 3.06 (s, 6H), 3.30 (m,2H), 3.34 (m, 2H, H-1'), 3.61 (m, 2H); 3.62 (m, 2H); 4.71 (t, *J*=5.3 Hz, 1H). ¹³C NMR (100MHz, CDCl₃, 25°C, TMS): δ= 14.0, 22.6- 32.5, 47.5, 61.5, 62.0, 66.0 ppm

N,N- dimethyl-*N*-cetyl-*N*-(2-hydroxybutyl)ammoniumBromide -HBA16Br: Yield 80%, ¹H NMR (400MHz, CDCl₃, 25°C, TMS): δ= 0.81 (t, *J* = 7 Hz, 3H, H-16'), 1.22 (m, 24H, H-14' - H-3'), 1.31 (m, 2H - H-15'), 1.48 (m, 2H), 1.67 (m, 2H, H-2'), 1.75 (m, 2H), 3.0 (s, 6H), 3.30 (m, 2H, H'1), 3.55 (m, 2H); 3.60 (m, 2H); 5.14 (t, *J* = 5.3 Hz, 1H). ¹³C NMR (100MHz, CDCl₃, 25°C, TMS): δ= 14.0, 19.4, 23.1- 32.5, 47.5, 63.0, 66.0 ppm.

N,N- dimethyl-*N*-cetyl-*N*-(2-hydroxypropyl)ammoniumBromide -H2PA16Br: Yield 90%. ¹H NMR (400MHz, CDCl₃, 25°C, TMS): δ= 0.96 (t, *J*=7 Hz, 3H, H-16'), 1.29 (m, 24H,

H-14'-H-3'), 1.32 (m, 2H- H-15'), 1.39 (m, 2H, H-2'), 2.38 (m, 2H), 2.27 (s, 6H), 2.63 (m, 2H), 2.36 (m, 2H, H-1'), 3.61 (m, 2H); 4.0 (t, $J=5.3$ Hz, 1H). ^{13}C NMR (100MHz, CDCl_3 , 25°C, TMS): $\delta= 14.1, 22.8- 31.9, 54.1, 62.6, 63.8, 68.0$ ppm

N,N- dimethyl-*N*-cetyl-*N*-(1,2-hydroxypropyl)ammoniumBromide – H1,2PA16Br: Yield 90%, ^1H NMR (400MHz, CDCl_3 , 25 °C, TMS): $\delta= 0.85$ (t, $J = 7$ Hz, 3H, H-16'), 1.29 (m, 24H, H-14'-H-3'), 1.31 (m, 2H- H-15'), 1.73 (m, 2H, H-2'), 3.24 (m, 2H), 3.30 (s, 6H), 5.32 (m, 1H), 3.24 (m, 2H, H-1'), 4.10 (m, 1H); 1.21 (m, 3H); 2.0 (t, $J=5.3$ Hz, 1H). ^{13}C NMR (100MHz, CDCl_3 , 25 °C, TMS): $\delta= 14.1, 22.8- 31.9, 46.6, 58.9, 66.8, 118.8$ ppm.

N,N- dimethyl-*N*-cetyl-*N*-ethylammoniumBromide- EA16Br: Yield 92%, ^1H NMR (400MHz, CDCl_3 , 25°C, TMS): $\delta= 0.96$ (t, $J = 6.7$ Hz, 3H, H-16'), 1.30 (m, 24H, H-14'-H-3'), 1.33 (m, 2H- H-15'), 2.22 (m, 2H, H-2'), 2.20 (m, 2H), 2.27 (s, 6H), 2.40 (m, 2H, H-1'); ^{13}C NMR (100MHz, CDCl_3 , 25°C, TMS): $\delta= 14.1, 22.8 - 31.9, 53.0, 62.5$ ppm

N,N- dimethyl-*N*-cetyl-*N*-propylammoniumBromide -PA16Br: Yield 92%, ^1H NMR (400MHz, CDCl_3 , 25°C, TMS): $\delta= 0.90$ (t, $J = 6.7$ Hz, 3H, H-16'), 1.22 (m, 24H, H-14'-H-3'), 1.30 (m, 2H- H-15'), 1.70 (m, 2H, H-2'), 2.21 (m, 2H), 3.05 (s, 6H), 3.20 (m, 2H), 3.24 (m, 2H, H-1'); ^{13}C NMR (100MHz, CDCl_3 , 25°C, TMS): $\delta= 14.0, 23.1- 32.5, 66.0, 68.0$ ppm.

N,N- dimethyl-*N*-cetyl-*N*-butylammoniumBromide -BA16Br: Yield 92%, ^1H NMR (400MHz, CDCl_3 , 25°C, TMS): $\delta= 0.96$ (t, $J = 6.7$ Hz, 3H, H-16'), 1.29 (m, 24H, H-14'-H-3'), 1.33 (m, 2H- H-15'), 1.39 (m, 2H, H-2'), 2.36 (m, 2H), 2.27 (s, 6H), 2.36 (m, 2H), 1.39 (m, 2H, H-1'); ^{13}C NMR (100MHz, CDCl_3 , 25°C, TMS): $\delta= 14.0, 22.8 - 31.9, 62.3, 53.8$ ppm.

N,N- diethyl-*N*-cetyl-*N*-(2-hydroxyethyl)ammoniumBromide -HDA16Br: Yield 92%, ^1H NMR (400MHz, CDCl_3 , 25 °C, TMS): $\delta= 0.96$ (t, $J = 7$ Hz, 3H, H-16'), 1.29 (m, 24H, H-14'-H-3'), 1.33 (m, 2H- H-15'), 1.39 (m, 2H, H-2'), 2.36 (m, 2H), 2.40 (m, 4H), 2.0 (s,

6H), 2.42 (m, 2H), 2.55 (m, 2H, H-1'), 3.63 (m, 2H); 4.0 (t, $J=5.3$ Hz, 1H). ^{13}C NMR (100MHz, CDCl_3 , 25°C, TMS): $\delta= 14.1, 22.8- 31.9, 50.4, 57.3, 61.6, 58.0$ ppm

N,N- dimethyl-N-cetyl-N-methylephidrine Bromide - N-MeEPh12Br: yield 75%, m.p. 96°C, ^1H NMR (400MHz, CDCl_3 , 25°C, TMS): $\delta= 0.87$ (t, $J=6.8$ Hz, 3H), 1.16 (d, $J=6.4$ Hz, 3H), 1.24-1.32 (m, 16H), 1.62-1.77 (m, 2H), 2.87 (s, 1H), 3.29 (s, 3H), 3.45 (s, 3H), 3.49 (m, 1H), 3.61 (q, $J=6.4$ Hz, 1H), 3.82 (td, 1H); 5.76 (d, 1H), 7.23-7.48 (m, 5H) ppm. ^{13}C NMR (100MHz, CDCl_3 , 25°C, TMS): $\delta= 7.3, 14.1, 22.7, 22.9- 31.9, 49.5, 49.7, 64.2, 67.8, 72.8, 125.9, 127.6, 128.5, 141.1$ ppm

N-methyl-N-cetyl-N,N -(DiHydroxyEthyl)ammonium Bromide - DHEA16Br: Yield 71%, ^1H NMR (400MHz, CDCl_3 , 25°C, TMS): $\delta= 0.96$ (t, $J =7$ Hz, 3H, H-16'), 1.29 (m, 24H, H-14'-H-3'), 1.33 (m, 2H- H-15'), 1.73 (m, 2H, H-2'), 3.30 (s, 3H), 3.24 (m, 2H, H-1'), 3.43 (t, $J=5.3$ Hz, 1H), 2.0 (m, 2H);). ^{13}C NMR (100MHz, CDCl_3 , 25°C, TMS): $\delta= 14.1, 22.8- 31.9, 50.3, 62.6, 65.5, 65.3$ ppm.

N-cetyl-N,N -(DiHydroxyEthyl)ammonium Bromide - DHA16Br: Yield 80%, ^1H NMR (400MHz, CDCl_3 , 25°C, TMS): $\delta= 0.96$ (t, $J =7$ Hz, 3H, H-16'), 1.29 (m, 24H, H-14'-H-3'), 1.33 (m, 2H- H-15'), 1.73 (m, 2H, H-2'), 3.24 (m, 2H, H-1'), 3.43 (t, $J=5.3$ Hz, 1H), 2.0 (m, 2H);). ^{13}C NMR (100MHz, CDCl_3 , 25°C, TMS): $\delta= 14.1, 22.8- 31.9, 50.3, 62.6, 65.5, 65.3$ ppm.

2.3.5. N-cetyl-N,N,N -(TrisHydroxyEthyl)ammonium Bromide - THEA16Br

In a two necked flask, hexadecylamine (16.7g, 62 mmol) and bromoethanol (19.5g, 230 mmol) were heated to reflux. Then, NaOH (8.16g, 204 mmol) in distilled water (75mL) was added dropwise. After 24h at reflux, the reaction mixture was cooled down and extracted with chloroform (3x50 mL). The organic phase was dried on MgSO_4 and chloroform was removed. The residue was recrystallized from Et-OH-EtOAc to give the final product as a white powder with a moderate yield (44%), m.p.: 94-96°C. ^1H NMR (400MHz, DMSO-d_6 , 25°C, TMS) δ /ppm: 0.84 (t, $J =7$ Hz, 3H, H-16'), 1.17-1.32 (m, 26H, H-15'-H-3'), 1.66-1.68(m, 2H- H-2'), 3.38-3.40 (m, 2H, H-1'), 3.48-3.50 (m, 6H, H_2),

3.73-3.79(m, 6H, H-1), 5.44 (t, $J=6$ Hz, 3H, OH). ^{13}C NMR (100MHz, DMSO- d_6 , 25°C, TMS): $\delta=$ 13.91, 21.32-31.25, 54.51, 60.13, 6.61 ppm.

2.3.6. *N,N*- dimethyl-*N*-cetyl-*N* -Oxide Amine (NOx16)

In a 100 mL flask fitted with a condenser and a dropping funnel, are added 2.5 mL (7.5 mmol) of dimethylalkylamine in 10 mL of methanol. The mixture is refluxed for 1h and then 1.15 mL (11.25 mmol, 1.5 equiv.) of 30% hydrogen peroxide are added dropwise. The mixture is stirred and heated to 70 ° C with vigorous stirring for 15 h. The progress of the reaction is followed by TLC. The solvent is then evaporated and the product was frozen, dried for 24 h. The final product is a white powder with a 97% yield. ^1H NMR (400 MHz, CDCl_3 , 25 ° C, TMS): $\delta =$ 0.81 (t, 3H, H16 '); 1.19 (m, 24H, H15'-H4'); 1.27 (m, 2H, H3 '); 1.79 (m, 2H, H2 '); 3.13 (s, 6H, Me); 3.20 (m, 2H, H1 '); ^{13}C NMR (100 MHz, CDCl_3 , 25 ° C, TMS): $\delta =$ 14.09, 22.66 - 31.90, 58.21, 71.66 ppm. TLC (eluent: ethyl acetate) $R_f = 0.74$.

2.4. Synthesis of gold nanoparticles in aqueous system

To prepare AuNRs by the seed-mediated method, the process consists on preparing two solutions: i) the seed solution, and ii) the growth solution.

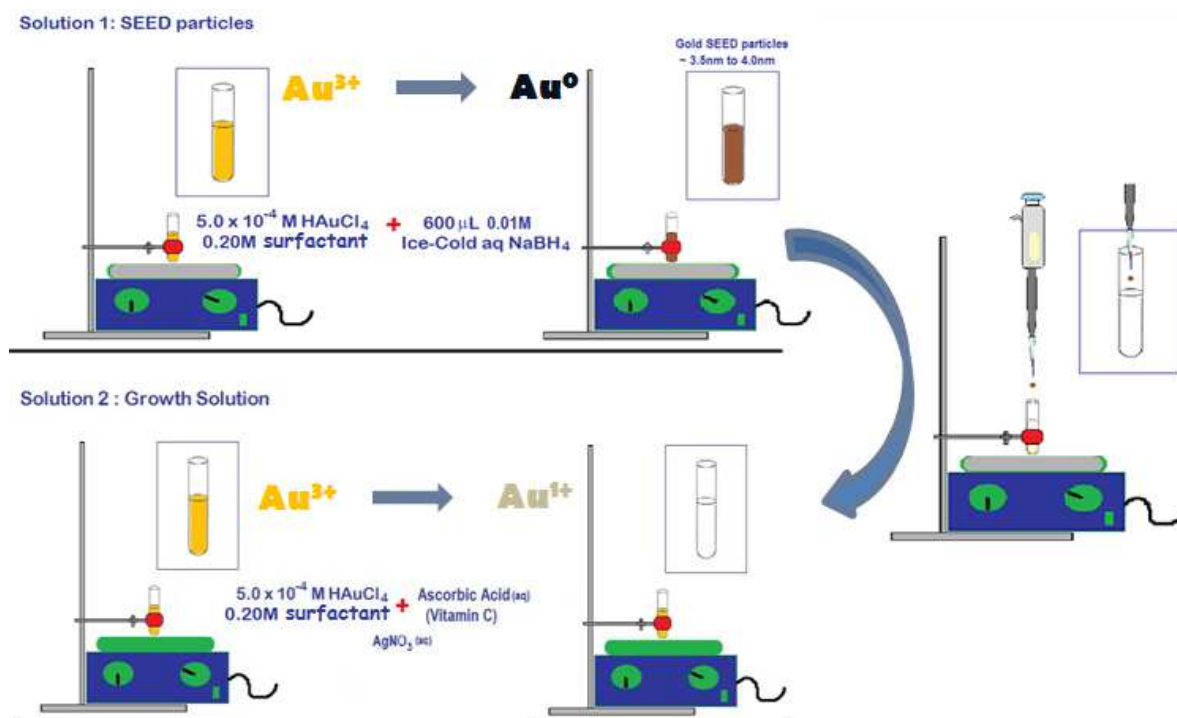
Seed solution: In a 25 mL flask, a Au^{3+} solution (0.1 mL, 1% w/v) was added to an aqueous solution of surfactant (7.4 mL, $0.2\text{mol}\cdot\text{L}^{-1}$). The solution color changed to dark or light yellow, depending on the surfactant. Then, an ice cold solution of sodium borohydride (5×10^{-1} mmol, 0.6 mL, $0.01\text{mol}\cdot\text{L}^{-1}$) was added. The solution color immediately turned to brown. The system remained under stirring for 2 min. and kept at room temperature for at least 2 h.

Growth Solution: In a 25 mL-flask, a Au^{3+} solution (0.2 mL, 1% w/v) was added to a surfactant solution (7.3 mL, $0.2\text{mol}\cdot\text{L}^{-1}$). The solution color changed to dark or light yellow, depending on the surfactant in question. Then, silver nitrate (0.150 mL, $0.40\text{mmol}\cdot\text{L}^{-1}$) was added under stirring, followed by ascorbic acid (and 0.070 mL, $0.0788\text{mol}\cdot\text{L}^{-1}$). The system turned to colorless, proving the reduction of Au^{3+} to Au^+ .

Growth process of AuNRs: 0.060 mL of seed particles was added to the growth solution freshly prepared. The system remained under stirring for just 10 s. Then it is allowed to

stand for 4 h prior to characterization to ensure the system stability. The solution darkens slowly between 10 to 15 min. to a dark brown colour. The solution is stocked in a flask under the absence of light.

Figure 20 - Illustration of gold nanorods preparation via seed mediated method.



Results and Discussions

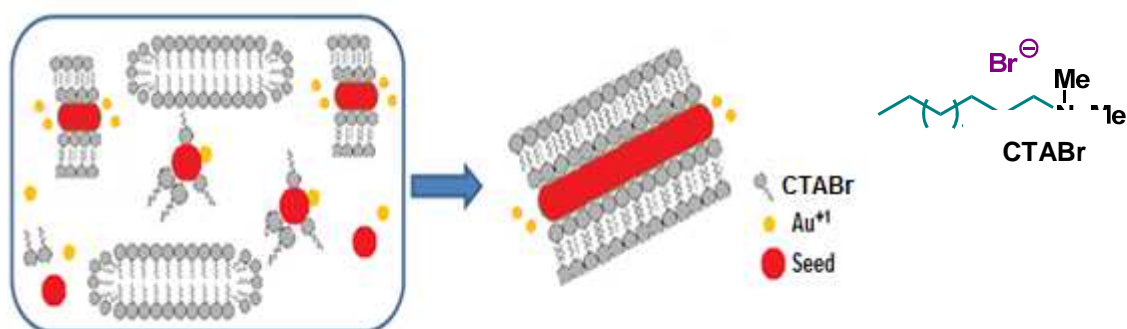
3.0. Introduction

As indicated on Chapter 1, Cetyltrimethylammonium bromide (CTABr) is the growth-driving agent classical choice for the syntheses of gold nanorods (AuNRs). This ammonium salt provides a well-controlled particle growth process. Murphy's group proposed that the CTABr ion-pair site binds better to the {100} faces that exist along the length of the rods than to the {111} gold faces that are at the ends of the rods.^{1,2} This interaction blocks the long axis crystal faces {100} and/or {110} through the surfactant bilayer structure and thus, promoting metal growth on the short-axis faces {111} to produce AuNRs.^{3,4} Also, it was observed, by SAXS (Small Angle X-ray Scattering) and optical spectroscopy, that the growth kinetic of AuNRs has an initial growth rate at the end of the AuNRs 5 times higher than that one on the side, but with time, both rates decrease exponentially.^{2,5}

On Figure 21 we can see a scheme illustrating the generation of AuNRs from seed particles, in the presence of CTABr, since the moment when the seed particles are added in the growth solution.

Recently, a theoretical study in Dynamic Molecular made by Meena et al. reported the simulation of the CTABr interaction on crystal surfaces of AuNRs. The innovative aspect is the inclusion of the role of surfactants, which are explicitly modeled. They found that on all facets of the AuNR, namely {110}, {100} and {111}, CTABr forms a layer of distorted cylindrical micelles where channels among the micelles provide the access of the ions to the surface.⁶ Moreover, they observed that channels among the micelles on the {111} facets (i.e. on the tips of the rods) present larger channels. This can explain the origin of the anisotropic growth of the particles.

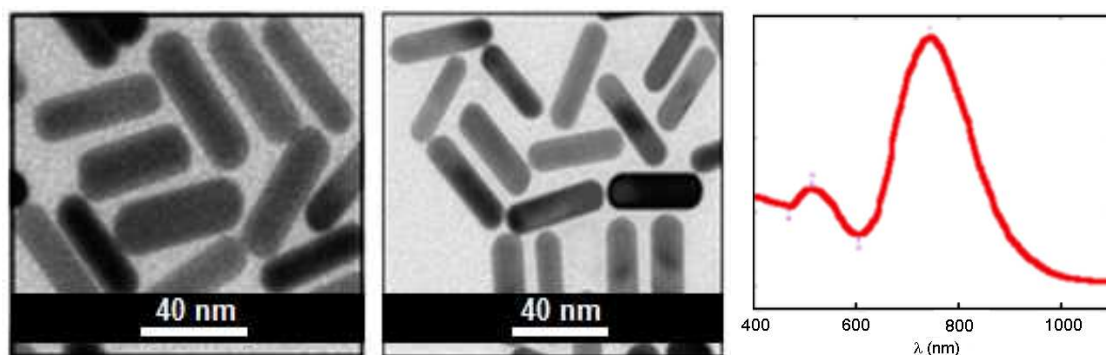
Figure 21 -Scheme illustrating the idealized formation of AuNRs from seed particles.



In our first set of experiments, we prepared AuNRs in the presence of CTABr in order to confirm and establish our synthetic conditions, and lately, we have compared with our experiments, using our set of surfactants.³

We can observe the typical Uv-vis spectrum of AuNRs obtained in the presence of CTABr (Figure22a). The presence of two typical absorption bands suggests a rod-like morphology in the colloidal dispersion. The Transmission Electron Microscopy (TEM) images confirm the formation of AuNRs (Figure 22b) in which AuNRs with sizes of 40.8 x 12.4 nm (\pm 4.8 x 2.3 nm), aspect ratio of 3.3, and 90% of selectivity were observed.

Figure 22. -AuNRs obtained in presence of CTABr, TEM images and Uv-vis spectrum.

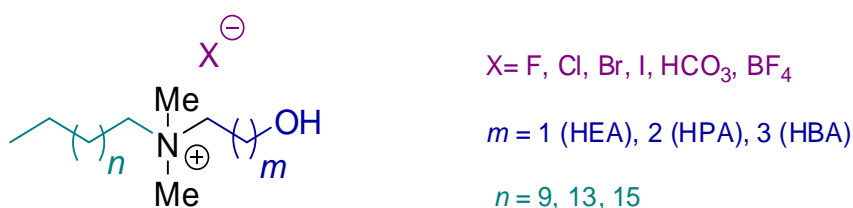


Some studies have been published with the aim to tune the aspect ratio of AuNRs, adding or modifying some synthetic parameters such as the amount of the driving agent,^{7,3} the size of the seeds used,⁸ the effect of additives⁹ etc. According to previous publications by Murphy et al., the nature of the growth-driving agents or even a mixture of these agents is essential in the AuNRs elongation.¹⁰ Thus, several studies have been done in order to improve reaction

yields and selectivity, but no significant improvements have been really carried out. To our knowledge, only the cetylpyridinium chloride (CPyCl), possessing a larger and more anisotropic head group, has been proposed as a potential growth-driving agent to produce AuNRs, but multi-shaped nanoparticles such as nanospheres, triangles, pentagons, were observed.¹¹ Also, binary mixtures such as CTABr/BDACl (benzyltrimethyl ammonium chloride),¹² and CTABr/OTABr (octyltrimethylammonium bromide),¹³ were tested, but only modest improvements have been obtained.

Considering this lack of options, we envisage new growth-driving agents in order to attempt anisotropic gold nanoparticles (AuNPs), more precisely gold nanorods (AuNRs). Thus, herein we show and discuss the results until now obtained. Indeed, we have developed a real alternative preparation of size and form-controlled AuNPs by the seed mediated growth in aqueous media with high yields and selectivities, using an original library of easily prepared *N,N*-dimethyl-*N*-cetyl-*N*-(hydroxyalkyl)ammonium salts (HAAX) as growth-driving agents (Figure 23), instead of the usual CTABr. These growth-driving agents, bearing hydroxyl groups, possess high water-solubility, as well as a good stability in a large range of pH. As already mentioned, they are easily synthesized in an one-step, with high-yielding, by quaternarization of the amino alcohol with a long chain bromoalkane that can undergo anionic metathesis to attain different counter-ions.

Figure 23 - Structure of surfactants HAAX.



3.1. Influence of counter-ions

Several research groups have demonstrated that the growth process of the AuNRs is governed by various chemical mechanisms such as halide adlayers and/or surfactant bilayer structure. Based on a series of control experiments by

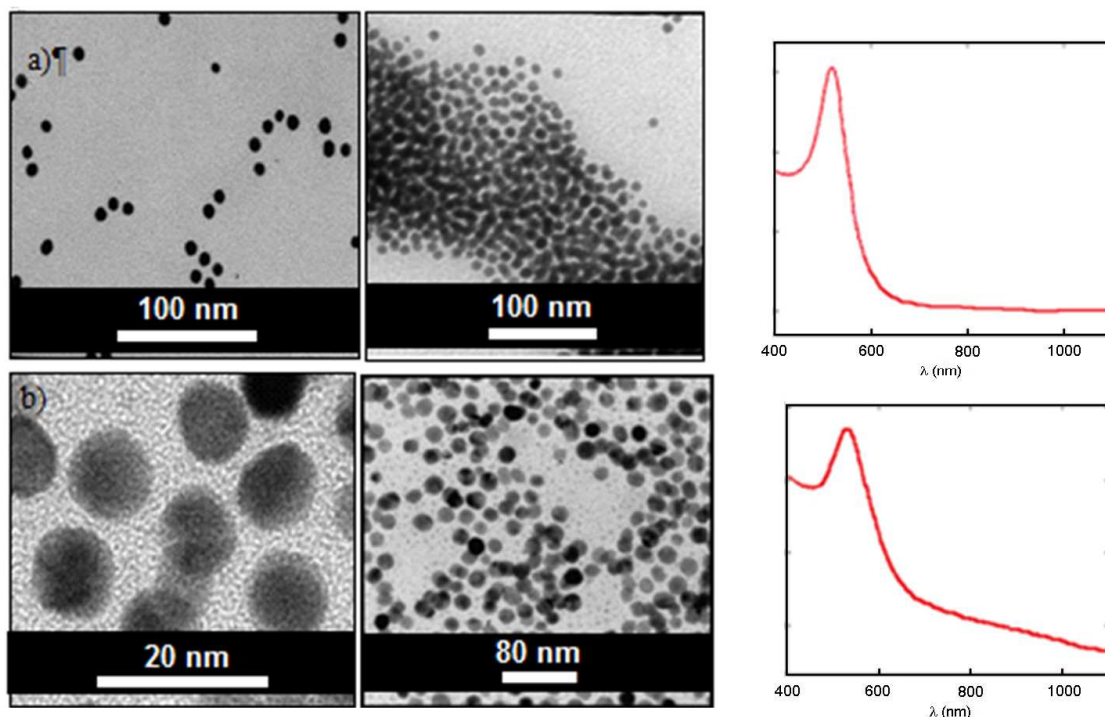
salt addition in the systems, it is now accepted that the presence of halide ions involves a mechanism of adsorption onto low indexed gold surfaces, i.e., Au {111}, Au {110}, and Au {100}, except for the fluoride ion.^{14,15}

On this context, we first evaluated the series of surfactant named HEA16X (X= F, Cl, Br, I, HCO₃, BF₄) as growth-driving agents in the production of AuNPs. The main aspect evaluated in this study was the influence of the counter-ion in terms of yields, size and shape control of the AuNPs produced.

Firstly, HEA16BF₄ could not be employ as driving agent due to its very low solubility in water. On the other hand, HEA16I displays just a poor solubility, i.e. this surfactant precipitates on concentrations required of our typical tests. Out of these two former surfactants, all display suitable solubility in water and could be tested.

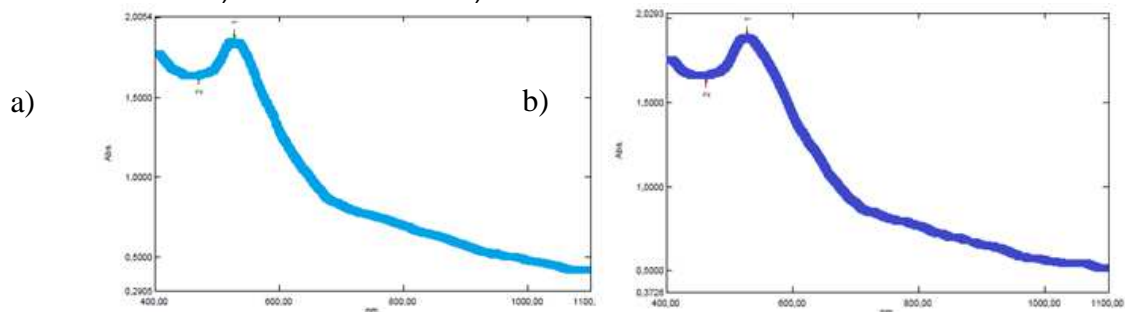
It is worth of mention that the first characterization to confirm AuNPs formation was Uv-vis absorption spectroscopy. And when gold colloidal solutions, containing HEA16F and HEA16Cl were analyzed by Uv-vis absorption spectra, they presented just one absorption band that strongly suggested the spherical AuNPs formed (Figure 24). This was confirmed by Transmission Electron Microscopy analysis. These results, indeed, were already expected since it is known that weak interactions of the fluoride and chloride ions on the gold surface.¹⁶ This trend was observed also under different concentration of the respective surfactants, but no changes in the Uv-vis spectra were observed, (Figure 25).

Figure 24 - Transmission Electron Microscopy images of gold nanoparticles obtained face to surfactants with different counter-ions. Spectrum of Uv-vis for each one. a) AuNP@HEA16F (8.5 nm) and b) AuNP@HEA16Cl (10nm).



The spherical AuNPs capped with HEA16F (8.5 nm) are smaller than those obtained by HEA16Cl (10 nm). Similar observations have already been reported by Kawasaki et al.,¹⁷ with spherical AuNPs obtained by hydrazine reduction in the presence of CTAF and CTACl, and it was attributed to a fast reduction rate, promoting the use of a fluoride salt.

Figure 25 -Uv-vis spectrum of AuNP@HEA16Cl in different levels of surfactant concentrations: a) 0.096 mol/L and b) 0.128 mol/L in final solution.



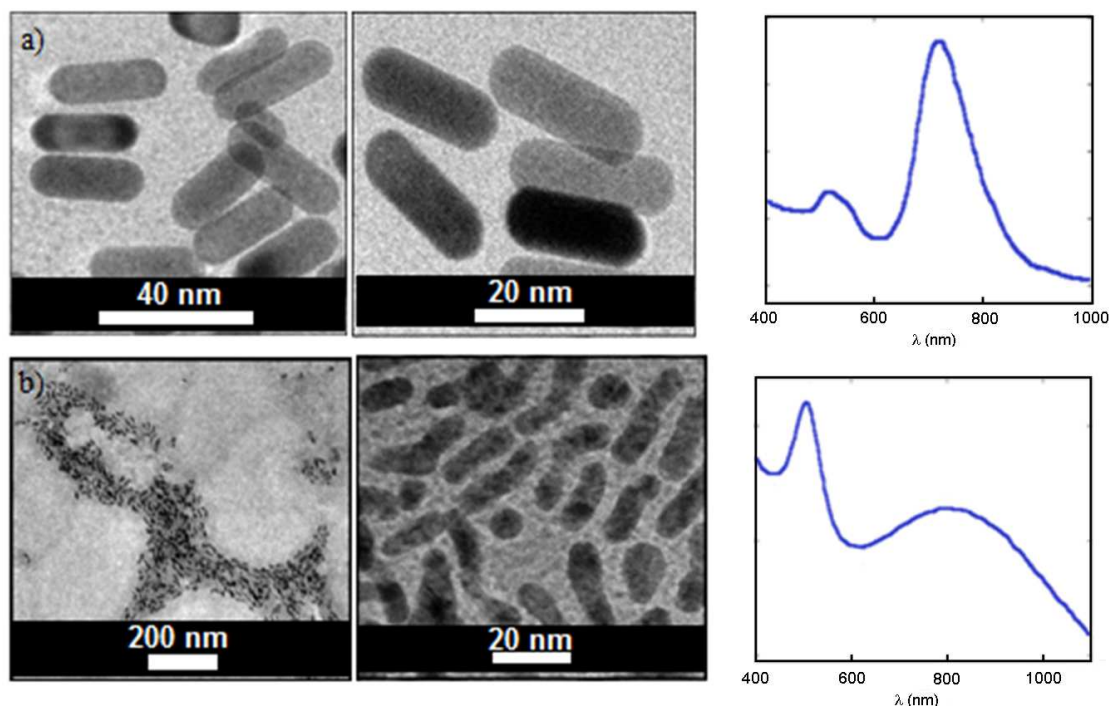
On the other hand, two absorption bands were observed in the Uv-vis absorption spectra of the colloids prepared in the presence of HEA16HCO₃ (Figure 26 b) and HEA16Br (Figure 26 a). These results suggested that rod-like

AuNPs were formed, which was lately confirmed by TEM analyses.

This anisotropic shape tendency, observed on the later AuNPs, is obtained due to the specific association of the ion-pair of the surfactant on the gold surface during the crystal growth.¹⁸ Similar tendency has already been observed with CTAX salts, and the interaction strength of the surfactant with the gold surface was associated to the measurements on the decrease of the frequent shift of Quartz Crystal Microbalance (QCM) in the following order: $\text{Br}^- > \text{Cl}^- > \text{F}^-$.^{17,18} Thus, the fluoride and chloride anions generate weak interactions within the particle surface, thus disfavoring the formation of a stable, compact double layer of the surfactant around the growing particle, while the high-affinity adsorption of Br^- onto Au surfaces produces anisotropic AuNRs. Moreover, in the synthetic method used, silver ions are also introduced into the reaction and thus, the influence of halides on crystal growth are more complex since the halides interact with the Au ions in solution and the Au surface, and also with the silver ions in solution. In fact, Mirkin et al.¹⁹ have found that in the presence of larger halides there is an increasing strength of the Au-halide interaction relative to the Ag-Au and Ag-halide interaction.

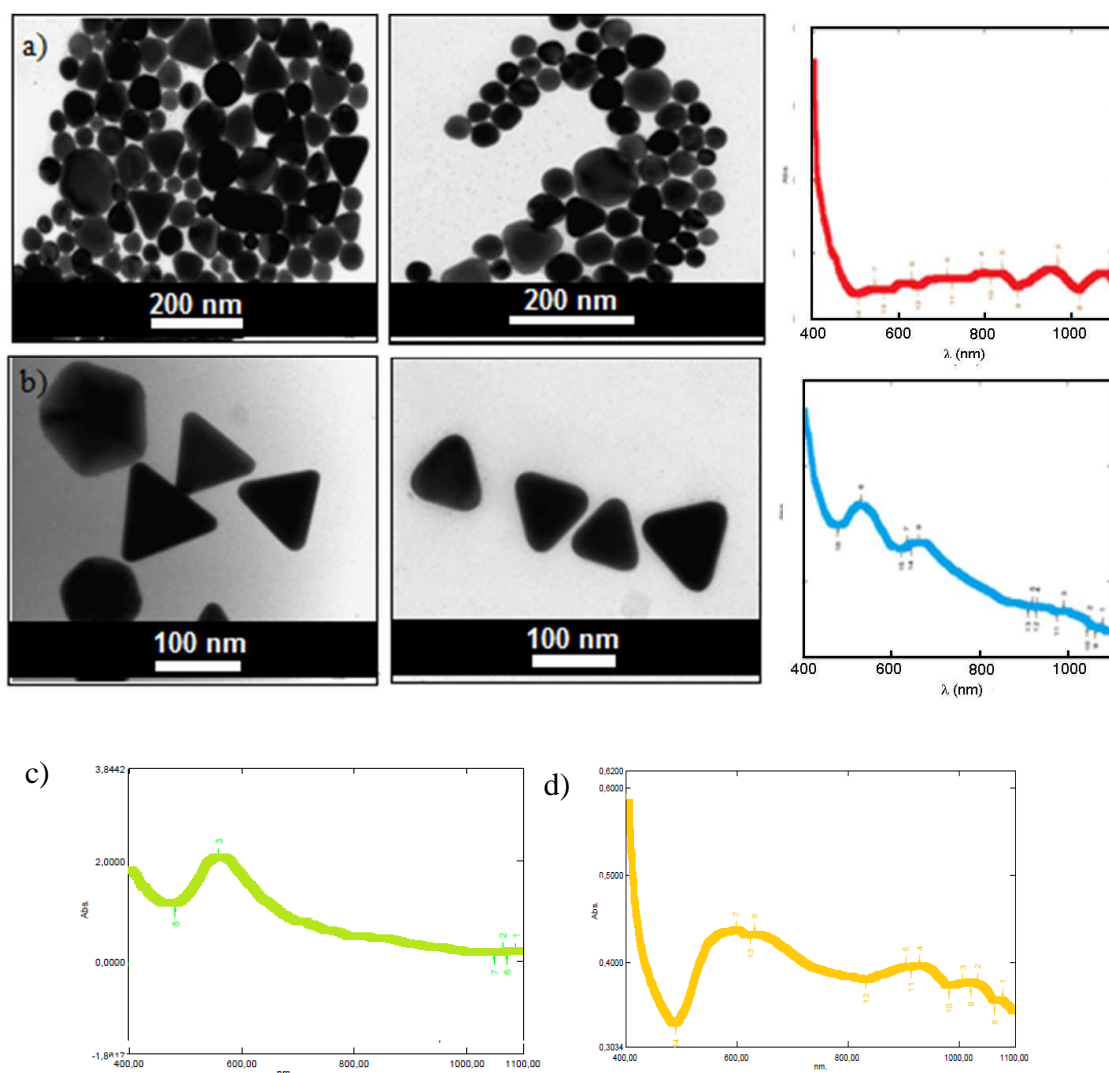
In the particular case of HEA16HCO_3 salt, we could presume that, by analogy to carboxylate anions or polycarboxylates such as citrate polyanions, the hydrogenocarbonate counter-ion provides an intermediate adsorption affinity at the growing AuNP surface, somehow between the bromide and the chloride ones. In fact, this must be the reason of the poor relationship between the two typical absorption bands observed when $X = \text{HCO}_3^-$, which could be attributed to a less efficient control of the NP growth. TEM images confirm this hypothesis, in which peanut pod shape AuNPs were formed (Figure 26 b).

Figure 26 - Transmission Electron Microscopy images of gold nanoparticles obtained face to surfactants with different counter-ions. UV-vis spectra for each one: a) AuNR@HEA16Br (30 x 10 nm; aspect ratio: 3.0) and b) AuNR@HCO₃ (29 x 7 nm; aspect ratio: 4.2).



Finally, the use of iodide counter-ion leads to the formation of well-formed nanoprisms (ca. 41%) and other morphologies (spheres, penta-twinned crystals), as shown by TEM analyses (Figure 27 b). This counter-ion is known to promote the formation of nanoprisms by preferential interaction on facets of the gold nanocrystal which are different of those observed when bromide one is used.²⁰ In this case, the binding energy follow this sequence: $\{111\} > \{110\} > \{100\}$ ^{21,22}, and in the case of bromide the sequence is $\{110\} \sim \{100\} > \{111\}$ ²³. This effect of iodide on the shape of AuNPs has already been described even in the presence of low concentrations of iodide impurities (< 3.0 ppm) in CTABr as growth-driving agent.^{24,25,26,27} Indeed, these gold triangular nanoprisms are promising materials with applications in optics and electronics,²⁸ and as biosensing platforms.²⁹

Figure 27 - Transmission Electron Microscopy images, histograms and Uv-vis spectra of gold nanoparticles obtained face an iodide counter-ion in presence of surfactant concentration: a) 0.016 mol/L; b) 0.0032 mol/L; c and d) 0.00064 and 0.0016 mol/L, respectively.



The uv-vis spectra of the colloids prepared with HEA16I do not present the characteristic absorption band of spherical or rod-like shaped AuNPs. Besides the strong interaction of iodide ions on the crystal faces, this surfactant displays a low degree of solubility in water, inducing the formation of large particles and instable colloidal systems. Thus, under low concentration, spheres and other different anisotropic NPs shapes have been obtained. In the figure 27a and 27b, we can see a system prepared with 4x less surfactant concentration (0.016 mol/L) than standard conditions, leading to 82.5% of spherical particles and 17.5% of anisotropic forms (prisms and others shapes). Under conditions of 2x less surfactant concentration (0.032 mol/L), 46.5% of

spherical particles and 48.5% of other anisotropic forms are obtained. The remaining percentage is related to agglomeration of particles. These percentage values of selectivity were based on the counts of nanoparticles from the TEM images, considering the form desired by all shapes formed. In the figure 27c and 27d, we can observe the Uv-vis spectra of the system in lower concentrations. The inhibition of the lateral facets increases in order $Cl < Br < I$ due to the different interaction forces between these counter ions and the gold surface.

Finally, with this study, it is possible to observe that the presence of bromide ions is crucial to obtain AuNPs with rod shapes. However, just the surfactant labeled HEA16Br was able to lead the formation of AuNRs with good control in terms of form, and yields. Table 4 summarizes these former results.

Table 4 - Characteristics of the gold nanorods obtained in presence of surfactants with different nature of counter ions.

Surfactant	Length (nm)	Width (nm)	Aspect Ratio	Selectivity
HEA16F	8.5 ± 1.0	8.5 ± 1.0	1.0	Spheres
HEA16Cl	10 ± 1.7	10 ± 1.7	1.0	Spheres
HEA16Br	30 ± 5.2	10 ± 1.3	3.0	Nanorods
HEA16I	100			Prisms
HEA16HCO ₃	29 ± 6.0	7 ± 2.3	4.1	Peanuts
CTABr	40.8 ± 4.8	12.4 ± 2.3	3.3	Nanorods
HEA16BF ₄	-	-	-	-

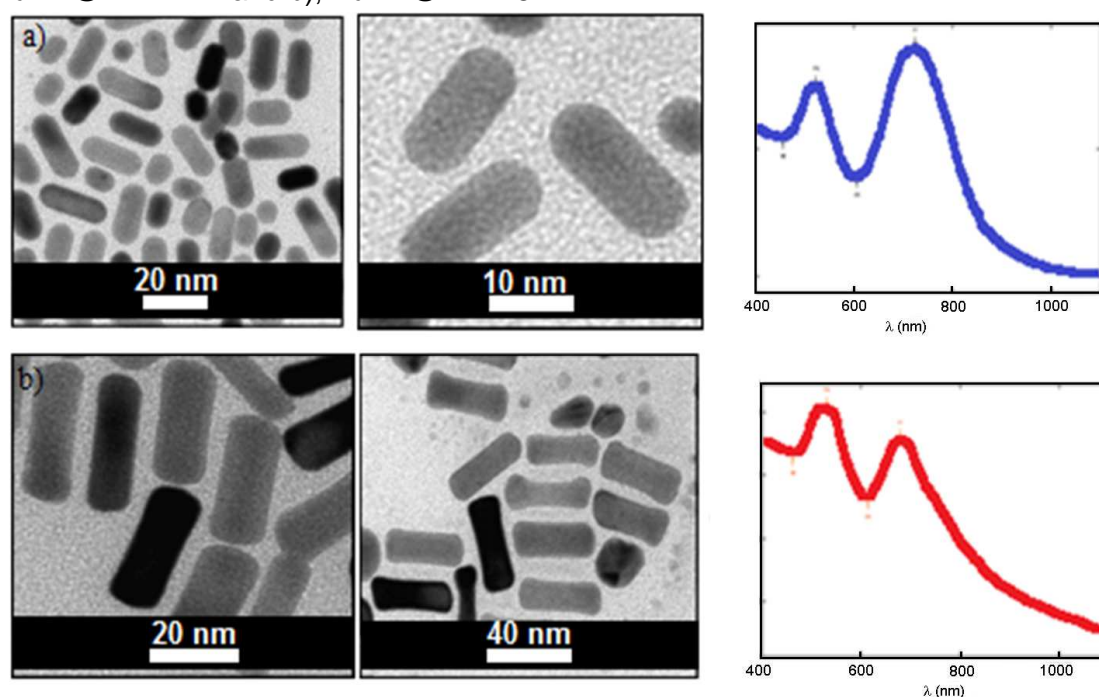
3.2. Influence of the alkyl chain length

In a second set of experiments, we investigated the influence of the length of the lipophilic chain (C12, C16, C18) on the particle morphology, considering a 2-hydroxyethylammonium (HEA) as polar head and bromide as counter-ion. Figure 28 shows the Uv-vis absorption spectra and TEM images of AuNPs as function of the different chain lengths for *N,N*-dimethyl-*N*-alkyl-*N*-(hydroxyethyl)ammonium bromide salts (HEA_nBr, with $n = 12, 16, 18$).

As already observed with various CTABr analogues, carrying different hydrocarbon chain lengths, the size of the lipophilic chain seems to have an important influence also in the AuNP morphology. For example, AuNRs with the

highest aspect ratios can be produced when CTABr analogues with longer lipophilic chains are employed as growth-driving agents. With a small lipophilic chain (HEA12Br), the growth control seems not very efficient, leading to a mixture of spherical particles (~ 10 nm) and low aspect ratio (2.4) AuNRs, with a selectivity of about 78% (Figure 28). In the case of HEA16Br, as previously discussed, the Uv-vis absorption spectrum of AuNPs presents two rod-shape typical absorption bands with a good correlation, suggesting the formation of high content of AuNRs (Figure 26). This result was confirmed by TEM analyses, showing rod-like particles with an aspect ratio of 3.0 (30 x 10 nm) with a high selectivity of 88%. Just for comparison, the aspect ratio of AuNRs obtained in the presence of CTABr, the aspect ratio was around 3.3 (40 x 12 nm), quite similar to values reported in the literature.³⁰

Figure 28 - Transmission Electron Microscopy images and Uv-vis spectra of the AuNRs obtained using growth-driving agents with different long alkyl chains. a) AuNR@HEA12Br and b), AuNR@HEA18Br.



In the case of the hydroxyalkylammonium bearing an alkyl chain with 18 carbons (HEA18Br), experimental difficulties were imposed, since its solubility is compromised due to the large hydrophobic chain. Nevertheless, under low concentration of the driving agent, dog-bone shape particles were produced (see Figure 28b). This must be probably owing to the low amount of capping

agents in the medium. It is also worth mentioning that without a hydroxyethyl substituent on nitrogen, only few anisotropic AuNPs are produced due to the lower water solubility of the surfactant in water. This trend has been already observed by Murphy et al., using CTABr analogues with different lipophilic chains.¹¹ Table 5 summarizes these last results.

Table 5 - Characteristics of the gold nanorods obtained in presence of surfactants with different length of alkyl chain

Surfactant	Length (nm)	Width (nm)	Aspect Ratio	Selectivity
HEA12Br	18.8 ± 3.4	8 ± 0.6	2.35	Nanorods
HEA16Br	30 ± 5.2	10 ± 1.3	3.0	Nanorods
HEA18Br	45 ± 11.6	14 ± 2.3	3.21	Nanorods

3.3. Influence of the length of the hydroxylated polar head

In a third set of experiments, we evaluated three surfactants with different length on the hydroxylated polar head (Figure 23), *i.e.* HEA16Br (HEA: HydroxyEthylAmmonium), HPA16Br (HPA: HydroxyPropylAmmonium) and HBA16Br (HBA: HydroxyButyl Ammonium) were investigated as growth-driving agents for the production of AuNRs at constant pH (3.5), according to the preparation conditions.

With this study, it was observed that whatever, the length of the hydroxylated polar head, the Uv-vis absorption spectra of AuNRs prepared with the HAA16Br series display two rod-shape typical absorption bands (Figure 29). This result was confirmed by TEM analyses, showing rod-like particles with various lengths and widths, providing modulated aspect ratios (Table 6), with very narrow size distribution. Higher values were achieved when the hydroxylated alkyl chain increased (3.0, 4.2, and 4.4 for HEA16Br, HPA16Br, and HBA16Br, respectively). For comparison, the aspect ratio of AuNRs obtained with CTABr by the same procedure is around 3.3 (40 x 12 nm), similar to the values reported by Murphy.³⁰ The selectivity was determined by the TEM image obtained from the crude solution without any centrifugation step, in opposition to the results usually reported in the literature. Due to this factor, our samples are more representative of the whole system (Table 6).

Figure 29 - Transmission Electron Microscopy images and Uv-vis spectrum of a) AuNR@HPA16Br, and b) AuNR@HBA16Br.

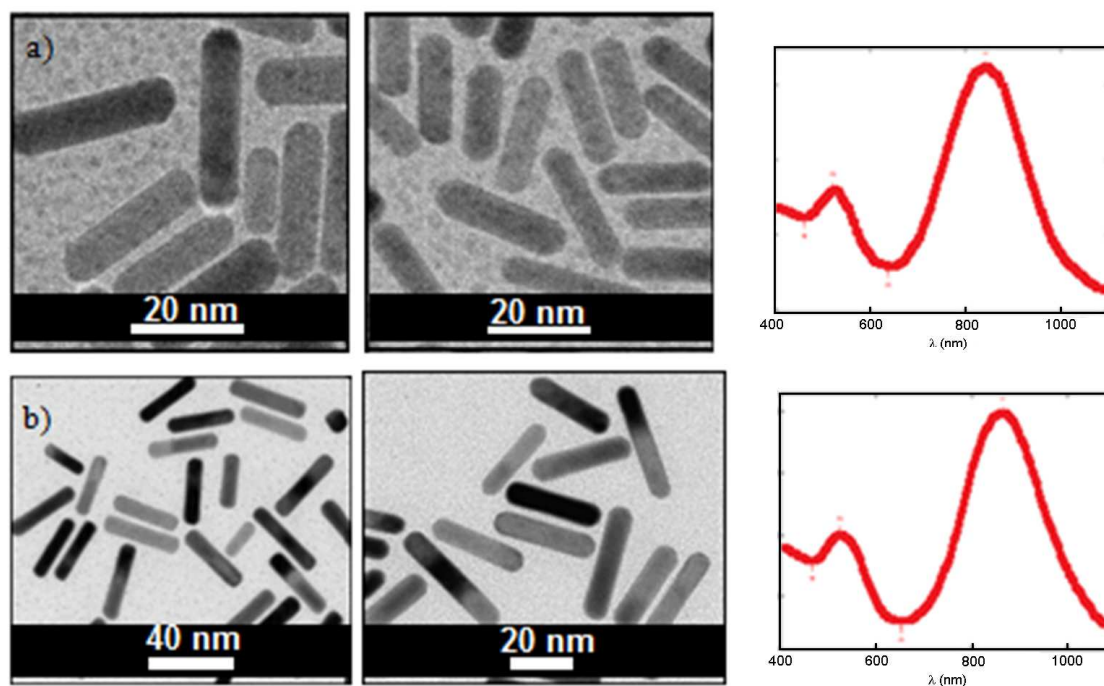


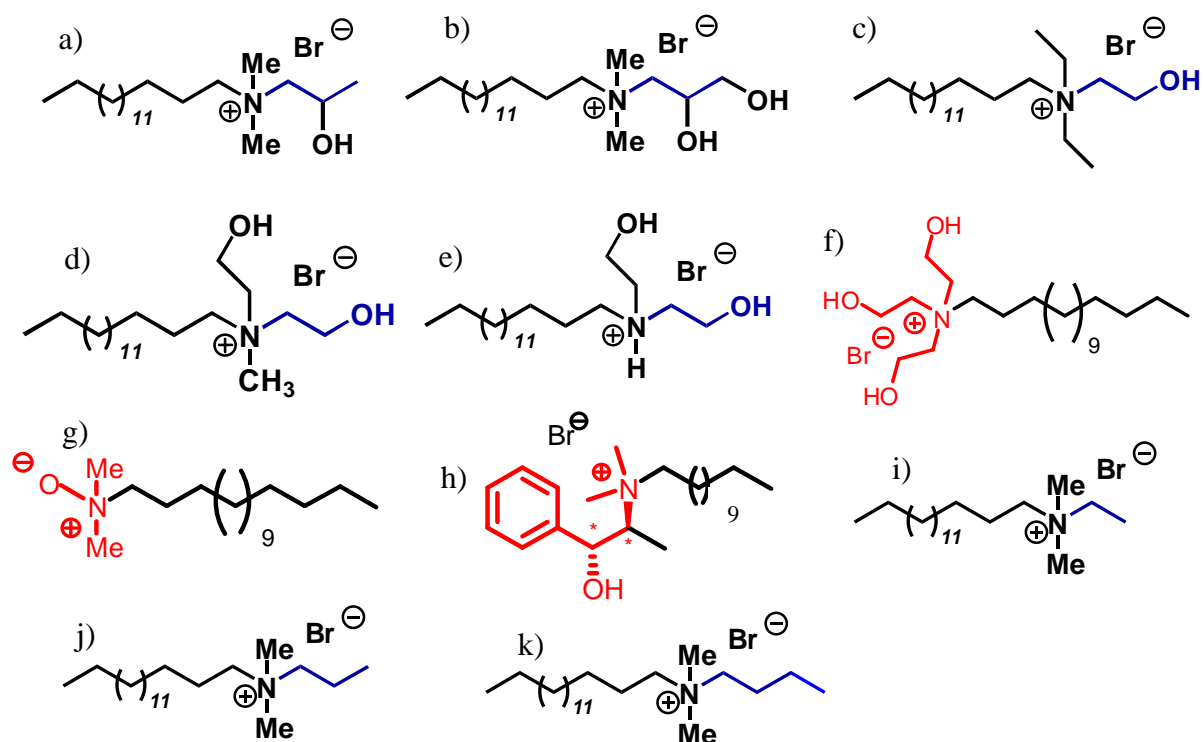
Table 6 - Characteristics of the gold nanorods obtained in presence of surfactants with different hydroxylated polar head

Surfactant	Length (nm)	Width (nm)	Aspect Ratio	Selectivity
HEA16Br	30 ± 5.2	10 ± 1.3	3.0	Nanorods
HPA16Br	30.2 ± 3.0	7.2 ± 0.8	4.2	Nanorods
HBA16Br	38.6 ± 6.4	8.8 ± 1.2	4.4	Nanorods

3.4. Influence of the polar head group

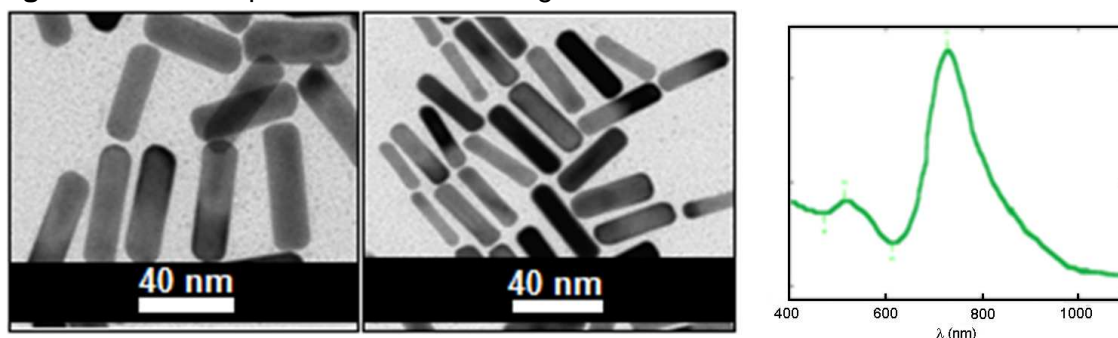
Surfactants with different polar head group were also prepared and tested as driving-growth agents (see Figure 30): H2PA16Br, H1,2PA16Br, HDA16Br, DHEA16Br, DHA16Br, THEA16Br, NOx16 (Nitrogen Oxide as polar head group), NMeEPh16Br (structure derived from N-methylephidrine as polar head group), EA16Br, PA16Br, and BA16Br.

Figure 30 - Chemical structures of the surfactants a) H2PA16Br, b) H1,2PA16Br, c) HDA16Br, d) DHEA16Br, e) DHA16Br, f) THEA16Br, g) NOx16, h) NMeEPh12Br, i) EA16Br, j) PA16Br, and k) BA16Br.



The branching present in the surfactant H2PA (Figure 30a) promoted the formation of gold nanorods with $48 \times 14.4 \text{ nm}$ ($\pm 4.5 \times 0.7 \text{ nm}$) and aspect ratio of 3.3 (Figure 31) that are longer in comparison with the system of AuNRs obtained in presence of HEA16Br, aspect ratio 3.0 (Figure 26a).

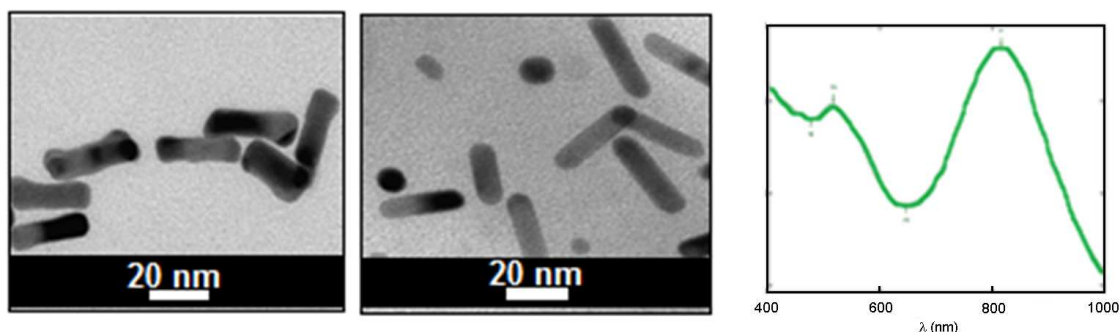
Figure 31 -Uv-vis spectrum and TEM images of AuNR@H2PA16Br.



The volume of the polar head group increased with the presence of the branched methyl group that provided a more efficient blockage of lateral facets of gold nanorods during their formation. Thus, the AuNRs grow mainly in length and consequently also in width (Figure 31).

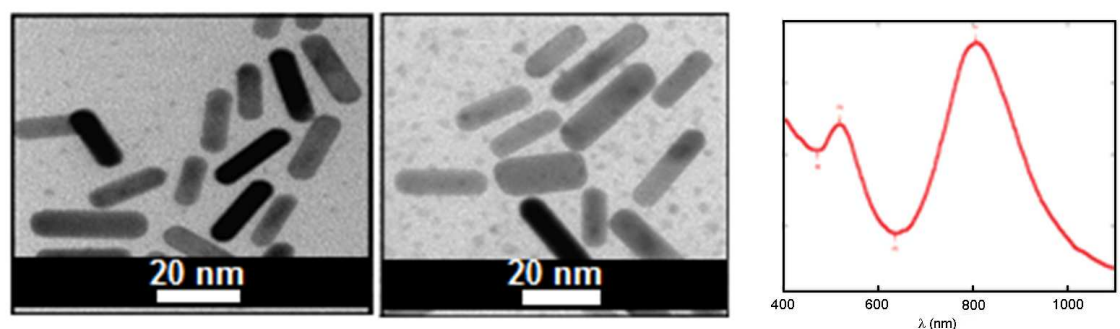
The presence of two hydroxyl groups in the surfactant H1,2PA16Br (Figure 31b) leads to the formation of AuNRs with size of $33.6 \times 8 \text{ nm}$ ($\pm 6.7 \times 1.8 \text{ nm}$) and aspect ratio of 4.2 (Figure 32). Probably, the inadequate steric effect on the crystal gold facets occurs during the well rod-shape particle formation. Due to this, in comparison with the particles obtained with HPA16Br, these AuNRs does not grow very homogeneously, they grow longer and consequently wider (Figure 32).

Figure32 -Uv-vis spectrum and TEM images of AuNR@H1,2PA16Br



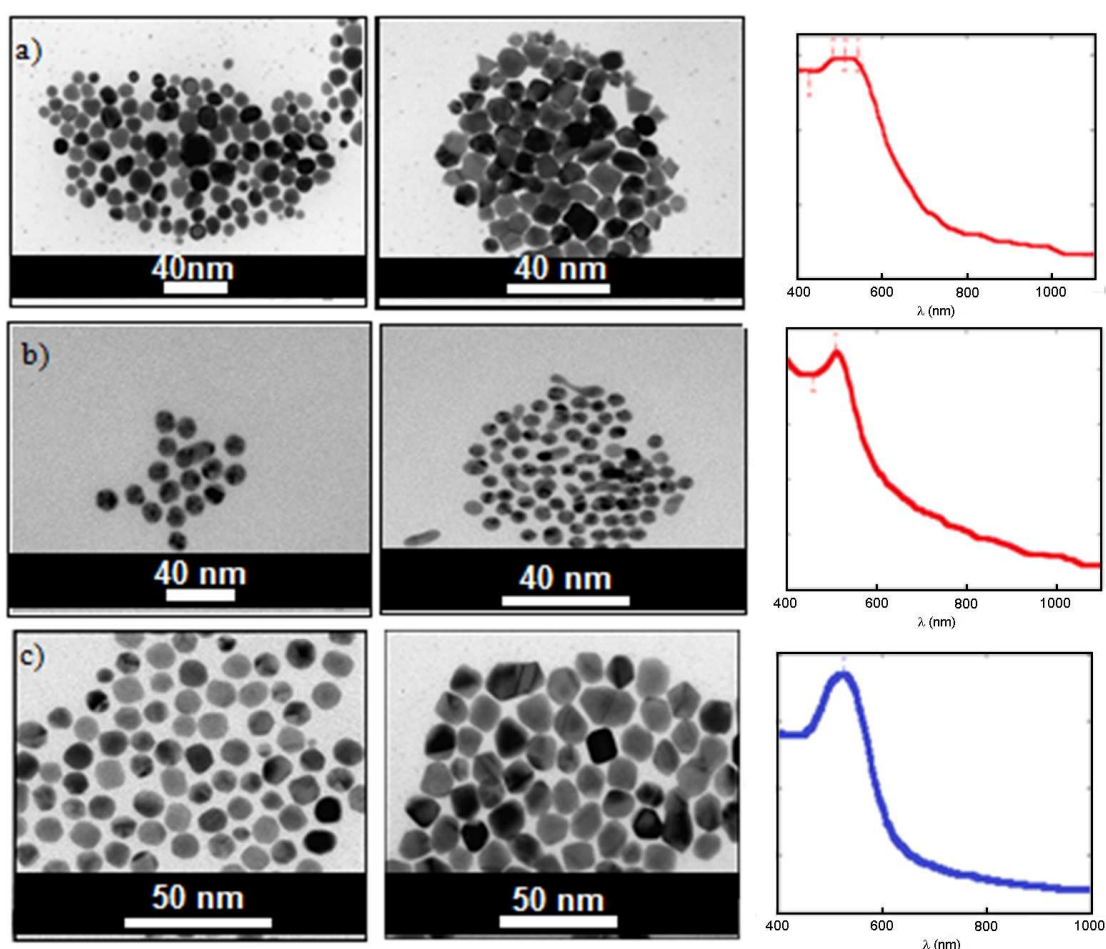
The substitution of two methyl(s) by two ethyl groups, the surfactant HDA16Br (Figure 30c), leads to the formation of AuNRs with size of $24 \times 6.8 \text{ nm}$ ($\pm 4.5 \times 0.7 \text{ nm}$) and aspect ratio of 3.5. Here, the particles are longer if compared to those obtained in presence of HEA16Br (aspect ratio 3.0). We suppose that the presence of the ethyl groups provided a significant hindrance on the lateral facets of the AuNRs during their formation. Thus, the growth of the AuNRs has a similar behavior to the other systems analysed before in the presence of surfactants with a bigger polar head. In this case, the particles grow mainly in length and consequently also in width (Figure 33).

Figure33 -Spectrum Uv-vis and TEM images of AuNR@HDA16Br



The nanoparticles obtained with DHEA16Br, DHA16Br and THEA16Br (Figure 30 d, e and f respectively) have a morphology close to spherical form that is already expected by the analysis of Uv-vis spectra which is confirmed by TEM images (Figure 34). The presence of more than one ethanol amino group as a substituent increases the steric effect caused by micelle formation, making the interaction with the crystal weak surface. Consequently, these surfactants are not adequate to drive the particle growth.

Figure 34 -TEM images and the Uv-vis spectra of a) AuNP@DHEA16Br, b) AuNP@DHA16Br and c) AuNP@THEA16Br.



The NOx16 and NMeEph12Br are not very soluble in water, and the system precipitated during the preparation of the seed solution, even under lower concentrations and soft heating. Consequently, they can not be considered a comparable system with the others due to the surfactant precipitation. The analysis of the final growth process solution by Uv-vis

spectroscopy showed just one absorption band even when prepared under lower concentration (Figure 35) that suggest the formation of spherical nanoparticles. In these cases, we did not perform microscopy analysis because the systems do not show any selectivity to well defined anisotropic shapes. Table 7 summarizes all last results.

Figure 35 -Uv-vis spectra of AuNP@NOx16 at a) 0.064 mol/L, and b) 0.016 mol/L; and AuNP@NMeEPh12Br at c) 0.016 mol/L, and d) 0.0064 mol/L, respectively.

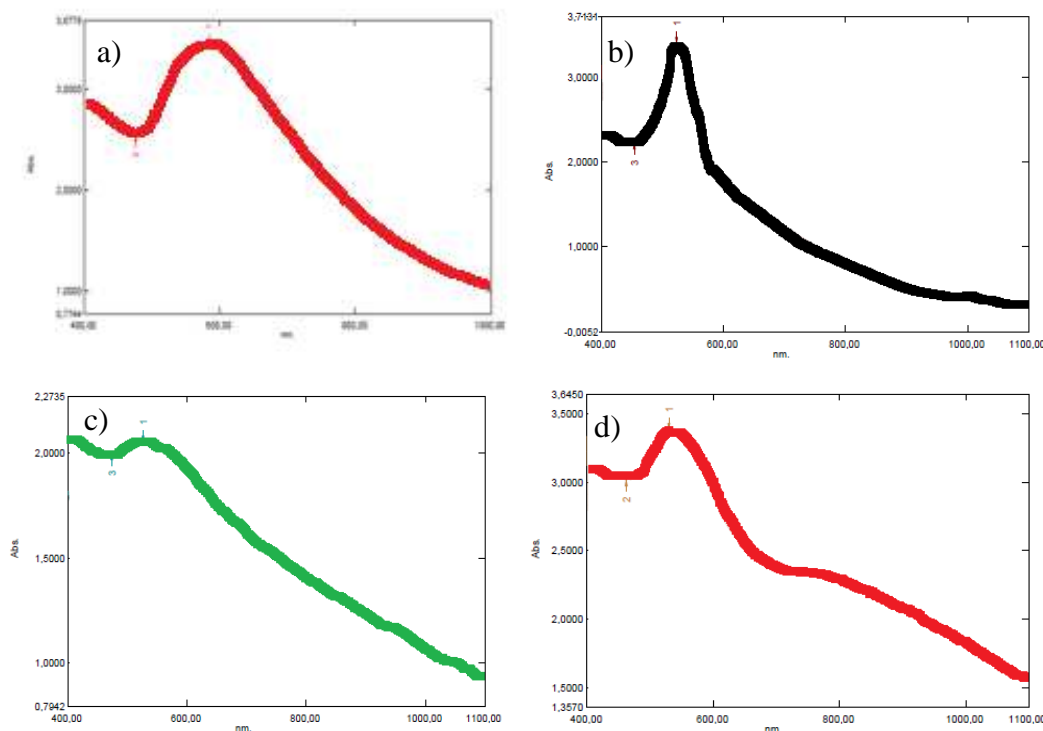


Table 7 - Characteristics of the AuNRs obtained in presence of surfactants with different polar head groups.

Surfactant	Length (nm)	Width (nm)	Aspect Ratio	Selectivity
H2PA16Br	48 ± 4.5	14.4 ± 0.7	3.3	nanorods
H1,2PA16Br	33.6 ± 6.7	8 ± 1.8	4.2	nanorods
HDA16Br	24 ± 4.5	6.8 ± 0.7	3.5	nanorods
DHEA16Br	7.25 ± 0.57	7.25 ± 0.57	~1	spheres, prisms, polyhedra
DHA16Br	27.6 ± 5.5	27.6 ± 5.5	~1	spheres
THEA16Br	11.2 ± 2.4	11.2 ± 2.4	~1	spheres, polyhedra
NOx16	-	-	-	probably spheres
NMeEph16Br	-	-	-	probably spheres

3.5. Influence of the hydroxyl group

In order to determine the influence of a hydroxyl group on the polar head of the surfactants on the formation of AuNRs, the non-hydroxylated surfactants *N,N*-dimethyl-*N*-cetyl-*N*-ethylammonium Bromide (EA16Br), *N,N*-dimethyl-*N*-cetyl-*N*-propylammonium Bromide (PA16Br), and *N,N*-dimethyl-*N*-cetyl-*N*-butylammonium Bromide (BA16Br) were prepared. The results obtained from their use as driving agents are shown in Figure 36 and summarized on Table 8.

High yield of AuNRs could be attained by using EA16Br as driving agent. It seems like the substitution of a methyl group on the polar head of CTABr by an ethyl (EA16Br) did not change the anisotropic growth processes of the AuNRs, i.e. the driving characteristics of CTABr and EA16Br are quite similar. Nevertheless, when an *n*-propyl or an *n*-butyl group is present on the polar head, a significant modification on the mechanism of the growth process occurs. In the case of PA16Br several particle shapes are produced, and for BA16Br, AuNRs with very low aspect ratio (1.5) are obtained (indeed they are close isotropic shape).

Here, it is interesting to compare the driving characteristics of the surfactants PA16Br with HEA16Br, and BA16Br with HPA16Br, since each set of surfactants presents almost the same steric hindrance, indeed one CH₃ group is substituted by an OH group. Nevertheless, many features are different, e.g. hydroxylated surfactants present higher solubility in water, and also display important growth-driving properties. It seems to be clear that the presence of the hydroxyl group is essential to obtain better driving properties during the growth processes. It suggests that the hydroxyl group allows a favorable polar long chain, packing through hydrogen bond thus, providing a better supramolecular organization and efficient protection of the lateral facets.

Figure 36 - Spectra of Uv-vis and TEM images of a) AuNP@EA16Br, b) AuNP@PA16Br, and c) AuNP@BA16Br

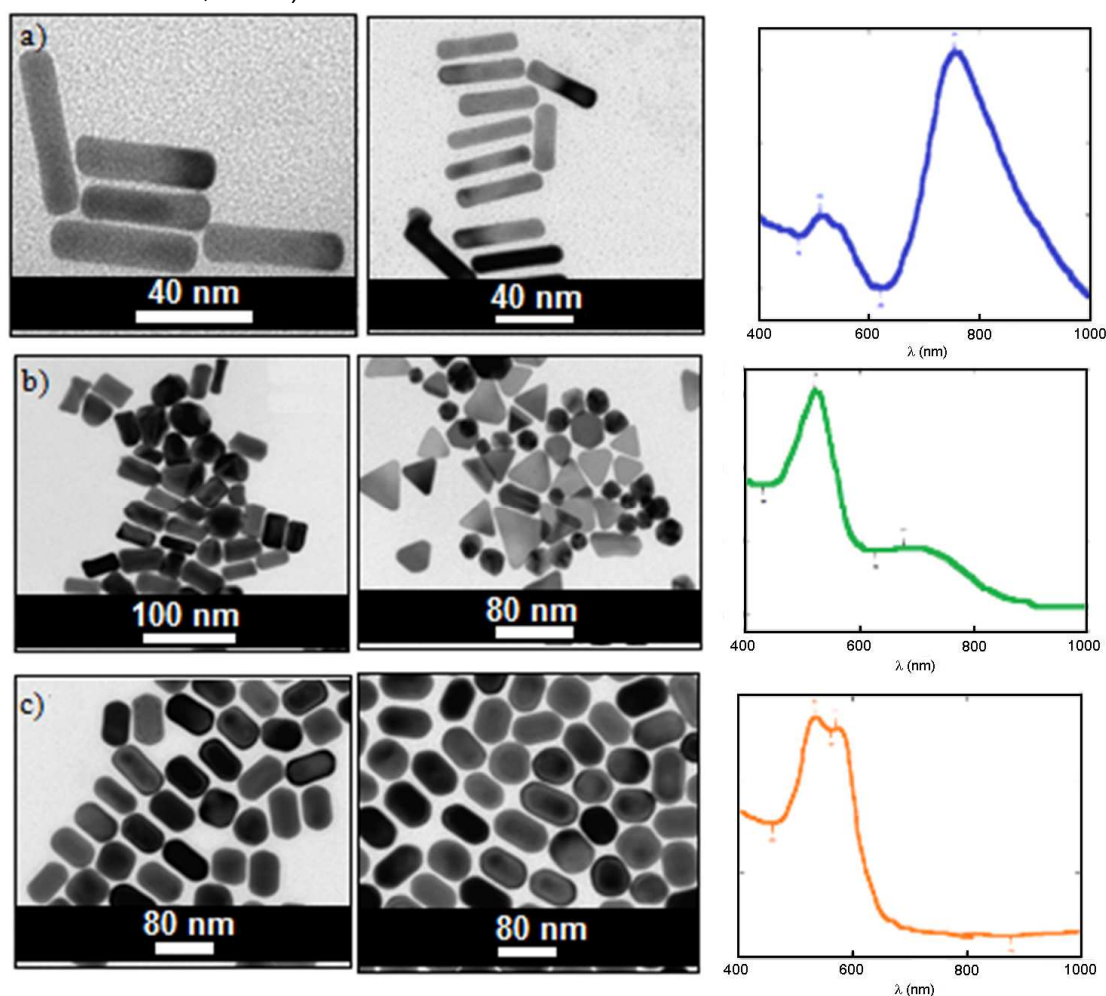


Table 8 - Characteristics of the gold nanorods obtained in presence of non-hydroxylated head groups.

Surfactant	Length (nm)	Width (nm)	Aspect Ratio	Selectivity
EA16Br	48.46 ± 5.28	11.39 ± 1.55	4.2	nanorods
PA16Br	-	-	-	different polyhedrons
BA16Br	42 ± 3.5	27 ± 1.6	1.5	nanorods

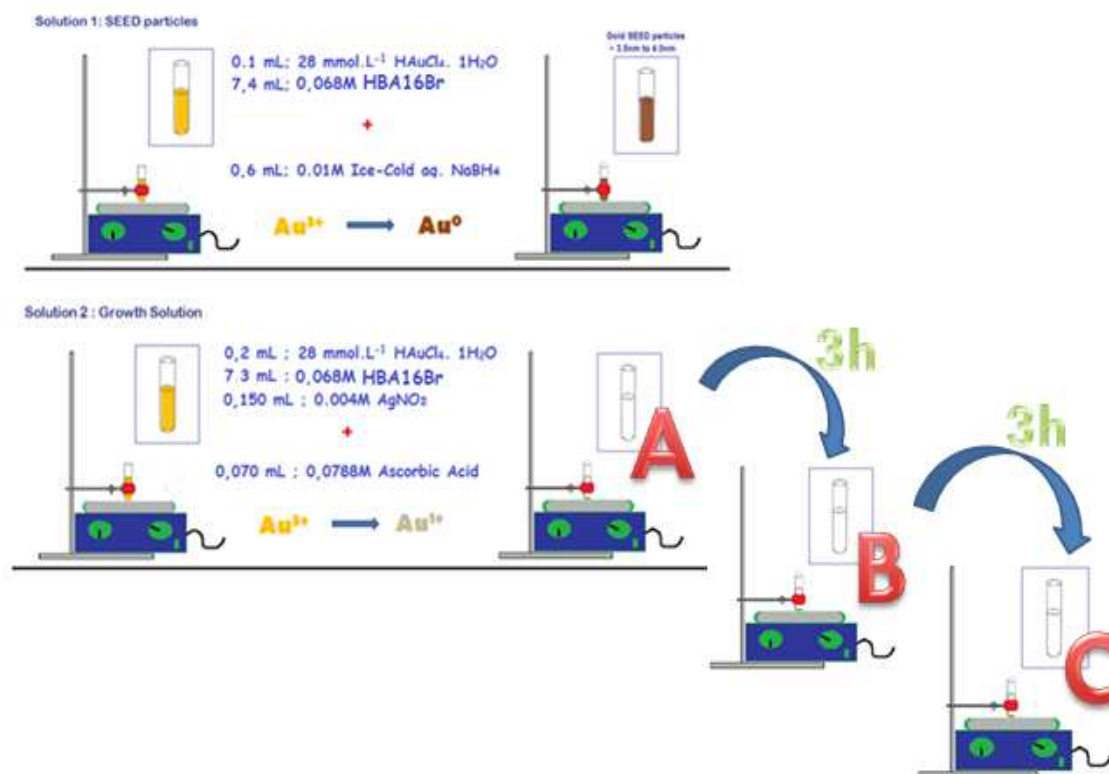
3.6. Synthesis of high aspect ratio AuNRs

We have used a three step seed mediated growth approach to scaling up AuNRs with different aspect ratios. Also, the reactions take place in water and room temperature (the same conditions to obtain shorter AuNRs). The process to prepare high aspect ratios AuNRs consisted in three steps: i) Seed solution, ii) First growth solution named “A”, iii) Second growth solution named “B” and iv) Third growth solution named “C”. All solutions are prepared in the same way of

the standard method, although in absence of silver ions. Figure 37 illustrate the whole procedure.

After two hours, a small aliquot of the seed solution is added in the growth solution A. After 3 hours, the solution A has a purple color and a small aliquot of this growth solution A is added in the solution B. Then 3 hours, a solution B has a pink color and a pink precipitate in the bottom of the flask. Due to this precipitation, the system was stirred before taking an aliquot to add in the solution C. This last one, in our conditions, did not present any colour keeping colorless with a brown precipitate in the bottom of the flask. At this work, the analysis was focused on the gold nanoparticles formed in solution B.

Figure 37 - Three steps to prepare high aspect ratios AuNRs



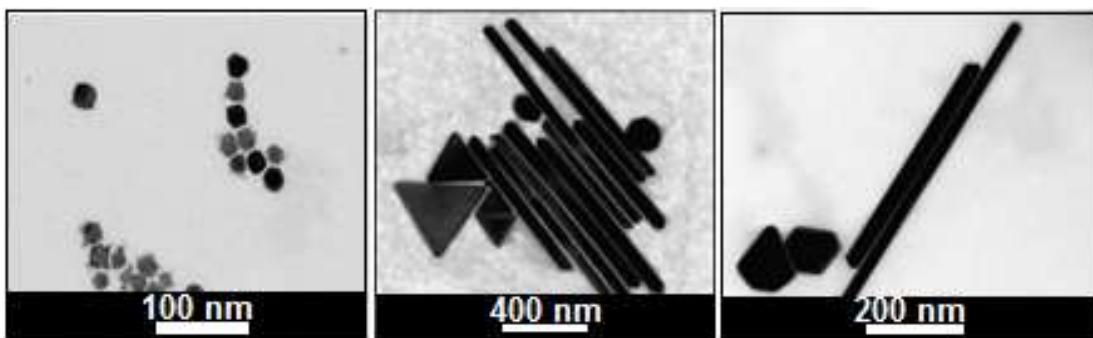
In this set of experiments, we adopted HBA16Br as a growth-driving agent to provide high aspect ratio AuNRs via three growth stages, since it demonstrated to attain AuNRs with the highest aspect ratio in the former studies. The morphological characteristics of the particles formed in each stage (i.e. in A, B and C solutions) are display in Figure 38.

The particles obtained in the solution "A" have polyhedral shapes, similar to spheres (ca. 20 nm). Here, we can observe that no AuNRs are formed on the first stage. It is important to remember that here no silver ions are present; but under the same conditions, in the presence of silver ions, AuNRs are formed on this stage.

The particles obtained in the solution "B", using the particles of solution "A" as the source of seed particles, larger rod shape particles with aspect ratio of 13.4 (860 x 64 nm) are formed. Indeed they present higher aspect ratio and a higher selectivity than that found when CTABr is used as driving agent.³¹

The particles in solution "C" display even higher aspect ratio (21; 1400 x 65 nm), but lower selectivity.

Figure 38 - TEM images of the solutions A, B, and C in absence of silver ions, using HBA16Br driving agent



These results prompted us to verify the features of the particles obtained with the other hydroxylated surfactants (see Figure 39). Then, under the same conditions of the former study, the particles obtained in solution B in presence of HEA16Br lead to the formation of large AuNRs, with an aspect ratio of 2.44 (159 x 65 nm; see Figure 39a). When HPA16Br was employed, also large AuNRs were obtained in solution B, with an aspect ratio of 7.4 (333 x 45 nm; see Figure 39b). And, finally, it is interesting to compare to the particles already presented in Figure 38b (and repeated in Figure 39c), in which HBA16Br was employed as driving agent. In this case, the aspect ratio is 13.4 (860 x 64 nm).

We can observe with this study that the growth of the AuNRs continues the same trend, in which the aspect ratio increases in function of the length of the polar head group as already discussed before in session 3.3 (Influence of

the length of the hydroxylated polar head), even with more stages of growth and in the absence of silver ions. Table 9 summarizes these results.

Figure 39 - TEM images of the solution B in presence of a) HEA16Br, b) HPA16Br, and c) HBA16Br

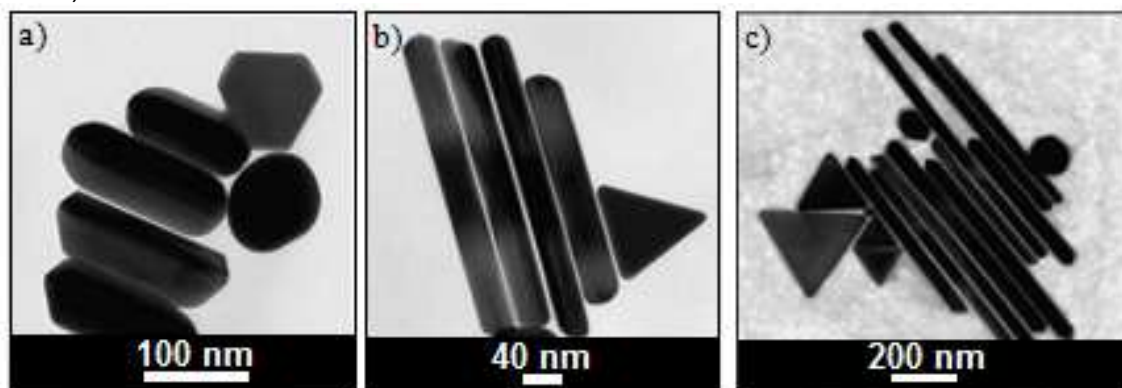
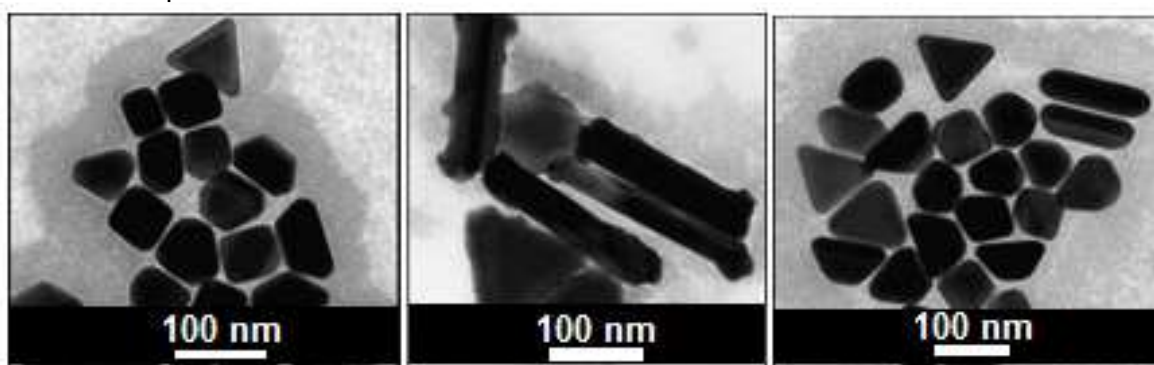


Table 9 - Characteristics of the gold nanorods obtained with high aspect ratio

Surfactant	Length (nm)	Width (nm)	Aspect Ratio	Selectivity
HEA16Br	159±23	65 ± 5	2.4	Nanorods
HPA16Br	333±114	45 ± 11	7.4	Nanorods
HBA16Br	860±214	64 ± 21	13.4	Nanorods

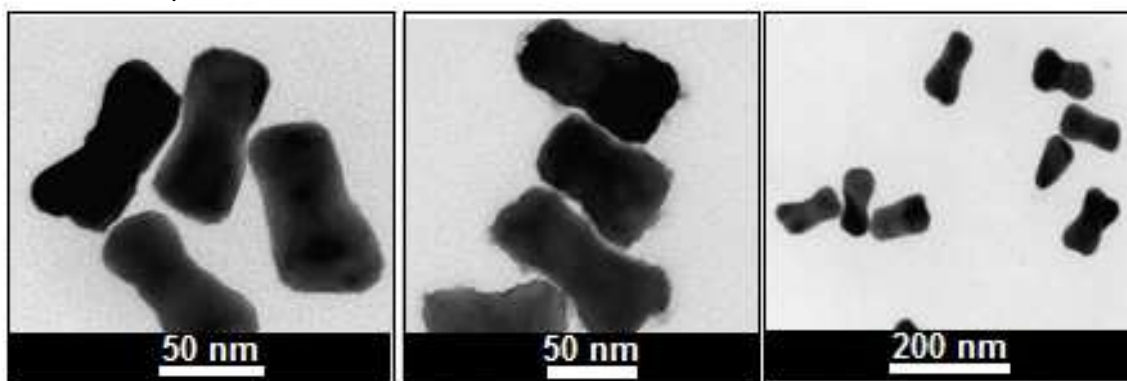
It is important to mention that when silver ions are present in the reaction medium, when multiple growth sequences are proposed, disform particles were obtained. For example, when AuNRs prepared like that displayed on Figure 29b (standard reaction conditions, in the presence of silver ions, using HBA16Br) are added in a second growth solution with absence of silver ions. Particles, like shown in Figure 40, are formed.

Figure 40 - TEM images of the solution B in absence of silver ions obtained from solution A in presence of silver ions



When the same AuNRs prepared, like in Figure 29b, are added in a second growth solution that contains silver ions, particles, like shown in Figure 41, are formed. In fact, the a full explanation for that reason is not developed yet.

Figure 41 - TEM images of the solution B obtained in presence of silver ions from solution A in presence of silver ions, too.



3.7. Effect of the number of seeds

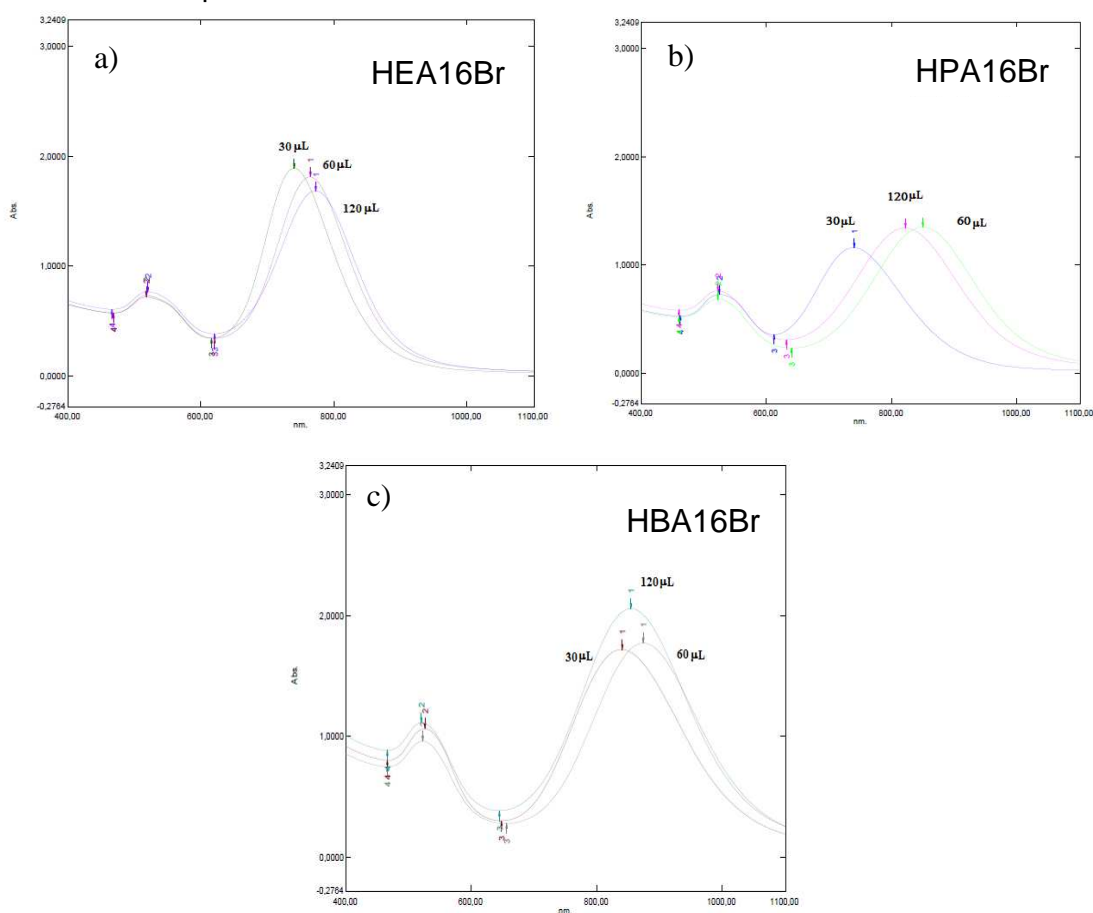
AuNRs were also prepared employing different numbers of seed particles into identical growth solutions. The Figure 42 shows the UV–vis absorption spectra of the particles obtained after 24 h of AuNR formation. At this point, it is important to consider that the number of AuNRs formed is the same as the number of seed particles added. Thus, if we increase the amount of seed particles added, keeping constant the amount of Au(I) species in the solution, i.e. if the Au(I):seed ratio decreases, smaller particles are produced.³

Indeed, we can see that, in presence of HEA16Br, increasing the number of seeds in the medium (30, 60, and 120 μ L of seed solution added), the aspect ratio of the AuNR also increase (Figure 42a). This phenomenon can be observed by the bathochromic shift of the second absorption band to longer wavelengths that is related to increased aspect ratios.

Now, in presence of HPA16Br and HBA16Br, we observed that increasing the number of seeds in the medium (30, 60, and 120 μ L of seed solution added), the aspect ratio of the AuNR increases when 30 and 60 μ L of seed solution are added, however decreases, i.e. an hipsochromic shift of the

second band is observed, when 120 μL of seed solution is added (Figure 42b and c, respectively).

Figure 42 -Absorption spectra of the colloids containing AuNRs prepared with different amounts of seed particles in the reaction medium.

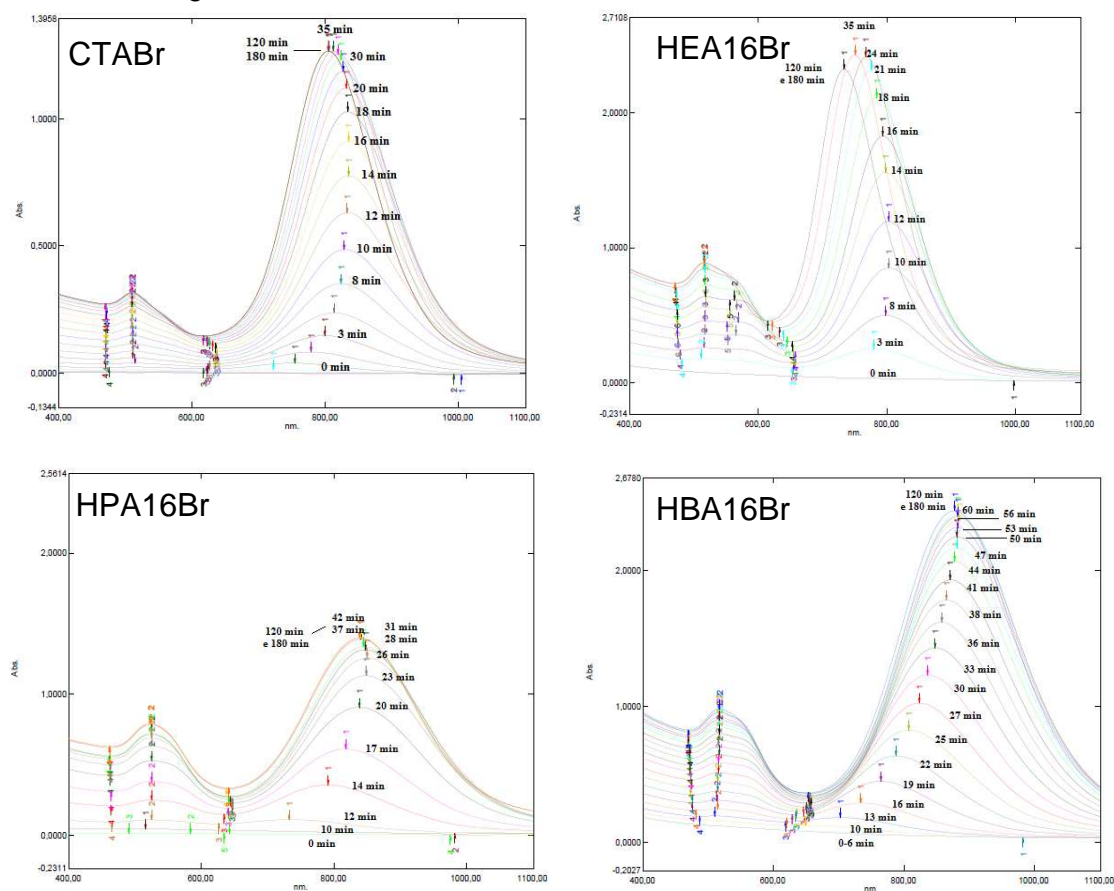


It seems to be a trend in which surfactants that lead to AuNRs with high aspect ratios, like HPA16Br and HBA16Br, need a higher content of Au(I) species (“monomers”) in relation to the amount of seeds present, in others to achieve the right conditions to reach AuNRs with high aspect ratios.^{32,33} Indeed, under a low Au(I)/seed ratio, it will have a scarce amount of Au(I) to attain high aspect ratio AuNRs. This study confirms that there is an ideal relation between “monomers” and seeds in the reaction medium to achieve AuNRs with higher aspect ratio.³

3.8. Stability study of gold nanorods formation

In order to spread more light on the understanding of the growth mechanism of AuNRs with these new series of driving agents, we carried out some kinetic Uv-vis spectroscopic studies to compare the rate of the particle formation, during the first 3 hours, comparing AuNRs prepared in the presence of CTABr, HEA16Br, HPA16Br, or HBA16Br as growth-driving agents (Figure 43).

Figure 43 -Uv-vis spectra of the colloids obtained from various growth-driving agents, collected during the first 3 hours of the NPs formation.



Whatever the growth-driving agent employed, the main growth step for AuNRs seems to take less than 1 hour, and these colloids are stable at least for 3 days without any significant changes on their Uv-vis spectra.

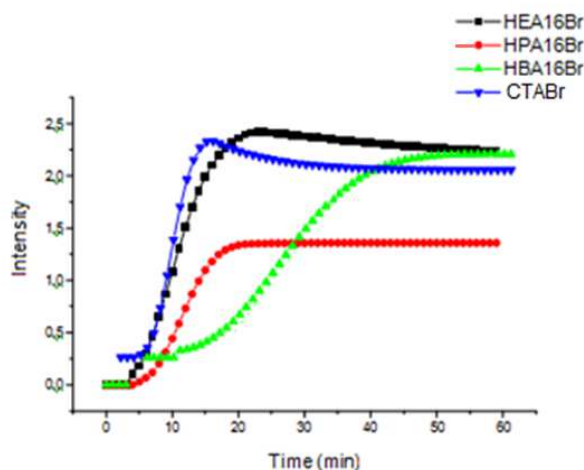
Moreover, during the first stages of the particle growth, a bathochromic effect can be observed. In the case of CTABr and HEA16Br a hypsochromic shift is clearly detected (around 14 min for both).

This behaviour suggests that the aspect ratio of the particle in formation decreases during its growth, since Au(I) ions can still reach the lateral facets of

the AuNRs. Thus, we can suggest that as more efficient is the protection of the double layer of surfactants on the lateral facets of the AuNR, the hypsochromic shift will be later observed in kinetic studies like presented before.

Also, from the Uv-vis spectra, we can obtain a qualitative measurement of the AuNP growth rate, measuring the rate in which intensity of the second band increases. Thus, plotting the intensity to the second band versus time, see Figure 43, we can evaluate how fast the growth process is. We can observe that growth rate follows this sequence: HBA16Br < HPA16Br < HEA16Br ~CTABr.* Again, we can see that HBA16Br must lead to a better coat effect around the particle, controlling indeed the access of the gold source on the particle surface, protecting even better the lateral facets of the crystal during growth process.

Figure 44 - Intensity of the second absorption band in function of time from 0 to 60 min, using four various growth-driving agents.



With this whole study we can suggest that slight modifications on the molecular structure of the surfactant can open new approaches to the development of new growth-driving agents. For example, it is known that the presence of larger carbon chains on the polar head disfavours the formation of AuNRs and decreases the solubility of the surfactant in water; however, these chains, containing OH groups, improve not only the solubility but also significantly the yields of high aspect ratio AuNRs.

*The rates (intensity/time) are: 0.144, 0.108, 0.071, and 0.048, respectively.

5. References

- ¹ J. Gao, C. M. Bender, C. J. Murphy. *Dependence of the Gold Nanorod Aspect Ratio on the Nature of the Directing Surfactant in Aqueous Solution*. Langmuir 2003, 19, 9065.
- ² A. Henkel, O. Schubert, A. Plech, C. Sonnichen. *Growth Kinetic of a Rod-Shaped Metal Nanocrystal*. J. Phys. Chem. C 2009, 113,10390.
- ³ M. G. Angelo da Silva, A. M. Nunes, S. M.P. Meneghetti, M. R. Meneghetti. *New aspects of gold nanorod formation via seed-mediated method*. Comptes Rendus Chimie 2013, 16, 640.
- ⁴ B. Nikoobakht, M. A. El-Sayed. *Preparation and Growth Mechanism of Gold Nanorods (NRs) Using Seed-Mediated Growth Method* Chem. Mater. 2003, 15, 1957.
- ⁵ C. J. Johnson, E. Dujardin, S. A. Davis, C.J. Murphy, S. Mann. *Growth and form of gold nanorods prepared by seed-mediated, surfactant-directed synthesis*. J. Mater. Chem. 2002, 12, 1765.
- ⁶ S. K. Meena, Sulpizi, M. *Understanding the Microscopic Origin of Gold Nanoparticle Anisotropic Growth from Molecular Dynamics Simulations*..Langmuir 2013, 29, 14954.
- ⁷ A. R. Ferhan, L. Guo, D. H. Kim. *Influence of Ionic Strength and Surfactant Concentration on Electrostatic Surface Assembly of Cetyltrimethylammonium Bromide-Capped Gold Nanorods on Fully Immersed Glass*. Langmuir 2010, 26, 12433.
- ⁸ A. Gole, C. J. Murphy. *Seed-Mediated Synthesis of Gold Nanorods: Role of the Size and Nature of the Seed*. Chem. Mater.2004, 16, 3633.
- ⁹ K.T. Yong, Y. Sahoo, M. Swihart, P. Schneeberger, P. Prasad. *Templated synthesis of gold nanorods (NRs): the effects of cosurfactants and electrolytes on the shape and optical properties*. Top. Catal.2008, 47, 49.
- ¹⁰ C. J. Murphy, T. K. Sau, A. M. Gole, C. J. Orendorff, J. Gao, L. Gou, S. E. Hunyadi, T. Li. *Anisotropic Metal Nanoparticles: Synthesis, Assembly, and Optical Applications* J. Phys. Chem. B2005, 109, 13857.
- ¹¹ J. Gao, C. M. Bender, C. J. Murphy. *Dependence of the Gold Nanorod Aspect Ratio on the Nature of the Directing Surfactant in Aqueous Solution*.Langmuir2003, 19, 9065.

-
- ¹² B. Nikoobakht, M. A. El-Sayed. *Preparation and growth mechanism of gold nanorods (NRs) using seed-mediated growth method.* Chem. Mater. 2003, 15, 1957.
- ¹³ Y. Takenaka, H. Kitahata. *High-aspect-ratio gold nanorods synthesized in a surfactant gel phase.* Chem. Phys. Lett. 2009, 467, 327.
- ¹⁴ M. Grzelczak, A. Sanchez-Iglesias, B. Rodriguez-González, R. Alvarez-Puebla, J. Pérez-Juste, L. M. Liz-Marzán. *Influence of Iodide Ions on the Growth of Gold Nanorods: Tuning Tip Curvature and Surface Plasmon Resonance.* Adv. Funct. Mater. 2008, 18, 3780.
- ¹⁵ M. Grzelczak, J. Pérez-Juste, P. Mulvaney, L. M. Liz-Marzán. *Shape control in gold nanoparticle synthesis.* Chem. Soc. Rev. 2008, 37, 1783.
- ¹⁶ T. H. Ha, H. Koo, B. H. Chung. *Shape-Controlled Syntheses of Gold Nanoprisms and Nanorods Influenced by Specific Adsorption of Halide Ions.* J. Phys. Chem. C 2007, 111, 1123.
- ¹⁷ H. Kawasaki, K. Nishimura, R. Arakawa. *Influence of the Counterions of Cetyltrimethylammonium Salts on the Surfactant Adsorption onto Gold Surfaces and the Formation of Gold Nanoparticles.* J. Phys. Chem. C 2007, 111, 2683.
- ¹⁸ V. Sharma, K. Park, M. Srinivasarao. *Colloidal dispersion of gold nanorods: Historical background, optical properties, seed-mediated synthesis, shape separation and self-assembly.* Mater. Sci. Eng. R 2009, 65, 1.
- ¹⁹ M. R. Langille, M. L. Personick, J. Zhang, C. A. Mirkin. *Defining Rules for the Shape Evolution of Gold Nanoparticles* J. Am. Chem. Soc. 2012, 134, 14542.
- ²⁰ K. Saha, S. S. Agasti, C. Kim, X. Li, V. M. Rotello. *Gold Nanoparticles in Chemical and Biological Sensing.* Chem. Rev 2012, 112, 2739.
- ²¹ V. R. Dugyala, S. V. Daware, M. G. Basavaraj. *Shape anisotropic colloids: synthesis, packing behavior, evaporation driven assembly, and their application in emulsion stabilization.* Soft Matter 2013, 9, 6711.
- ²² O. M. Magnussen. *Ordered anion adlayers on metal electrode surfaces.* Chem. Rev., 2002, 102, 679.

-
- ²³ S. K. Meena, M. Sulpizi. *Understanding the Microscopic Origin of Gold Nanoparticle Anisotropic Growth from Molecular Dynamics Simulations*. Langmuir 2013, 29, 14954.
- ²⁴ J. E. Millstone, W. Wei, M. R. Jones, H. Yoo, C. A. Mirkin. *Iodide ions control seed-mediated growth of anisotropic gold nanoparticles*. Nano Lett. 2008, 8, 2526.
- ²⁵ D. K. Smith, N. R. Miller, B. A. Korgel. *Iodide in CTAB prevents gold nanorod formation*. Langmuir 2009, 25, 9518.
- ²⁶ M. R. Langille, M. L. Personick, J. Zhang, C. A. Mirkin. *Defining rules for the shape evolution of gold nanoparticles*. J. Am. Chem. Soc. 2012, 134, 14542
- ²⁷ T. H. Ha, H. J. Koo, B. H. Chung. *Shape-controlled syntheses of gold nanoprisms and nanorods influenced by specific adsorption of halide ions*. J. Phys. Chem. C 2007, 111, 1123.
- ²⁸ D. Lee, S. Hong, S. Park. *Controlled Assembly of Gold Nanoprism and Hexagonal Nanoplate Films for Surface Enhanced Raman Scattering*. Bull. Korean Chem. Soc. 2011, 32, 3575.
- ²⁹ Z. Guo, X. Fan, L. Liu, Z. Bian, C. Gu, Y. Zhang, N. Gu, D. Yang, J. Zhang. *Achieving high-purity colloidal gold nanoprisms and their application as biosensing platforms*. J. Colloid Interface Sci. 2010, 348, 29.
- ³⁰ T. K. Sau, C. J. Murphy. *Seeded high yield synthesis of short Au nanorods in aqueous solution*. Langmuir 2004, 20, 6414.
- ³¹ N. R. Jana, L. Gearheart, C. J. Murphy. *Wet chemical synthesis of high aspect ratio cylindrical gold nanorods*. J. Phys. Chem. B 2001, 105, 4065.
- ³² X. Xu, M. B. Corti. *Shape change and color gamut in gold nanorods, dumbbells, and dog bones*. Adv. Funct. Mat. 16 2006, 2170.
- ³³ F. Ratto, P. Matteini, F. Rossi, R. Pini. *Size and shape control in the overgrowth of gold nanorods*. J. Nanopart. Res. 2010, 12, 2029

Applications on catalysis and self-assembly studies

4.0. Introduction

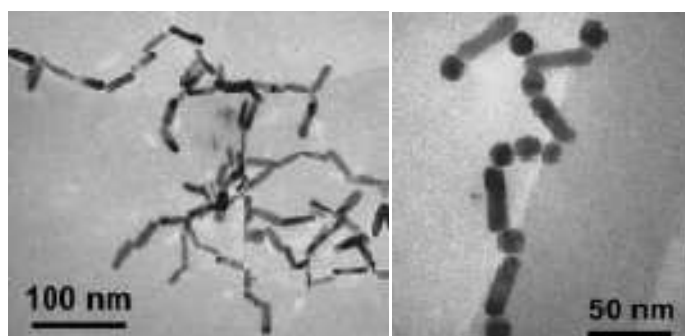
Nanomaterials are important in diverse areas, from basic research to various technological applications such as electronics, biochemical sensors, catalysis, and energy. They have emerged as sustainable alternatives to conventional materials as robust high surface area heterogeneous catalysts, and catalyst supports. The nanosized particles increase the exposed surface area of the active component of the catalysts, thereby enhancing the contact between reactants and catalysts dramatically, and mimicking the homogeneous catalysts.

One slope of this chapter focuses on the nanocatalysis for green-chemistry by hydrogenation of unsaturated compounds with aqueous gold colloidal dispersion.^{1,2} The second slope is related to the surface modification, and self-assembling of AuNPs.

Functionalization of AuNRs@CTABr with derivatives of thiols has been shown to be very regioselective for the extremities of the particles. This behavior has opened the possibility to link together rods in an end-to-end fashion way (see Figure 45).³ Indeed, AuNRs can be linked to each other in an end-to-end way by using cheaper thiols such as cysteine⁴, glutathione or thioalkylcarboxylic acid⁵ as molecular bridges.

These assembled nanostructures may be used as the precursors for future nanodevices such as electromagnetic waveguides^{6,7}, biosensing^{8,9}, liquid crystal properties, and catalysts.

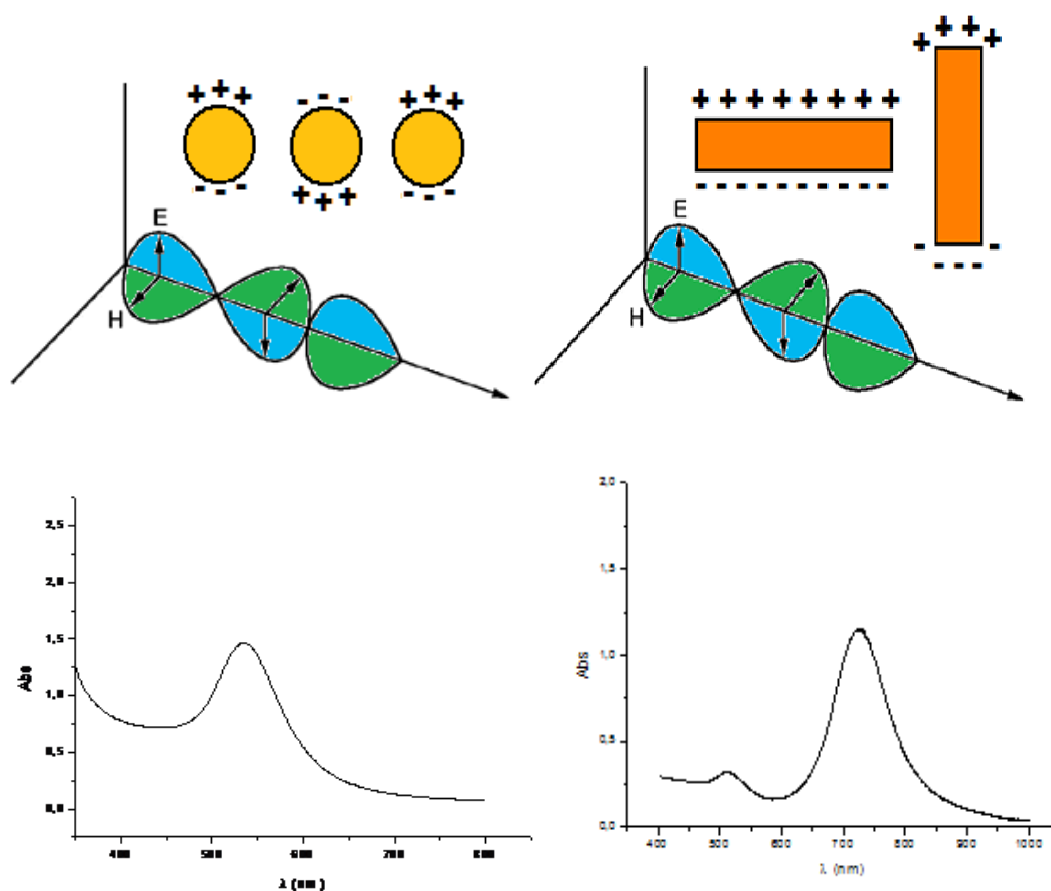
Figure 45 - TEM images showing the selective interaction among AuNRs via end-to-end fashion.³



4.0.1. Optical properties of gold nanoparticles

Many noble metals, such as gold, and silver, display a size-dependent plasmonic behavior to a certain degree. However, by manipulating the architecture of the nanoparticles, researchers have been able to access even more notable plasmonic absorbance, and scattering phenomena that are simply not seen in spherical nanoparticles.^{10,11,12,13} The plasmon resonance is an optical phenomenon that occurs when a metallic nanoparticle of particular size interacts with incident photons in such a way as to confine the resonant photon within the dimensions of the nanoparticle.^{10,11,12} This induces an electron oscillation of the conduction band at the particle surface. Spherical AuNPs display just one surface plasmon resonance (SPR) that is broken when the particle presents different axes and vertices on the surface. When it occurs, the particle possesses multiple SPRs. In case of AuNRs, they possess two distinct SPR: a transversal SPR, corresponding to the short axis of the rod, and a longitudinal SPR, corresponding to the long axis (Figure 46). Like the energy of the SPR for spherical AuNPs is relatively constant for different core diameters, in other words, the λ_{\max} does not change very much, the energy of the transversal SPR of AuNRs does not change very much, however their longitudinal SPR depend strongly on their aspect ratios, and any displacement is related to this phenomenon.^{10,11,12,14} Therefore, the energy of the longitudinal SPR can be tuned from the middle of the visible region of the electromagnetic spectrum (~600 nm) to the infrared region (~1800 nm), simply by changing the aspect ratio of AuNR.

Figure 46 - Schematic representation of plasmon absorbance in spherical rod, and gold nanoparticles.¹⁵



4.0.2. Catalytic properties

Nanoparticles have emerged as sustainable alternatives to conventional materials with a high surface area as heterogeneous catalysts, and catalyst supports. The nanosized particles increase the exposed surface area of the active component of the catalysts, thereby enhancing the contact between reactants and catalysts dramatically, and mimicking the homogeneous catalysts. However, their “insolubility” in reaction solvents renders them separately, under some conditions, from the reaction mixture like heterogeneous catalysts. Also, the activity and selectivity of nanocatalysts can be manipulated by tailoring chemical, physical properties like size, shape, composition, and morphology.¹⁶

The scientific challenge is the synthesis of specific size, shape nanocatalysts to allow facile movement of materials in the reacting phase and control over morphology of nanostructures to tailor their physical, chemical

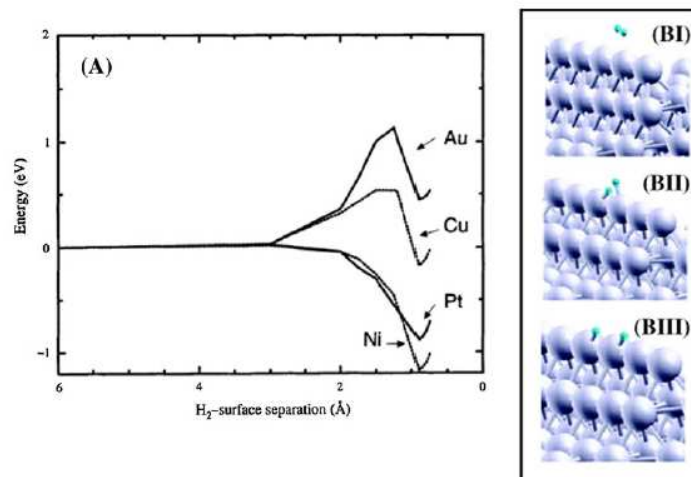
properties. However, the rapid advancement of nanotechnology made possible the preparation of a variety of nanoparticles with controlled size, shape, morphology, and composition.

4.0.3. Catalytic Hydrogenation reactions

Gold was less studied in the field of catalysis because gold bulk is chemically inert and it has considered uninteresting for many years. However, ever since Hutchings' discovery that gold is the catalyst of choice for acetylene hydrochlorination^{17,18} and Harutas' discovery that gold nanoparticles supported on a certain kind of materials are very active for CO oxidation at low temperatures^{17,19,20}, the study of the catalytic properties of gold nanoparticles has been prospering^{21,22}. One major reason for ignoring gold catalysts for many years is that, in most cases, supported gold nanoparticles, prepared by traditional impregnation method, exceed a critical nanosized range of which the gold catalysts are not active. To overcome this problem, deposition-precipitation,²³ and co-precipitation²⁴ methods have been adopted, and have proven effective for many oxide supports.

In 1970, Bond et al.²⁵, in studying the hydro treatment of buta-1,3-diene, and but-2-yne, reported what would constitute the first publication, dealing with the use of gold in catalytic hydrogenation where the requirement of surface defects, and smaller AuNPs for significant activity was proposed. The catalytic activity of gold in hydrogen-mediated reactions is significantly lower when compared with conventional transition metals as Platinum, Palladium, and Nickel, a response that has been attributed to less effective activation/dissociation of H₂^{26,27} (Figure 47). Molecular hydrogen does not chemisorb on bulk gold^{28,29}, but weakly interacts at 78K, desorbing (at 125 K) with a desorption activation energy of 12 kJ mol⁻¹.³⁰

Figure 47 - A) Calculated energy along the minimum-energy reaction path for H₂ dissociation on the (111) surface of Ni, Cu, Pt, and Au; (B) optimized geometry for adsorbed H₂ (I), transition state (II) and dissociated H₂ (III) at the edge of a monoatomic row on a defective Au (111) surface. Adapted from Reference 31.



The use of supports such as inorganic oxide or amorphous carbon to anchor Au particles can guarantee well-dispersed metal phase at the nanoscale. While the nature of H₂-Au interactions in supported systems has not been well settled yet., the consensus that emerges suggests a high activation energy barrier for dissociative adsorption³² where uptake is dependent on Au coordination.^{33,34,35} Dissociative chemisorption of H₂ appears to occur on low-coordination Au sites, i.e. at edges (Figure 4.3) and corners.^{36,37,38} It has been demonstrated, both theoretically³⁹ and experimentally,^{36,40} that H₂ chemisorbs on defect sites, with a measurable uptake on AuNPs < 10 nm.⁴¹ Supported AuNPs exhibit a higher number of defects when compared with bulk gold form⁴².

The review of Cárdenas-Lizana et al.³¹ presents an interesting compilation of literature on gas-phase hydrogenation over Au catalysis in which few carried out, using colloidal nanoparticles; it just cited the hydrogenation of the Anthracene compound but any data is reported in the study.

Thus, due to this lack, we prompted to carried out hydrogenation studies of unsaturated compounds with colloidal gold as catalysts.

4.1. Colloidal gold for catalytic hydrogenation of unsaturated compounds

For economic, ecological reasons, biphasic catalysis based on two immiscible liquid phases, e.g. water and hydrocarbons have attracted increasing attention⁴³. In fact, such catalytic systems offer a way to separate and recycle the catalyst by simple decantation or extraction.

During the last decade, nanoparticles dispersed in liquid media⁴⁴ have been studied⁴⁵ in catalytic reactions such as hydrogenation,^{43,46} oxidation.^{47,48} These small metal particles can work efficiently as catalyst if aggregation does not occur during the reaction. To prevent this phenomenon and to facilitate recycling, particles must be stabilized by a highly water-soluble protective agent. Three main methods are known to prevent colloids from aggregating in water: i) electrostatic stabilization with ionic species,⁴⁹ ii) steric protection based on the use of polymers,⁵⁰ and iii) electrosteric stabilization generated by surfactants or polyoxoanions.⁵¹ We have chosen an ionic surfactant to prepare and to protect the aqueous colloidal suspension of gold particles. We have synthesized *N*-alkyl-*N*-(2-hydroxyethyl)ammonium salts (HEA) which provide sufficiently hydrophilic character to maintain the catalytic species within aqueous phase.⁵² The hydrogenation of unsaturated compounds represents an important industrial catalytic transformation.⁵³ Generally, this reaction is carried out with heterogeneous catalysts.⁵⁴ Some pure homogeneous⁵⁵ or microheterogeneous⁵⁶ systems have been reported, but they require in many, if not most, cases drastic conditions (high pressure and/or temperature). However, colloidal catalysts do give satisfactory results for unsaturated reduction in organic mixtures.⁵⁶ In this thesis, we show that our catalytic system (AuNP@HEA16Br) can efficiently catalyze the hydrogenation of unsaturated compounds in biphasic liquid ± liquid (water/organic phase) media at room temperature and under H₂ pressure. We have demonstrated that surfactant-protected colloids can be used in pure biphasic conditions with a satisfactory recycling process.

4.1.1. Experimental description

All catalytic tests were carried out in a close steel reactor (Figure 48) equipped with magnetic stirring, under room temperature, and specific reaction times. In general, a some amount of the gold colloidal solution freshly prepared (usually

containing 0.0015 mmol of gold) is added in the reactor, together with the unsaturated substrate (usually 1.0 mmol of toluene, anisole, styrene or acetophenone, leading to a solution in which the substrate:gold molar ratio is 704:1). In order to keep the same volume for all catalytic tests, a specific amount of distilled water was added until reach a final volume of 10 mL. Finally, the reactor is pressurized with H₂ (1 to 30 bars). After the reaction period, the organic products are extracted with diethyl ether (3x with 3 mL), and analyzed with Gas Chromatography. In some experiments, the colloid was reintroduced in the reactor for reuse tests.

Figure 48—Image of the reactor employed to the hydrogenation reaction.



4.1.2. Results and discussions

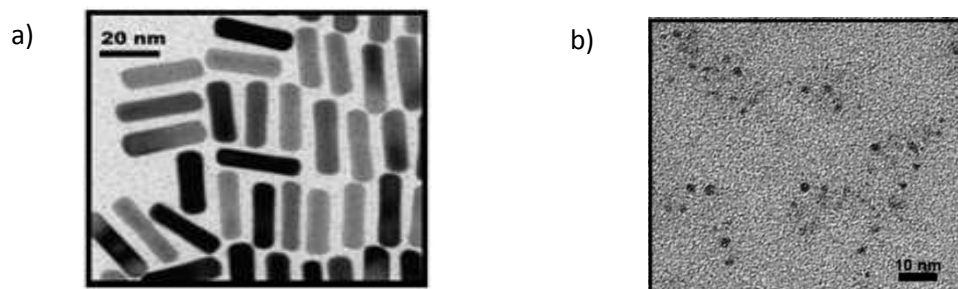
4.1.2.1. Catalytic Hydrogenation Reaction

The control of the growth process with this series of surfactants allows the modulation of the structural parameters of AuNRs and opens interesting perspectives in terms of applications. Without one unprecedented in the literature, these AuNRs were evaluated as catalysts for hydrogenation of aromatic compounds.

Our set of experiments had two goals: i) evaluate the catalytic activity of gold nanoparticles, and ii) verify the influence of the particle morphology (gold nanorods and spherical nanoparticles) in the catalytic properties.

Thus two different gold nanoparticles were tested, rod shape-like and spherical (Figure 49).

Figure 49 - TEM images of AuNR@HEA16Br (30 x 10 nm) and spherical AuNP@HEA16Br (3 nm).



With this study, as we can observe in the following tables, that both aqueous catalytic systems based on AuNRs or spherical AuNPs are active in the hydrogenation of alkenes, ketones, nitro, and aromatics compounds such as toluene (Figure 50), anisole (Figure 51), styrene (Figure 52), acetophenone (Figure 53) and nitrobenzene (Figure 54), as we can see in the following tables (Table 10 to 13). Of course, it is highly possible that other substrates can be hydrogenated.

Figure 50 - Toluene hydrogenation reaction product using gold nanoparticles as catalysts

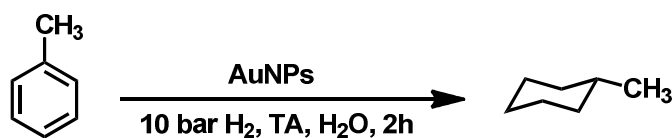


Table 10 - Reaction conditions for toluene hydrogenation reaction using gold nanoparticles as catalysts (AuNRs: gold nanorods; AuNPs: gold nanospheres).

Catalyst	HEA16Br (mol/L)	Au (mmol)	S/Au	P (bar)	Time (h)	Methylcyclohexane (%)
AuNRs	0.0128	0.0015	704	30	1	100
AuNRs	0.0128	0.0015	704	30	0.5	55
AuNRs	0.0128	0.0015	704	10	2	100
AuNRs	0.0128	0.0015	704	10	1	60
AuNRs	0.0128	0.0015	704	10	0.5	20
AuNRs	0.0128	0.0015	704	1	6	0
AuNRs	0.0128	0.0015	704	1	20	0.1
AuNRs	0.0128	0.0015	704	5	3	100
AuNRs	0.0128	0.0015	704	5	2	84
AuNPs	0.027	0.0015	704	10	2	100
AuNPs	0.027	0.0015	704	10	1	70

Figure 51 - Anisole hydrogenation reaction products using gold nanoparticles as catalysts.



Table 11—Reaction conditions for anisole hydrogenation reaction using gold nanoparticles as catalysts (AuNRs: gold nanorods; AuNPs: gold nanospheres; and A: Methoxy-cyclohexane; B: Cyclohexanone)

Catalyst	HEA16Br (mol/L)	Au ⁰ (mmol)	S/Au	P (bar)	Time (h)	A (%)	B (%)
AuNRs	0.0128	0.0015	704	1	3	1	0
AuNRs	0.0128	0.0015	704	30	3	99	0.3
AuNRs	0.0128	0.0015	704	10	2	53	1
AuNRs	0.0128	0.0015	704	5	3	59	2
AuNPs	0.027	0.0015	704	1	3	0.1	0
AuNPs	0.027	0.0015	704	30	3	85	1
AuNPs	0.027	0.0015	704	10	2	49	1
AuNPs	0.027	0.0015	704	5	3	45	1

Figure 52 - Styrene hydrogenation reaction products using gold nanoparticles as catalysts

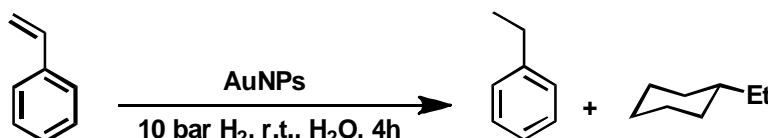


Table 12- Reaction conditions for styrene hydrogenation using gold nanoparticles as catalysts (AuNRs: gold nanorods; AuNPs: gold nanospheres; and A: Ethyl-benzene; B: Ethyl- Cyclohexane)

Catalyst	HEA16Br (mol/L)	Au (mmol)	S/Au	P (bar)	Time (h)	A (%)	B (%)
AuNRs	0.0128	0.0015	704	10	2	20	80
AuNRs	0.0128	0.0015	704	10	3	9.5	90.5
AuNRs	0.0128	0.0015	704	10	4	0	100
AuNPs	0.027	0.0015	704	10	2	24	76
AuNPs	0.027	0.0015	704	10	3	13	87
AuNPs	0.027	0.0015	704	10	4	10	90

Figure 53 - Acetophenone hydrogenation reaction products using gold nanoparticles as catalysts

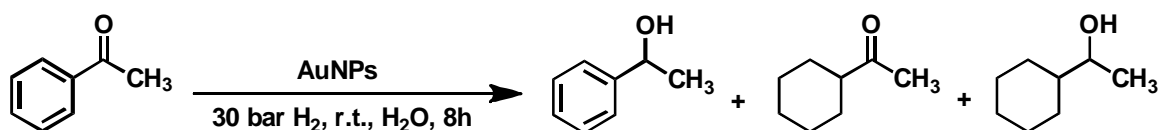


Table 13 - Reaction conditions for acetophenone hydrogenation using gold nanoparticles as catalysts (AuNRs: gold nanorods; AuNPs: gold nanospheres; and A: Phenylethanol; B: Cyclohexylethanone; C: Cyclohexylethanol)

Catalyst	HEA16Br (mol/L)	Au (mmol)	S/Au	P (bar)	Time (h)	A (%)	B (%)	C (%)
AuNRs	0.0128	0.0015	704	1	3	0	0	0
AuNRs	0.0128	0.0015	704	10	2	16	10	14
AuNRs	0.0128	0.0015	704	30	3	24	16	56
AuNRs	0.0128	0.0015	704	30	6	8	2	90
AuNRs	0.0128	0.0015	704	30	8	4.5	0.5	95
AuNPs	0.027	0.0015	704	1	3	0	0	0
AuNPs	0.027	0.0015	704	10	2	8	5	7
AuNPs	0.027	0.0015	704	30	3	20	15	55
AuNPs	0.027	0.0015	704	30	6	18	7	73
AuNPs	0.027	0.0015	704	30	8	10	9	78

Figure 54 - Nitrobenzene hydrogenation reaction products using gold nanoparticles as catalysts

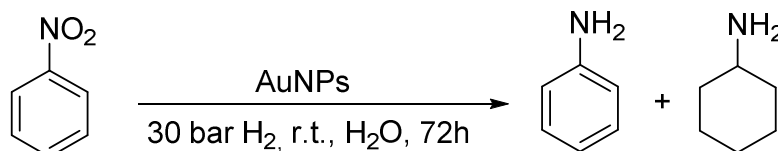


Table 14 - Reaction conditions for nitrobenzene hydrogenation using gold nanoparticles as catalysts (AuNRs: gold nanorods; AuNPs: gold nanospheres; and A: Aniline; B: Cyclohexylamine)

Catalyst	HEA16Br (mol/L)	Au (mmol)	S/Au	P (bar)	Time (h)	A (%)	B (%)
AuNRs	0.0128	0.0015	704	30	72	3	97
AuNRs ^a	0.0580	0.0015	704	30	72	18	82
AuNRs ^b	0.000	0.0015	704	30	72	7	93
AuNRs ^c	0.000	0.0015	704	30	72	9	91
AuNRs	0.0256	0.0029	352	30	72	11	89
AuNRs	0.0450	0.0056	176	30	72	20	80
AuNRs ^d	0.0450	0.0056	176	30	72	5	95
AuNPs	0.0450	0.0028	176	15	3	100	0
AuNPs	0.0450	0.0028	176	30	18	68	32
AuNPs	0.0450	0.0028	176	30	72	10	90

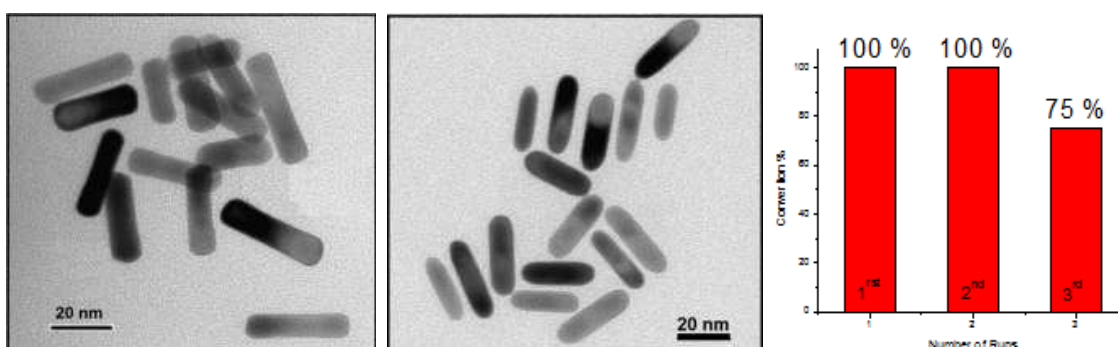
^a Addition of more surfactant; ^b Elimination of the excess of surfactants by centrifugation; ^c Elimination of the surfactant and treatment with NaCl (70mmol); ^d addition of NaCl. (70mmol)

For comparison, we have found that those AuNPs, whatever shape, are active as catalysts in hydrogenation reactions. The AuNRs have shown excellent catalytic activity in the process of hydrogenation of aromatic rings in all tests, reaching 100% conversions. Some nitrobenzene hydrogenation reactions, NaCl were added to the system. Interestingly, no significant change was observed in the analysis of the extracted products. It was also observed the efficiency of the AuNRs catalysts in absence of the surfactant. The AuNRs were centrifuged under 13500 rpm during 20 minutes to remove the excess of surfactant before the catalytic reaction, but no significant influence of the catalytic performance was detected. On the other hand, the addition of more surfactant in the reaction system decrease the catalytic activity, probably due to the hindrance of the gold surface created by the high excess of surfactant, avoiding the substrate interaction with the catalytic surface.

4.1.2.2. Reuse of Colloidal Dispersion of AuNRs

We have conducted the reuse tests of the nanocatalyst for toluene hydrogenation. After reaction, the hydrogenated products are extracted with ethyl ether and the aqueous colloidal dispersion of AuNPs are reused (added again into the reactor) with fresh quantity of substrate. In these tests, the conversion reaches also 100%. TEM images were obtained from the AuNRs before and after the first hydrogenation reaction of toluene (Figure 55). We can clearly see that the tips of the AuNRs are more wastage. This result suggest that probably the substrate interacts more on the tips that on the lateral facets of the rod particle.

Figure 55 - TEM images of AuNRs before and after the first hydrogenation reaction of toluene.



4.2. Interaction among gold nanoparticles

Gold nanoparticles in the spherical, rod shapes have different properties due to differences in their sizes and also in the arrangement of their atoms (morphology). Therefore, each one has an intrinsic, unique feature. However, the union of both particles can lead to a singular highly organized nanostructured system with more innovative properties. This interaction control among the particles is named self-organization or self-assembly, and can lead a new range of materials, and potential applications.

Aiming to promote the self-organization among AuNPs with similar or distinct morphologies, we have carried out studies based on the NP surface modification, adding bifunctionalized compounds, bearing an anchoring and a linking group, in order to allow controlled interaction or associations among the NPs.

4.2.1. Experimental description

Materials

AuNRs were prepared and used according chapter 2 of this work. Acetonitrile (99,9% HPLC, TEDIA), deionized water (DEIONIZER DIRECT – Q3 MILLIPORE), 4,4'-thiobisbenzenethiol (TIOB). All glassware was cleaned with aqua regia and rinsed with deionized water before each experiment.

Self-assembly by homo-organization

Initially 7.8 mL of the colloidal solution of AuNRs were centrifuged (13500 rpm, 10 min). After that, the supernatant was removed and the precipitate was redispersed in water. Subsequently, it was added an equimolar amount to gold of TIOB in acetonitrile: water (equivalent in gold). Then different amounts of glutathione were added (an equimolar amount, 10x more, 10x less to gold).

Characterization of the samples

Freshly prepared solutions were analyzed by Uv-vis/Near IR (400-1000 nm, spectrophotometer VARIAN Cary 50), Dynamic Light Scattering (DLS, Nanotrak Particle Size Analyser, series S3000/S3500 from Microtrac Inc.), and

transmission electron microscopy (TEM, Model Tecnai 20). Some TEM images of the samples are still processing.

4.2.2. Results and discussions

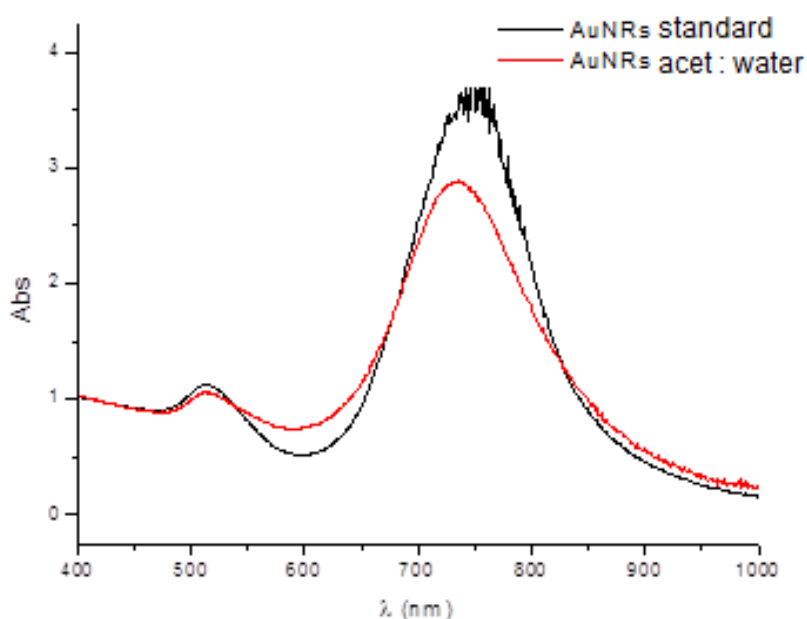
The promotion of interparticle interactions and realization of the self-assembly phenomenon can be observed through various interactions of different chemical nature.

Most systems described in this work occur in aqueous media. The presence of low water soluble connectors was a challenge to be overcome. Thus, it was necessary to use another solvent in which most of the connectors had to be sufficiently soluble. Thus, the AuNP-assembling tests were carried out in acetonitrile: water (4:1).

In order to prove that this new condition is suitable to stabilize AuNPs, with agglomeration or precipitation of the particles, due to the presence of this new solvent, we have checked the stability of the AuNRs under these conditions.

After the characterization by UV-vis, it was possible to verify a decrease in the intensity of the spectrum which indicates only dilution of the process, without direct influence on the system like agglomeration (Figure 56).

Figure 56 - UV-vis spectra of AuNRs in water and in presence of acetonitrile: water (4:1)

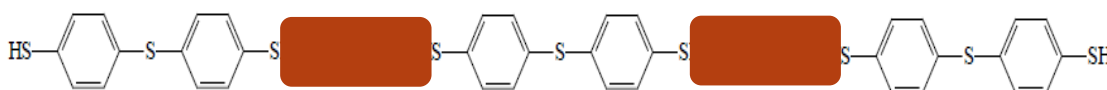


4.2.2.1 Homo-organization

The literature has demonstrated the strong interaction of thiol groups (SH) with metallic gold surface. More recently, this chemical interaction was further elucidated, and the general phenomenon that occurs is the result of this reaction: $\text{Au}_{(\text{surface})} + \text{RS-H} \rightarrow \text{Au}_{(\text{surface})} + \text{H}_2$.^{57,58}

As we added a compound bearing two thiol groups on its structure, a possibility of AuNRs assembling can be expected, as illustrated in Figure 57.

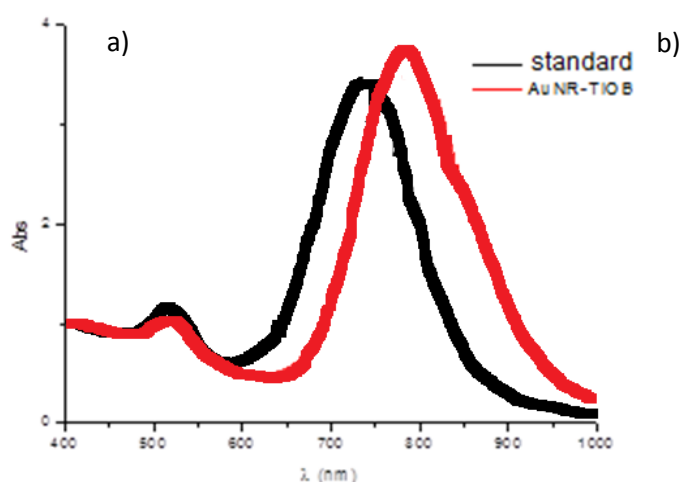
Figure 57 - Scheme of homo-organization using the TIOB.



Through the Uv-vis spectrum (Figure 58a), it is possible to observe the shift of the second band to the right after treatment with TIOB. This phenomenon can be related to the association among the AuNRs (a self-assembly of the particles). This phenomenon was also observed by Dynamic Light Scattering (DLS) that shows at least an increase of the longitudinal values for the AuNPs (see Figure 4.58b).

In order to observe these interactions of particles after treatment with this connector (TIOB), and even other potential connectors, via TEM still in course.

Figure 58 - UV-vis spectrum of gold nanorods treated with TIOB and the values of dynamic light scattering of the sample.



REFERENCES

- ¹F. P. Silva, L. M. Rossi. *Palladium on magnetite: magnetically recoverable catalyst for selective hydrogenation of acetylenic to olefinic compounds*. Tetrahedron 2014, 70, 3314.
- ²C. H. Pelisson, L. L. R. Vono, C. Hubert, A. Denicourt-Nowicki, L. M. Rossi, A. Roucoux, *Catalysis Today* 2011, 183, 124.
- ³S. Zhang et al. *Nanonecklaces assembled from gold rods, spheres, and bipyramids*. Chem. Commun.2007, 1816.
- ⁴X. Hu, W. Cheng, T. Wang, E. Wang, S. Dong. *Well-ordered end-to-end linkage of gold nanorods*.Nanotechnology 2005, 16, 10, 2164.
- ⁵K. G.Thomas, S. Barazzouk, B. I. Ipe, S. T. S. Joseph, P. V. Kamat. *Uniaxial plasmon coupling through longitudinal self-assembly of gold nanorods*. J. Phys Chem. B2004, 108, 35, 13066.
- ⁶S. A. Maier, P. G. Kik, H. A. Atwaker, S. Meltzer, E. Harel, B. E. Koel, A. A. G. Requicha. *Local detection of electromagnetic energy transport below the diffraction limit in metal nanoparticle plasmon waveguide*.Nat Mater 2003, 2, 4, 229.
- ⁷S.A. Maier, M. L. Brongersma, P. G. Kik, S. Meltzer, A. A. G. Requicha, H. A. Atwater. *Plasmonics—a route to nanoscale optical devices*.Advanced Materials 2001, 13, 19, 1501.
- ⁸P. K. Sudeep, S. T. S. Joseph, K. G. Thomas. *Selective detection of cysteine and glutathione using gold nanorods*.J. Am. Chem. Soc. 2005, 127, 18, 6516.
- ⁹F. de A. dos S.Silva, M. G. Angelo da Silva, P. R. Lima, M. R. Meneghetti, L. T.Kubota, M. O. F. Goulart. *A very low potential electrochemical detection of< i>L</i>-cysteine based on a glassy carbon electrode modified with multi-walled carbon nanotubes/gold nanorods*.Biosensors and Bioelectronics2013, 50, 202.
- ¹⁰S. E. Lohse, C. J. Murphy,Chem. *The quest for shape control: a history of gold nanorod synthesis*. Mater.2013, 25, 1250.

-
- ¹¹ P. K. Jain, X. Huang, I. H. El-Sayed, M. A. El-Sayed. *Noble Metals on the Nanoscale: Optical and Photothermal Properties and Some Applications in Imaging, Sensing, Biology, and Medicine*. *Acc. Chem. Res.* 2008, 41, 1578.
- ¹² E. C. Dreaden, A. M. Alkilany, X. Huang, C. J. Murphy, M. A. El-Sayed. *The golden age: gold nanoparticles for biomedicine*. *Chem. Soc. Rev.* 2012, 41, 2740.
- ¹³ L. Vigderman, B. P. Khanal, E. R. Zubarev. *Functional Gold Nanorods: Synthesis, Self-Assembly, and Sensing Applications*. *Adv. Mater.* 2012, 24, 4811.
- ¹⁴ P. K. Jain, M. A. El-Sayed. *Universal scaling of plasmon coupling in metal nanostructures: extension from particle pairs to nanoshells*. *Nano Lett.* 2007, 7, 2854.
- ¹⁵ M. G. Angelo da Silva, A. M. Nunes, S. M. P. Meneghetti, M. R. Meneghetti. *New aspects of gold nanorod formation via seed-mediated method*. *Comptes R. Chimie* 2013, 16, 640.
- ¹⁶ V. Polshettiwar, R. S. Varma. *Green chemistry by nano-catalysis*. *Green Chem.* 2010, 12, 743.
- ¹⁷ Y. Chen, J. Qiu, X. Wang, J. Xiu. *Preparation and application of highly dispersed gold nanoparticles supported on silica for catalytic hydrogenation of aromatic nitro compounds*. *Journal of Catalysis* 2006, 242, 227.
- ¹⁸ G. J. Hutchings. *Vapor phase hydrochlorination of acetylene: Correlation of catalytic activity of supported metal chloride catalysts*. *J. Catal.* 1985, 96, 292.
- ¹⁹ M. Haruta, T. Kobayashi, H. Sano, N. Yamada. *Novel gold catalysts for the oxidation of carbon monoxide at a temperature far below 0 °C*. *Chem. Lett.* 1987, 405.
- ²⁰ M. Haruta, N. Yamada, T. Kobayashi, S. Iijima. *Gold catalysts prepared by coprecipitation for low-temperature oxidation of hydrogen and of carbon monoxide*. *J. Catal.* 1989, 115, 301.

-
- ²¹ M.D. Hughes, Y.J. Xu, P. Jenkins, P. McMorn, P. Landon, D.I. Enache, A.F. Carley, G.A. Attard, G.J. Hutchings, F. King, E.H. Stitt, P. Johnston, K. Griffin, C.J. Kiely. *Tunable gold catalysts for selective hydrocarbon oxidation under mild conditions*. *Nature* 2005, 437, 1132.
- ²² D.I. Enache, J.K. Edwards, P. Landon, B. Solsona-Espriu, A.F. Carley, A.A. Herzing, M. Watanabe, C.J. Kiely, D.W. Knight, G. J. Hutchings. *Solvent-Free Oxidation of Primary Alcohols to Aldehydes Using Au-Pd/TiO₂ Catalysts*. *Science* 2006, 311, 362.
- ²³ F. Moreau, G. C. Bond, A. O. Taylor. *Gold on titania catalysts for the oxidation of carbon monoxide: control of pH during preparation with various gold contents*. *J. Catal.* 2005, 231, 105.
- ²⁴ S. Miao, Y. Deng. *Au-Pt/Co₃O₄ catalyst for methane combustion*. *Appl. Catal. B Environ.* 2001, 31, L1.
- ²⁵ G. C. Bond, P. A. Sermon, G. Webb, D. A. Buchanan, P. B. Wells, *Hydrogenation over supported gold catalysts*. *J Chem Soc Chem Commun* 1973, 13, 444.
- ²⁶ G. C. Bond, C. Louis, D. T. Thompson. *Catalysis by gold*. 2006 Imperial College Press, London
- ²⁷ C. Mohr, H. Hofmeister, P. Claus. *The influence of real structure of gold catalysts in the partial hydrogenation of acrolein*. *J Catal* 2003, 213, 86.
- ²⁸ P. Claus. *Heterogeneously catalysed hydrogenation using gold catalysts*. *Appl Catal A* 2005, 291, 222.
- ²⁹ L. Barrio, P. Liu, J. A. Rodríguez, J. M. Campos-Martín, J. L. G. Fierro. *A density functional theory study of the dissociation of H₂ on gold clusters: Importance of fluxionality and ensemble effects*. *J Chem Phys* 2006, 125, 164715.
- ³⁰ L. Stobinski, L. Zommer, R. Dus. *Molecular hydrogen interactions with discontinuous and continuous thin gold films*. *Appl Surf Sci* 1999, 141, 319.
- ³¹ F. Cárdenas-Lizana, M.A. Keane. *The development of gold catalysts for use in hydrogenation reactions*. *J Mater Sci* 2013, 48, 543.
- ³² J. Harris. *On vibrationally-assisted dissociation of H₂ at metal surfaces*. *J. Surf. Sci* 1989, 221, 335.
- ³³ B. Campo, M. Volpe, S. Ivanova, R. Touroude. *On vibrationally-assisted dissociation of H₂ at metal surfaces*. *J Catal* 2006, 242, 162.

-
- ³⁴C. Milone, R. Ingoglia, L. Schipilliti, C. Crisafulli, G. Neri, S. Galvagno. *Selective hydrogenation of α , β -unsaturated ketone to α , β -unsaturated alcohol on gold-supported iron oxide catalysts: Role of the support.* *J Catal*2005, 236, 80.
- ³⁵M. Liu, W. Yu, H. Liu, J. Zheng. *Preparation and Characterization of Polymer-Stabilized Ruthenium–Platinum and Ruthenium–Palladium Bimetallic Colloids and Their Catalytic Properties for Hydrogenation of o-Chloronitrobenzene.**J Colloid Interface Sci*1999, 214, 231.
- ³⁶E. Bus, J. T. Miller, J. A. van Bokhoven. *Hydrogen chemisorption on Al₂O₃-supported gold catalysts.**J PhysChem B*2005, 109, 14581.
- ³⁷A. C. Gluhoi, H. S. Vreeburg, J. W. Bakker, B. E. Nieuwenhuys. *Activation of CO, O₂ and H₂ on gold-based catalysts.**ApplCatal A*2005, 291, 145.
- ³⁸M. Boronat, P. Concepcion, A. Corma. *Unravelling the nature of gold surface sites by combining IR spectroscopy and DFT calculations. Implications in catalysis.* *J Phys Chem C*2009, 113, 16772.
- ³⁹A. Corma, M. Boronat, S. Gonzalez, F. Illas. *On the activation of molecular hydrogen by gold: a theoretical approximation to the nature of potential active sites.**Chem. Commun*2007, 32, 3371.
- ⁴⁰M. Boronat, F. Illas, A. Corma. *Active Sites for H₂ Adsorption and Activation in Au/TiO₂ and the Role of the Support.**J PhysChemA*2009, 113, 3750.
- ⁴¹A. S. K. Hashmi, G. J. Hutchings. *Gold catalysis.**Angew.Chem.Int*2006, Ed 45, 7896.
- ⁴²A. G. Sault, R. J. Madix, C. T. Campbell. *Adsorption of oxygen and hydrogen on Au (110)-(1 \times 2).* *Surf Sci*1986,169, 347.
- ⁴³J. Schulz, A. Roucoux, H. Patin. *Stabilized Rhodium(0) Nanoparticles: A Reusable Hydrogenation Catalyst for Arene Derivatives in a Biphasic Water-Liquid System.**Chem. Eur. J.* 2000, 6, 4.
- ⁴⁴a) C. Larpent, H. Patin. *Catalytic Hydrogenations in Biphasic Liquid-Liquid Systems: Part 2: Utilization of Sulfonated Tripod Ligands for the Stabilization of Colloidal Rhodium.* *J. Mol. Catal.* 1988, 44, 191. b) C. Larpent, E. Bernard, F. Brisse-Le Menn, H. Patin. *Biphasic liquid-liquid hydrogenation catalysis by aqueous colloidal suspensions of rhodium: The choice of the protective-colloid agent and the role of interfacial phenomena.* *J. Mol. Catal.* A1997, 116, 277. c)

-
- J. Schulz, A. Roucoux, H. Patin. *Unprecedented efficient hydrogenation of arenes in biphasic liquid-liquid catalysis by re-usable aqueous colloidal suspensions of rhodium*. Chem. Commun. 1999, 535.
- ⁴⁵ a) G. Schmid. *Large clusters and colloids. Metals in the embryonic state*. Chem. Rev. 1992, 92, 1709. b) L. N. Lewis. *Chemical catalysis by colloids and clusters*. Chem. Rev. 1993, 93, 2693. c) G. Schmid, V. C. H. Weinhem, *In Clusters and Colloids*, 1994, 459.
- ⁴⁶ For the hydrogenation of C=C double or triple bonds, see for example: a) H. Bönemann, W. Brijoux, K. Siepen, J. Hormes, R. Franke, J. Pollmann, J. Rothe. *Surfactant stabilized palladium colloids as precursors for cis-selective alkyne-hydrogenation catalysts*. Appl. Organomet. Chem. 1997, 11, 783. b) H. Bönemann, W. Brijoux, A. S. Tilling, K. Siepen. *Application of heterogeneous colloid catalysts for the preparation of fine chemicals*. Top. Catal. 1997, 4, 217. c) W. Yu, M. Liu, H. Liu, X. Ma, Z. Liu. *Preparation, characterization, and catalytic properties of polymer-stabilized ruthenium colloids*. J. Colloid Interface Sci. 1998, 208, 439. d) H. Hirai, N. Yakura, Y. Seta, S. Hodoshima. *Characterization of palladium nanoparticles protected with polymer as hydrogenation catalyst*. React. Funct. Polym. 1998, 37, 121. e) E. Sulman, Y. Bodrova, V. Matveeva, N. Semagina, L. Cervený, V. Kurtc, L. Bronstein, O. Platonova, P. Valetsky. *Hydrogenation of dehydrolinalool with novel catalyst derived from Pd colloids stabilized in micelle cores of polystyrene-poly-4-vinylpyridine block copolymers*. Appl. Catal. A 1999, 176, 75.
- ⁴⁷ a) F. Launay, A. Roucoux, H. Patin. *Ruthenium colloids: A new catalyst for alkane oxidation by tBHP in a biphasic water-organic phase system*. Tetrahedron Lett. 1998, 39, 1353. b) Y. Shiraishi, N. Toshima. *Colloidal silver catalysts for oxidation of ethylene*. J. Mol. Catal. A 1999, 141, 187.
- ⁴⁸ G. Schmid, H. West, H. Mehles, A. Lehnert, *Hydrosilation reactions catalyzed by supported bimetallic colloids*. Inorg. Chem. 1997, 36, 891.
- ⁴⁹ C. Larpent, H. Patin. *Catalytic Hydrogenations in Biphasic Liquid-Liquid Systems: Part 2: Utilization of Sulfonated Tripod Ligands for the Stabilization of Colloidal Rhodium*. J. Mol. Catal. 1988, 44, 191.

-
- ⁵⁰ a) C. W. Chen, M. Akashi. Synthesis, characterization, and catalytic properties of colloidal platinum nanoparticles protected by poly (N-isopropylacrylamide). *Langmuir* 1997, 13, 6465.
- ⁵¹ a) Y. Lin, R. G. Finke. *Novel Polyoxoanion- and Bu₄N⁺-Stabilized, Isolable, and Redissolvable, 20-30-Å Ir₃₀₀₋₉₀₀ Nanoclusters: The Kinetically Controlled Synthesis, Characterization, and Mechanism of Formation of Organic Solvent-Soluble, Reproducible Size, and Reproducible Catalytic Activity Metal Nanoclusters*. *J. Am. Chem. Soc.* 1994, 116, 8335. b) Y. Lin, R. G. Finke. *A More General Approach to Distinguishing "Homogeneous" from "Heterogeneous" Catalysis: Discovery of Polyoxoanion- and Bu₄N⁺-Stabilized, Isolable and Redissolvable, High-Reactivity Ir_{approx.190-450} Nanocluster Catalysts*. *Inorg. Chem.* 1994, 33, 4891.
- ⁵² J. Schulz, A. Roucoux, H. Patin. *Unprecedented efficient hydrogenation of arenes in biphasic liquid-liquid catalysis by re-usable aqueous colloidal suspensions of rhodium*. *Chem. Commun.* 1999, 535.
- ⁵³ K. Weissermel, H. J. Arpe, *In Industrial Organic Chemistry*, 2nd ed., VCH, New York, 1993, 343.
- ⁵⁴ a) S. Siegel, *In Comprehensive Organic Synthesis*, Vol. 5 (Eds.: B. M. Trost, I. Fleming), Pergamon Press, New York, 1991. b) M. S. Eisen, T. J. Marks. *Supported organoactinide complexes as heterogeneous catalysts. A kinetic and mechanistic study of facile arene hydrogenation*. *J. Am. Chem. Soc.* 1992, 114, 10358.
- ⁵⁵ a) I. P. Rothwell. *A new generation of homogeneous arene hydrogenation catalysts*. *Chem. Commun.* 1997, 1331. b) L. Plasseraud, G. Süß-Fink. *Catalytic hydrogenation of benzene derivatives under biphasic conditions*. *J. Organomet. Chem.* 1997, 539, 163.
- ⁵⁶ a) P. Drognat, L. André, M. Lemaire, D. Richard, P. Gallezot. *A stereoselective reduction of dibenzo-18-crown-6 ether to dicyclohexyl-18-crown-6 ether*. *J. Mol. Catal.* 1993, 78, 257. b) K. Nasar, F. Fache, M. Lemaire, J.C. BeÂziat, M. Besson, P. Gallezot. *Stereoselective reduction of disubstituted aromatics on colloidal rhodium*. *J. Mol. Catal.* 1994, 87, 107±115.
- ⁵⁷ S. Pierrat, I. Zins, B. Aaron, C. Sönnichsen. *Self-Assembly of Small Gold Colloids with Functionalized Gold Nanorods*. *Nano Lett.* 2007, 7, 259.

-
- ⁵⁸ K. K. Caswell, J. N. Wilson, U. H. F. Bunz, C. J. Murphy. *Preferential End-to-End Assembly of Gold Nanorods by Biotin–Streptavidin Connectors*. *J. Am. Chem. Soc.* 2003, 125, 13914.

Final considerations

In summary, a novel library of easily tunable hydroxylated ammonium surfactants were synthesized and used as versatile growth-driving agents of AuNPs. This original family provides more flexible shape templates than the CTABr, giving rise to AuNPs of various morphologies (rods, spheres, prisms...), and different sizes through the easy modulation of the capping agent (length of the lipophilic chain or of the polar head, and the counter-ion), with good yields and selectivities without size/shape selection step. The novelty concerns the presence of the hydroxylated group which proves to be essential to increase the steric hindrance on the particle surface, thus leading to the formation of rod-like particles of modulated aspect ratios. Further investigations on the interaction of the driving agent within the facets of AuNRs will constitute a breakthrough to better understand the influence of the hydroxyl group in the growth process.

The kinetics of the NRs growth was studied through Uv-vis measurements to understand how fast these particles growth under the influence of the different driving agents are, as well the differences in size and aspect ratio observed among these agents. These promising results open new perspectives in the design of original growth driving agents to produce anisotropic gold nanoparticles with well-controlled morphologies and dimensions according to the desired application, in aqueous solution without any mixture with CTABr or addition of different additives as ions and solvents.

This control of the growth process generated by this series of surfactants allows the modulation of the structural parameters of gold nanorods and opens interesting perspectives in terms of applications. Unprecedented in the literature, these nanorods were evaluated for catalytic hydrogenation of aromatic compounds such as toluene, anisole, styrene, and acetophenone. They showed good catalytic activity in the hydrogenation of these alkenes and aromatics as the spherical nanoparticles.

Another way to reach this kind of control is to functionalize the gold nanorods with thiol derivatives which have been shown to be regioselective for the extremities of the rods and total spherical surface. This behavior has opened the possibility to link together nanoparticles with the same or different

shapes such as in an end-to-end fashion way in case of rod forms. Thus, the main contribution of this study is to offer new possibilities of interactions of interparticles, favoring the preparation of materials with innovative properties.

The results of this thesis work are promising and cover a range of perspectives as: i) changing different parameters of the surfactants structures, and investigating their influence on the dynamic formation of these metal nanoparticles, ii) performance of more catalytic tests with nanoparticles obtained in both shapes (rod and spheres) to define the selectivity degree of these colloidal dispersion as catalysts as function of their morphologies, iii) performance of catalytic reactions with different conditions to define the kinetic selectivity conversion among the products of the hydrogenation reactions, iv) tests of new substrates, v) syntheses of anisotropic nanoparticles with other metals and evaluate their catalytic activities, and vi) improvement of strategies to promote the interaction between particles by self-assembly process.

APPENDIX

APPENDIX

Synthesis conditions:

Figure 22 - Synthesis conditions: 0.005 mmol de HAuCl_4 (0.2 mL; 25 mmol/L); 0.0006 mmol of AgNO_3 (0.6 mL; 0.0040 mol/L); 0.0055 mmol of ascorbic acid (0.07 mL; 0.0788 mol/L); 0.060 mL of seed and 7.3 mL of surfactant (0.064 mol/L).

Figure 24 - Synthesis conditions: 0.005 mmol of HAuCl_4 (0.2 mL; 25 mmol/L); 0.0006 mmol of AgNO_3 (0.6 mL; 0.0040 mol/L); 0.0055 mmol of ascorbic acid (0.07 mL; 0.0788 mol/L); 0.060 mL of the seed solution, and 7.3 mL of the surfactant solution (0.064 mol/L).

Figure 25 - Synthesis conditions: 0.005 mmol de HAuCl_4 (0,2 mL; 25 mmol/L); 0.0006 mmol of AgNO_3 (0.6 mL; 0.0040 mol/L); 0.0055 mmol of ascorbic acid (0,07 mL; 0.0788 mol/L); 0.060 mL of seed and (a) 7.3 mL of surfactant (0.096 mol/L) and b) 7.3 mL of surfactant (0.128 mol/L).

Figure 26 - Synthesis conditions: 0.005 mmol de HAuCl_4 (0,2 mL; 25 mmol/L); 0.0006 mmol of AgNO_3 (0.6 mL; 0,0040 mol/L); 0.0055 mmol of ascorbic acid (0.07 mL; 0.0788 mol/L); 0.060 mL of seed and 7.3 mL of surfactant (0.064 mol/L).

Figure 27 - Synthesis conditions: a) 0.005 mmol de HAuCl_4 (0.2 mL; 25 mmol/L); 0.0006 mmol of AgNO_3 (0.6 mL; 0.0040 mol/L); 0.0055 mmol of ascorbic acid (0.07 mL; 0.0788 mol/L); 0.060 mL of seed and 7.3 mL of surfactant (0.016 mol/L). b) 0.005 mmol de HAuCl_4 (0.2 mL; 25 mmol/L); 0.0006 mmol of AgNO_3 (0.6 mL; 0.0040 mol/L); 0.0055 mmol of ascorbic acid (0.07 mL; 0.0788 mol/L); 0.060 mL of seed and 7.3 mL of surfactant (0.0032 mol/L). c and d) 0.005 mmol de HAuCl_4 (0.2 mL; 25 mmol/L); 0.0006 mmol of AgNO_3 (0.6 mL; 0.0040 mol/L); 0.0055 mmol of ascorbic acid (0.07 mL; 0.0788 mol/L); 0.060 mL of seed and 7.3mL of surfactant (0.00064 ; 0.0016 mol/L,

respectively).

Figure 28 - Synthesis conditions: a) 0.005 mmol de HAuCl_4 (0.2 mL; 25 mmol/L); 0.0006 mmol of AgNO_3 (0.6 mL; 0.0040 mol/L); 0.0055 mmol of ascorbic acid (0.07 mL; 0.0788 mol/L); 0.060 mL of seed and 7.3 mL of surfactant (0.064 mol/L). b) 0.005 mmol de HAuCl_4 (0.2 mL; 25 mmol/L); 0.0006 mmol of AgNO_3 (0.6 mL; 0.0040 mol/L); 0.0055 mmol of ascorbic acid (0.07 mL; 0.0788 mol/L); 0.060 mL of seed and 7.3 mL of surfactant (0.032 mol/L).

Figure 29 - Synthesis conditions: 0.005 mmol de HAuCl_4 (0.2 mL; 25 mmol/L); 0.0006 mmol of AgNO_3 (0.6 mL; 0.0040 mol/L); 0.0055 mmol of ascorbic acid (0.07 mL; 0.0788 mol/L); 0.060 mL of seed and 7.3 mL of surfactant (0.064 mol/L).

Figure 31 - Synthesis conditions: 0.005 mmol de HAuCl_4 (0.2 mL; 25 mmol/L); 0.0006 mmol of AgNO_3 (0.6 mL; 0.0040 mol/L); 0.0055 mmol of ascorbic acid (0.07 mL; 0.0788 mol/L); 0.060 mL of seed and 7.3 mL of surfactant (0.064 mol/L).

Figure 32 - Synthesis conditions: 0.005 mmol de HAuCl_4 (0.2 mL; 25 mmol/L); 0.0006 mmol of AgNO_3 (0.6 mL; 0.0040 mol/L); 0.0055 mmol of ascorbic acid (0.07 mL; 0.0788 mol/L); 0.060 mL of seed and 7.3 mL of surfactant (0.064 mol/L).

Figure 33 - Synthesis conditions: 0.005 mmol de HAuCl_4 (0.2 mL; 25 mmol/L); 0.0006 mmol of AgNO_3 (0.6 mL; 0.0040 mol/L); 0.0055 mmol of ascorbic acid (0.07 mL; 0.0788 mol/L); 0.060 mL of seed and 7.3 mL of surfactant (0.064 mol/L).

Figure 34 - Synthesis conditions: 0.005 mmol de HAuCl_4 (0.2 mL; 25 mmol/L); 0.0006 mmol of AgNO_3 (0.6 mL; 0.0040 mol/L); 0.0055 mmol of ascorbic acid (0.07 mL; 0.0788 mol/L); 0.060 mL of seed and 7.3 mL of surfactant (0.064 mol/L).

Figure 35 - Synthesis conditions: 0.005 mmol de HAuCl_4 (0.2 mL; 25 mmol/L); 0.0006 mmol of AgNO_3 (0.6 mL; 0.0040 mol/L); 0.0055 mmol of ascorbic acid (0.07 mL; 0.0788 mol/L); 0.060 mL of seed and 7.3 mL of surfactant NOx16: 0.064 mol/L, and 0.016 mol/L; NMeEph16Br: 0.016 mol/L, and 0.0064 mol/L)

PUBLICATIONS OF THIS THESIS WORK



Full paper/Mémoire

New aspects of gold nanorod formation via seed-mediated method

Monique G.A. da Silva, Ábner M. Nunes, Simoni M.P. Meneghetti, Mario R. Meneghetti*

Grupo de Catálise e Reatividade Química–GCaR, Instituto de Química e Biotecnologia da Universidade Federal de Alagoas, Av. Lourival de Melo Mota, s/n CEP 57072-970, Maceió, AL, Brazil

ARTICLE INFO

Article history:

Received 29 August 2012

Accepted after revision 16 January 2013

Available online 21 February 2013

Keywords:

Colloids
Nanostuctures
Nanoparticles
Gold nanorods
Nanotechnology
Nanoparticle growth

ABSTRACT

Gold nanorods (AuNRs) were obtained via a wet chemistry technique, in aqueous medium, employing crystallisation seeds. The kinetics of formation, the aspect ratio, and the selectivity of the particles were evaluated according to the parameters of synthesis: the growth-driving agent, seed, and gold precursor concentrations. In 2–4 h, the rod particles attained the expected size and shape under kinetic control, and were stable for at least 2 days. In order to obtain good quality AuNRs in good yields, without enrichment, we suggest keeping the growth-driving agent/gold molar ratio, the Au^I/seed ratio, and the concentration of the reagents in the final solution within specific ranges. For example, even if good molar ratios between the reagents are maintained, relatively highly concentrated reaction solutions lead to AuNRs with lower aspect ratios. The main properties of the prepared colloidal systems and the nanoparticles were evaluated by UV–vis spectroscopy and transmission electron microscopy, respectively.

© 2013 Académie des sciences. Published by Elsevier Masson SAS. All rights reserved.

1. Introduction

For centuries, the search for new materials with precise characteristics and applications has been one of the most important stimulants of technological development [1]. In general, to fabricate the most simple or complex device or object, it is essential to search for materials that exhibit the desired physico-chemical properties for the aspired application. But can a particular material, with identical chemical composition and structural arrangement, display different properties? The answer is yes, but this largely depends on the dimensions of the material itself or the dimensions of the components [2,3].

Outstanding properties can arise when materials are in the nanometric scale, but this is not only due to dimensional features, like the surface/volume ratio (very high for nanostructures), but it also depends on the form, environment, and organisation of the particles that

comprise the nanostructured material. Indeed, these features are consequence of a “nano-effect”, and most of them are associated with quantum-like laws [4,5].

Metal particles, like Au, Ag, and Cu, are known to absorb specific wavelengths of the visible spectrum when they possess nanometric dimensions. This singular absorption is due to the collective resonant oscillation of the electrons of the conducting band promoted by the electric field of the incident light at the particle surface [6,7]. This effect is called surface plasmon resonance (SPR), and was first elucidated by Mie in 1908 [8,9]. For that reason, for example, the optical properties of gold nanoparticles (AuNPs) can be significantly modified if their dimensions are in the range of 1 to 100 nm [10,11]. Indeed, with precise synthesis control, it is possible to prepare colloidal solutions of AuNPs with different colours [12].

Spherical AuNPs typically display one absorption band in the visible or near-infrared spectrum, and just one range of these electromagnetic radiations can induce the expected SPR (Fig. 1). On the other hand, anisotropic nanoparticles display different absorption bands since different SPR energies are generated [6]. Nanorods and

* Corresponding author.

E-mail address: mrm@qui.ufal.br (M.R. Meneghetti).

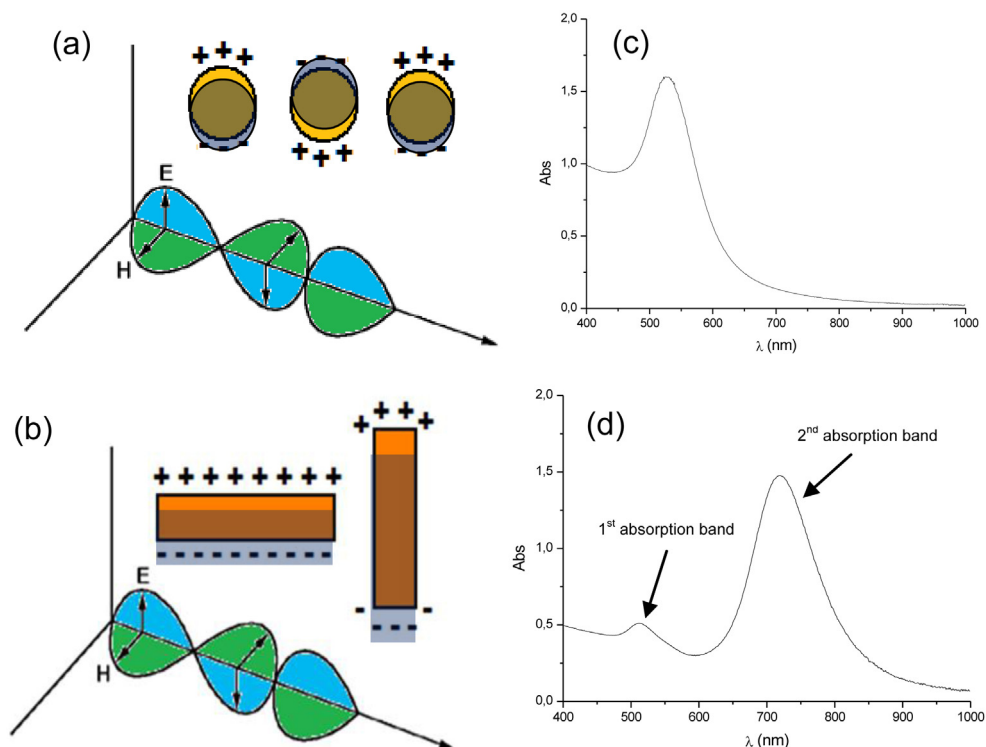


Fig. 1. (a) Illustration showing the single surface plasmon resonance on a spherical (a) and rod-like (b) gold nanoparticles, generated due to the interaction of the particle with the electromagnetic field of the incident light. (c) and (d) are an illustration of the respective typical outline UV–vis absorption spectrum expected for those colloidal solutions.

nanowires, for example, display two typical absorption bands; one related to the longitudinal, and the other to the transversal SPR (Fig. 1) [13].

It is worth noting that one can profit from the optical features of AuNP-based structured systems and use relatively simple UV–vis(-NIR) spectroscopy to evaluate and follow the synthetic procedures and the characteristics of the final product [14,15].

This great versatility of colloidal systems of AuNPs, in terms of optical properties, continues to attract the attention of several research groups. New synthetic strategies to obtain specific AuNPs in high yields, for precise applications [16,17], are frequently observed in the modern literature [10,18,19]. In addition to studies in the field of photonics [20] and optics [6,21], applications of AuNPs can also be found in areas like catalysis [22], sensors [23], medical diagnosis [24,25], and tumour treatment [26,27].

Metal nanoparticles can be prepared on the bases of physical and chemical methods, following two main approaches: (i) bottom-up or (ii) top-down methodologies. Nanoparticles obtained via the top-down approach are based on physical methods, and are normally generated from larger particles. Sputtering [18,28,29], sonolysis [30], and nanolithography [31,32] are examples of techniques based on this practice. On the other hand, methods based on “wet chemistry” follow, in general, the bottom-up approach. In this latter case, nanoparticles are frequently

prepared from molecular metal precursors that, after specific chemical transformations, generate very reactive “solvated” metal atoms that soon interact to each other via metal–metal bonds until they reach the size and shape of the desired metal nanoparticle. These nanoparticles remain, in many cases, dispersed in the liquid matrix, like colloidal solutions [33,34].

Of all the possible metal nanoparticle shapes that can be generated, the spherical ones are the most thermodynamically stable, since, with this shape, the lowest surface potential is achieved, and, for this reason, the particles are easier to obtain. However, depending on the concentration of the metal source in the solution and/or the presence of particular chemical compounds (growth-driving agents), other forms of nanoparticles can be obtained [35,36]. Indeed, there are a series of studies that report on the preparation of nanoparticles of several different forms, i.e. tetrahedral [37], cubic [38], prismatic [39], cylindrical [40], star-like [41], hollow [42], disk [43], etc. [44].

Several research groups have focused on anisotropic nanoparticle synthesis, especially because of their optical properties, which are closely related to the presence of different surface plasmons [45]. The most common strategies used to control the shape and size of anisotropic nanoparticles are based on wet chemistry methodologies [46–50].

Among the range of shapes possible for AuNP, rod-like particles are particularly well studied. In particular, many

aspects of AuNRs synthesis have been discussed in the literature, especially regarding how to obtain particles with different sizes and shapes [2,44,51,52]. Indeed, AuNRs can be obtained with a high level of morphological control and different aspect ratios (the ratio between the particle length and width). They can also achieve dimensions of a few nanometres to ca. 1 μm [16,44,53–55].

Different procedures can be used to obtain AuNRs [56–59], but the seed-mediated methods are the most commonly employed [60]. The reference works by Murphy et al. [44,61] and El-Sayed et al. [62] showed that AuNRs can be prepared from very small AuNPs (“seeds” of 3 to 4 nm in diameter), which act as nucleation sites for the formation of the desired particles. The seeds are added into a growth solution, which basically contain Au^{I} species that can be seen as the “monomer precursors” that are easily reduced to $\text{Au}(0)$ at the surface of an AuNP in the presence of a mild reducing agent, such as ascorbic acid (AA). A small amount of silver nitrate (AgNO_3) is also added to the growth solution. It seems to play an important role in obtaining AuNRs in high yields, but its role still incites discussion [63].

It is important to remark that, in this methodology, the presence of a chemical species that interact with the growing particle is essential, as it acts as a growth-driving agent – normally surfactants, like cetyltrimethylammonium bromide (CTAB). The role of these molecules is not just for particle protection, by avoiding particle agglomeration, but also to allow dissymmetric particle growth [47,64–68].

In this case, dissymmetric growth is mainly due to the dissimilar force interactions between the distinct crystal facets of the growing particle, which display different surface potentials [69], and the growth-driving agent. This leads to distinct rates of facet growth, permitting the formation of anisotropic nanoparticles. In other words, some facets are blocked by the growth-driving agent, provoking different rates of facet growth [64].

Fig. 2 illustrates, in a very simple way, the dissymmetric growth mechanism of AuNRs. Of course, other factors

like reaction temperature [70], seed and/or metal source concentrations [60], and surfactant chemical structure and concentration are variables that must be controlled for optimal AuNR production [67,71].

Although AuNRs can currently be produced with a high level of control, with different sizes, aspect ratios, and low polydispersity, there are some aspects of their formation that are not yet fully understood. It is in this context that this study was proposed, to improve our understanding of AuNR formation.

2. Experimental

2.1. Materials

Tetrachloroauric acid ($\text{HAuCl}_4 \cdot 3 \text{H}_2\text{O}$, 99.9%, Aldrich), sodium borohydride (NaBH_4 , > 98%, Acros Organics), AA (99%, Vetec), CTAB (99%, Acros Organics) and AgNO_3 (> 99%, Reagen) were used as purchased. Deionised water (Deionizer Direct-Q3 Millipore) was used in the preparation of all aqueous solutions. All the glassware was cleaned with aqua regia and rinsed with deionised water prior to experiments.

2.2. Synthesis of gold nanorods

All colloidal solutions containing AuNR were prepared from the mixture of two solutions, i.e. the seed and growth solutions, according to seed-mediated methods, and adapted from reference [54].

The seed solution was prepared in a 20 mL flask in which two aqueous solutions of $\text{HAuCl}_4 \cdot 3 \text{H}_2\text{O}$ (5.0 mL; 0.5 mmol/L) and CTAB (2.5 mL; 0.20 mol/L) were added. In the sequence, an ice-cold aqueous solution of NaBH_4 (0.6 mL; 0.01 mol/L) was added at one time. Immediately, the colour changed from dark yellow to brownish. The resulting solution was kept under gentle magnetic stirring for 2 min. The resulting solution was used for a period of 2 h after the preparation. This solution contained ca. 1.25×10^{14} particles of 4 nm/mL, and was used in all experiments.

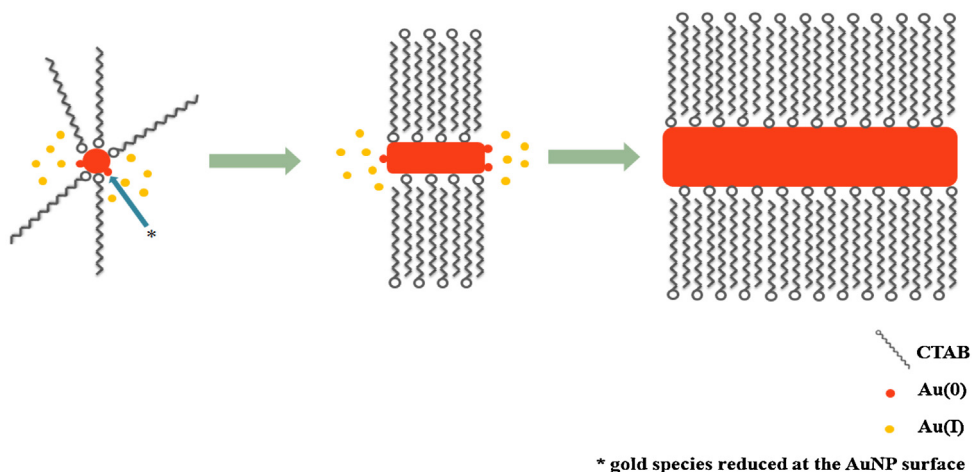


Fig. 2. Schematic illustration of the dissymmetric growth of an gold nanorods from a seed particle and Au^{I} ion species that are reduced to $\text{Au}(0)$ at the surface of the metal particle.

According to the experiment, different growth solutions were prepared. For example, for illustration, in a 20 mL glass tube, three aqueous solutions of $\text{HAuCl}_4 \cdot 3 \text{H}_2\text{O}$ (5.0 mL; 1.0 mmol/L), CTAB (2.5 mL; 0.20 mol/L), and AgNO_3 (0.150 mL; 0.40 mmol/L) were added. Under stirring, an aqueous solution of AA (0.070 mL; 0.80 mmol/L) was added all at once. Immediately, the colour changed from yellow to colourless.

Finally, the different colloids containing AuNRs were obtained by mixing appropriate quantities of seed and growth solutions, as well as CTAB. In a typical experiment, the seed solution (12 μL) was added, under gentle stirring for 10 s, into a recently prepared growth solution (7.72 mL; 0.64 mmol/L of Au^{I} species), and left undisturbed for at least 4 h.

2.3. Characterisation

Electronic absorption spectra of the colloidal solutions were obtained using a Varian Model Cary 50 Scan UV-Vis/near-IR spectrophotometer. The setup was configured to fix the baseline of the deionised water absorption band from 400 to 1 000 nm, using quartz cells with path length of 1.0 cm. The particle size and shape analysis of the AuNRs were performed using a FEI-Tecnaï 20 transmission electron microscope operating at 200 kV or a FEI-Morgani 268D operating at 100 kV. The samples were prepared by evaporating a thin film of nanoparticle solution on Holey carbon or formvar-coated copper grids for at least 24 h in a desiccator. Micrographs from transmission electron microscopy (TEM) were evaluated using the Sigma Scan program to determine the particle size distribution, measuring approximately 100 nanoparticles from each sample.

3. Results and discussion

The AuNRs were prepared by the seed-mediated method, adapted from the method developed by Murphy et al. [71]. As already mentioned, this method leads to high yields of AuNRs with a high degree of size and aspect ratio control. Nevertheless, slight changes in the synthesis conditions, for example, the quality of the water used to prepare the solutions, the amount of matter, and the concentration of the components, can induce significant modifications on the features of the AuNR. For this reason, we carried out a systematic study related to the formation of AuNR by modifying three parameters of synthesis, i.e.

CTAB, seed, and monomer amounts in the reaction medium. It is worth remarking that all analyses performed here used samples on which no previous treatment has been carried out.

3.1. Kinetic study of gold nanorods formation

In order to verify the dynamic of formation and range of stability of the aqueous AuNR-based colloids, we carried out a kinetic study of particle formation using UV-vis spectroscopy; (Fig. 3). We evaluated the growth process (AuNR formation) from the first moments until a period of one week, taking a series of electronic absorption spectra of samples prepared like solution B (Table 1). During this time, the colloid displayed dynamic behaviour in terms of colour change and colour intensity. Nevertheless, it is possible to divide the formation process of AuNRs into three main stages after the addition of the seed into the growth solution:

- the period from 0 to 2 h is characterised by the time needed for the AuNRs to form, with depletion of the Au^{I} source;
- from 2 to 48 h, no significant change in the colloidal system is detected. This is the best period in which the colloid can be manipulated and studied;
- from two days on, the main mechanism of the growth process seems to be characterised by the occurrence of Ostwald ripening [72], i.e. larger particles continue to grow, while smaller ones (more unstable, with a higher surface potential) get smaller [2].

This last process explains the significant increase in the absorption bands. In this case, the smaller particles are a second reservoir of gold species for the growth process.

In the first hour of particle formation, it was possible to verify the regular growth of nanorods since the intensities of their respective surface plasmon absorption bands increased relatively quickly. After this stage, the intensities of the absorption bands did not change significantly over a period of 48 h. However, from this period on, Ostwald ripening dictated the growth process, characterised by an enhancement in the intensity of the plasmon absorption bands (Fig. 3).

It was also interesting to note that, during the first 2 h of AuNR formation, the maximum absorption of the second band shifted to the red region of the UV-vis spectrum and

Table 1

Reaction conditions^a for the preparation of gold nanorods in the presence of different amounts of CTAB and some characteristics of the colloids obtained.

Sample	Volume of CTAB stock solution (mL) ^b	[CTAB] (mmol/L) ^c	CTAB: Au molar ratio	$\lambda_{\text{max}1}$ (nm)	$\lambda_{\text{max}2}$ (nm)	AuNR length (nm)	Aspect ratio
A	5.0	97	200	514	730	45 ± 4	2.8
B	2.5	64	100	515	732	45 ± 3	3.0
C	1.0	32	40	513	735	50 ± 10	–
D^d	0.5	17	20	527	775	–	–

^a Reagent amounts employed: 5.0 mL of tetrachloroauric acid ($\text{HAuCl}_4 \cdot 3 \text{H}_2\text{O}$) (1.0 mmol/L), 0.150 mL of silver nitrate (AgNO_3) (4.0 mmol/L), 0.070 mL of ascorbic acid (80 mmol/L), and 12 μL of seed solution.

^b Concentration of the CTAB stock solution: 0.20 mmol/L.

^c Concentration of the CTAB in the colloidal system.

^d Low yield of AuNR, large amount of spherical AuNP are present.

turned back (blue shift) to around 790 nm (maintaining this wavelength and absorption intensity from 4 to 48 h after the start of the particle formation; Fig. 3). The observation of this shift suggests that there is a significant change in the aspect ratio (length \times width) of the particles during particle formation.

3.2. Effect of the CTAB:Au molar ratio

In this study, four growth solutions containing relatively low and high CTAB:Au molar ratios were prepared.

Those solutions contained different amounts of CTAB, keeping the other component quantities constant. Into them, the same amount of seed particles was added. According to the method employed, the same amount of particles must be formed in all solutions, since the same amounts of seeds were used. The reaction conditions for this study are summarised in Table 1.

Fig. 4 shows the electronic absorption spectra of the colloids obtained 24 h after the addition of the seeds in the respective growth solution. In all measurements, the presence of two maximum absorption bands that are

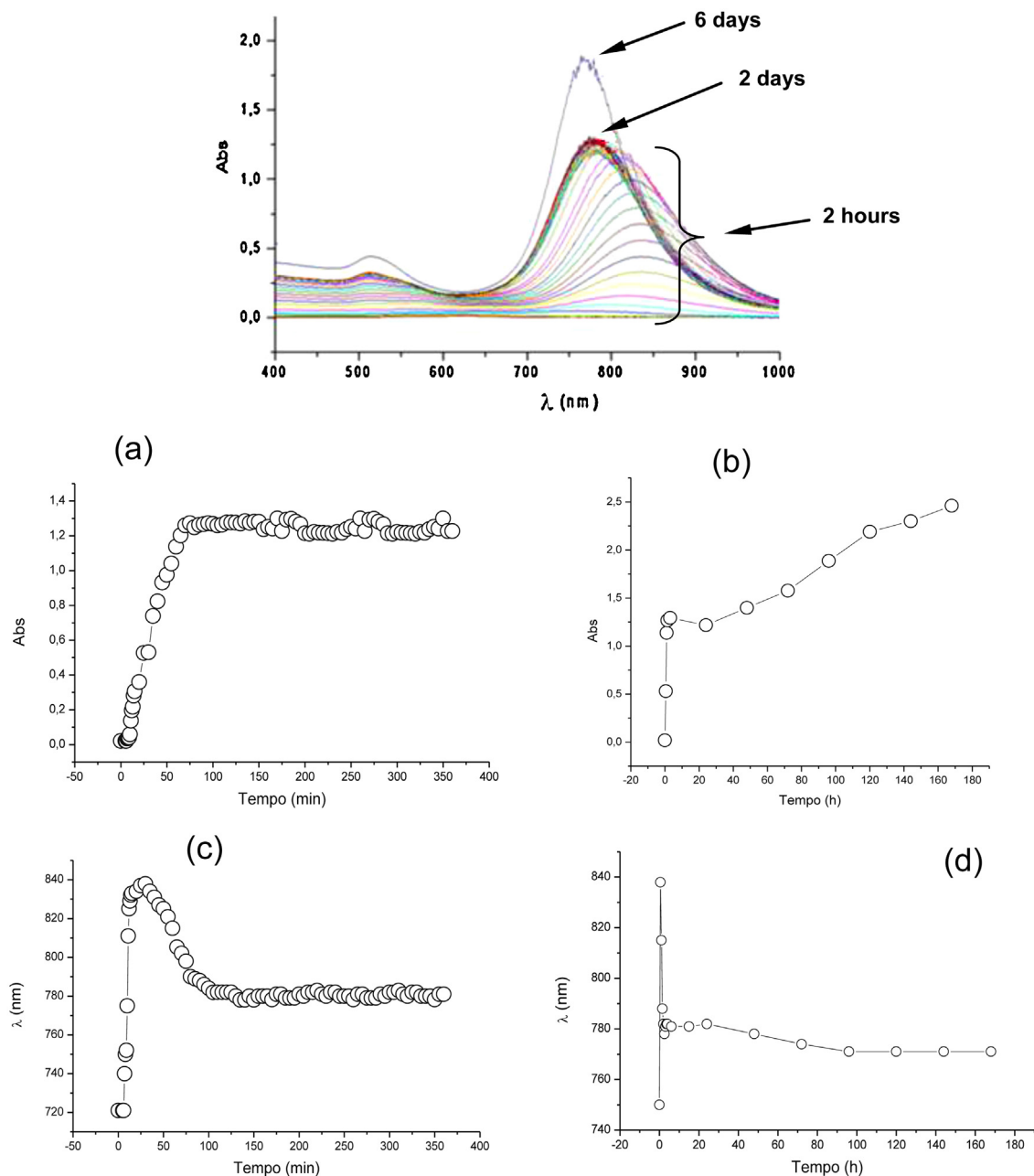


Fig. 3. Absorption spectra of the colloid containing the gold nanorods recorded from the first moments of nanorod formation until day 6 (Top). Graphics (a) and (b) indicate the evolution of the maximum absorption intensity of the second band as a function of time, during the first 6 h and 7 days, respectively. Graphics (c) and (d) indicate the evolution of the of maximum absorption wavelength of the second band as a function of time.

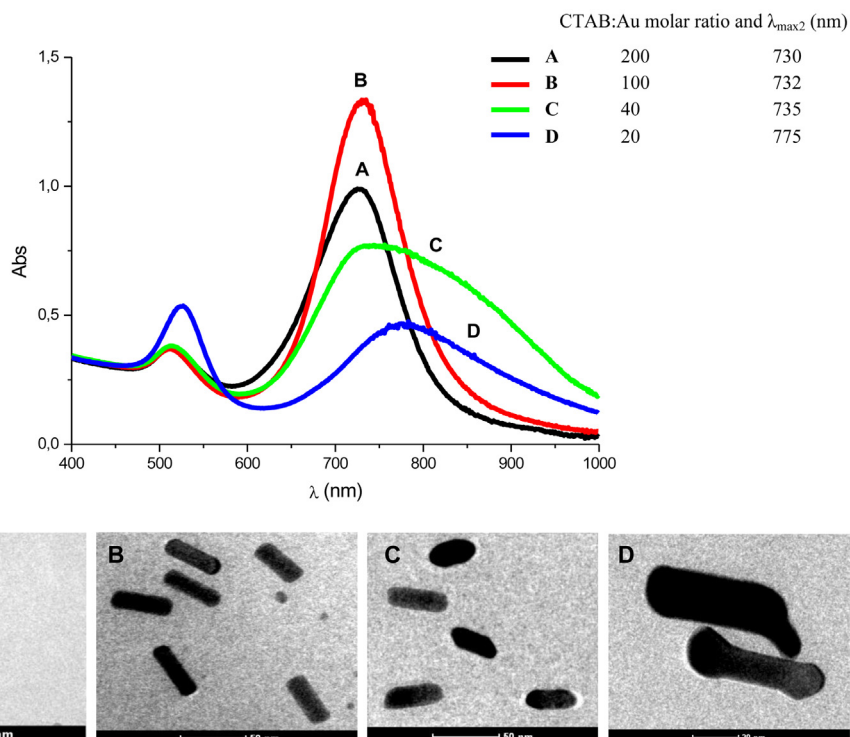


Fig. 4. Electronic absorption spectra of the colloids with different CTAB: Au molar ratio, obtained 24 h after rods formation. Sample **A**, **B**, **C** and **D** prepared with CTAB: Au molar ratio of 200, 100, 40, and 20, respectively (Top). TEM images showing the typical size and shape of the respective AuNRs obtained.

typical for colloids containing AuNRs was observed. The resulting spectra also show different correlations between the two absorption bands ($\lambda_{\max 1} < \lambda_{\max 2}$), which can be an indication of AuNR formation with different aspect ratios. Additionally, one can observe that the relative intensity between the two maximum absorptions in each spectrum are different. According to the optical law, the extinction coefficient of a metal nanoparticle is dependent on its size, and the longitudinal section has a higher extinction coefficient than the transversal one [9]. Thus, a typical UV–vis absorption spectrum of a colloid containing high numbers of AuNRs must have its $\lambda_{\max 1}$ less intensive than its correspondent $\lambda_{\max 2}$. This was the case for samples **A** and **B**, suggesting that we attained AuNRs in high yields. This was not the case for samples **C** and **D**, in which other

forms of nanoparticles were present, probably the more thermodynamically stable spherical ones.

The conclusions derived from the UV–vis absorption spectra were corroborated by the TEM images (Fig. 4). Most of the nanoparticles observed were rod-like and very homogenous in samples **A** and **B**. Both samples presented the same aspect ratio (3.0), with length and width around 45 and 15 nm, respectively (a slightly higher degree of homogeneity was seen in sample **B**). As we decreased the CTAB: Au molar ratio, as in the solutions **C** and **D**, the rod-shape appearance was strongly affected, leading to irregular rod-shaped particles and other different irregular forms.

Indeed, in this study, it was possible to verify that if we carried out a synthesis with CTAB: Au molar ratios between 100 and 200, we could reach a safe range of work to obtain

Table 2

Reaction conditions^a for the preparation of gold nanorods (AuNRs) in the presence of different amounts of seed particles and characteristics of the particles obtained.

Sample	Seed solution ^b (μL)	Au ^I :seed ^c × 10 ⁵	$\lambda_{\max 1}$ (nm)	$\lambda_{\max 2}$ (nm)	AuNR length (nm)	Aspect ratio
E	2.4	100	516	650	56 ± 3	1.7
B	12	20	511	732	45 ± 3	3.0
F	60	4.0	509	784	42 ± 4	3.7
G	120	2.0	509	777	54 ± 4	3.6
H^c	300	0.8	511	770	–	–
I^c	600	0.4	516	707	–	–

^a The growth solution was prepared from: 5.0 mL of Au^{III} (1.0 mmol/L), 2.5 mL of CTAB (0.2 mol/L), 0.150 mL of AgNO₃ (4.0 mmol/L), and 0.070 mL of AA (80 mmol/L).

^b Ratio of Au^I species and seed particles in the reaction medium.

^c Dog-bone shape AuNRs predominate.

AuNRs with the same size and aspect ratio, without significant variations, i.e. AuNRs with a length of 45 nm and an aspect ratio of 3.0.

3.3. Effect of the number of seeds

AuNRs were prepared with the addition of different numbers of seed particles into identical growth solutions (7.72 mL; CTAB: Au molar ratio of 100; 0.64 mmol/L of Au³⁺). The respective experimental conditions adopted in this study are presented in Table 2, as well as some of the

respective experimental results. Fig. 5 shows the UV–vis absorption spectra and TEM images of the particles obtained after 24 h of AuNR formation.

At this point, it is important to consider that the number of AuNRs formed is the same as the number of seed particles added. Thus, if we increase the amount of seeds added, keeping constant the amount of Au³⁺ species in the solution, i.e. if the Au³⁺:seed ratio decreases, smaller particles are produced.

From the data depicted on Table 2 and Fig. 5, one can see that solution E (2.4 μ L of seed solution added) led to larger

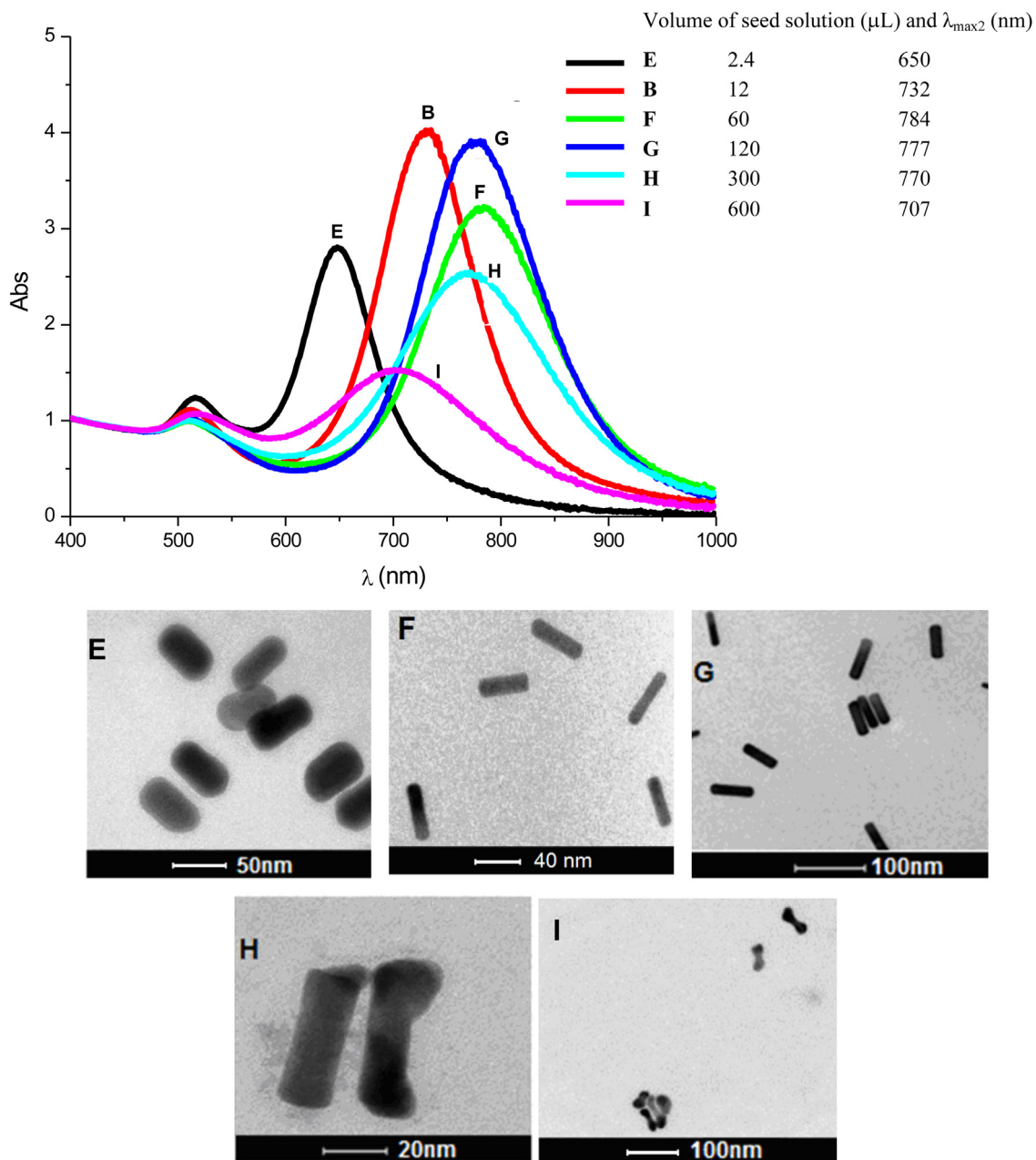


Fig. 5. Absorption spectra of the colloids containing gold nanorods prepared with different amounts of seed particles in the reaction medium, after 24 h. Samples B, E, F, G, H, and I were prepared with different amounts of seed particles (top). TEM images of the respective gold nanorods prepared from different amounts of seed particles. (E) 2.4 μ L; (B) 12 μ L; (F) 60 μ L; (G) 120 μ L; (H) 300 μ L; (I) 600 μ L added to the growth solution.

Table 3

Reaction conditions^a for the preparation of gold nanorods in the presence of different volumes of growth solution (0.64 mmol/L of Au^I species) and characteristics of the particles obtained.

Sample	V (mL) of Au ^{III} (1.0 mmol/L)	V (mL) of CTAB (0.2 mol/L)	V (mL) of AgNO ₃ (4.0 mmol/L)	V of AA (mL)	Total V (mL)	Au ^I :seeds ^b x 10 ⁵	λ _{max1} (nm)	λ _{max2} (nm)	AuNR length (nm)	Aspect ratio
J ^c	2.50	1.25	0.075	0.035	3.86	1.0	509	697	22 ± 3	3.2
G ^d	5.00	2.50	0.150	0.070	7.72	2.0	509	777	54 ± 4	3.6
K	10.0	5.00	0.300	0.140	15.4	4.0	510	774	38 ± 6	4.0
L	20.0	10.0	0.600	0.280	30.9	8.0	513	725	32 ± 5	2.9
M	50.0	25.0	1.50	0.700	77.2	20	514	720	11 ± 4	2.2

CTAB: Cetyltrimethylammonium bromide; AgNO₃: silver nitrate; AA: ascorbic acid; AuNRs: gold nanorods.

^a Seed solution: 120 μL.

^b Ratio of Au^I species and seed particles in the reaction medium.

^c Many spherical nanoparticles also present.

^d TEM images, (Fig. 5).

AuNRs; however, their aspect ratios were smaller (~2.0). Indeed, we can see that, until a certain level, by increasing the number of seeds in the medium (**B** < **F** < **G**), the aspect ratio of the AuNR also increased. If one were to increase even more the number of seed particles in the growth solution, the amount of Au^I species (“monomers”) becomes too scarce to produce rod-shape particles with elevated aspect ratios. Furthermore, by adding more seeds to the growth solution, more AuNRs are formed, but of a smaller size; consequently, the CTAB necessary to produce the double layer around the particles becomes scarce. This also explains the production of dog-bone-shaped particles,

since, at a certain level of rod growth, the amount of CTAB becomes insufficient to drive the preferential access of “monomers” at the tip of the rods during formation [19,73,74]. This study confirms that there is an ideal relation between “monomers” and seeds in the reaction medium to achieve highly selective production of rod-like particles, as verified in solutions and **G** [71].

3.4. Effect of monomer amount

In this study, we carried out two different set of experiments in order to evaluate the influence of the

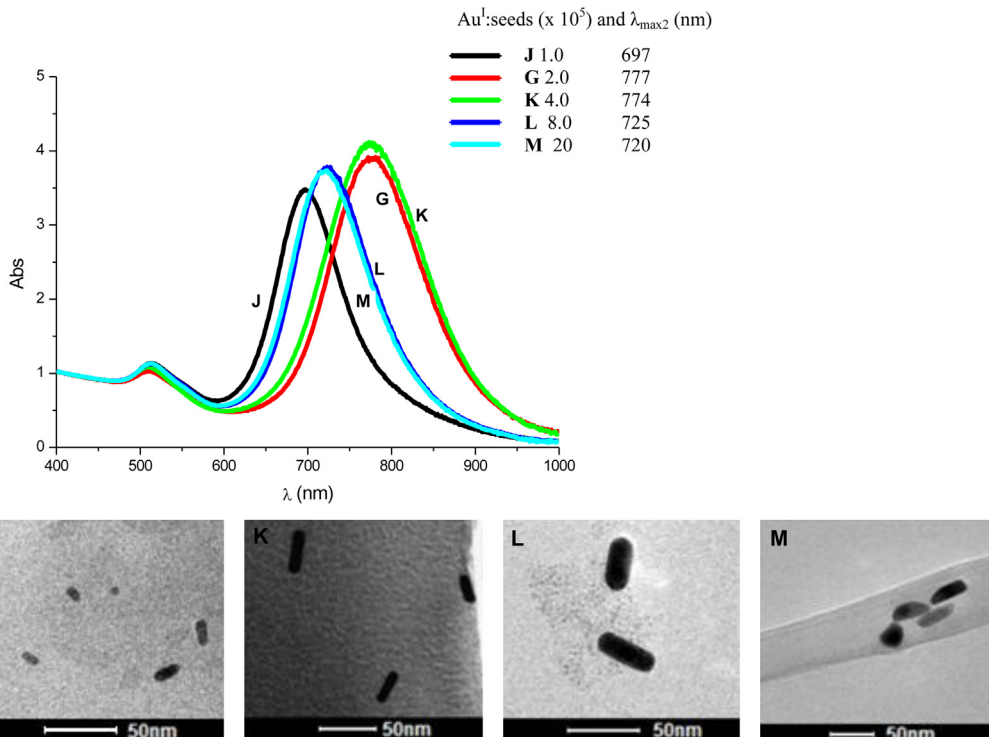


Fig. 6. Absorption spectra of the colloids containing gold nanorods prepared with different amounts of “monomers” in the reaction medium. All spectra were obtained 24 h after rod formation. Samples **J**, **G**, **K**, **L**, and **M** were prepared from different volumes of the growth solution (top). TEM images of gold nanorods prepared from different volumes of the growth solution (0.64 mmol/L of Au^I species): (**J**) 2.5 mL; (**K**) 10 mL; (**L**) 20 mL; (**M**) 50 mL. Volume of seed solution added: 120 μL.

“monomer” (Au^{I}) amount on the production of AuNRs. In both studies, we added the same amount of seeds into growth solutions with different amounts of “monomers”.

3.4.1. Method 1

In this first set of experiments, we added the same amount of seed solution ($120 \mu\text{L}$) into different volumes of growth solutions with the same characteristics (0.64 mmol/L of Au^{I} species; CTAB: Au molar ratio of 100). Table 3 summarises the experimental conditions adopted and shows some experimental results. Fig. 6 shows the UV–vis absorption spectra and TEM images of the particles obtained 24 h after AuNR formation started.

Using the reaction conditions adopted here, one can see that AuNRs were produced in all tests, but with different aspect ratios. Again, it was possible to verify that there is an

ideal ratio between the amount of “monomers” and seeds in the reaction medium to obtain rod nanoparticles with higher aspect ratios. As expected, it is possible to observe that as we increased the volume of the growth solution, larger particles were obtained, but this does not mean that the aspect ratio increased. This trend was also observed in the previous study (compare with Fig. 5).

3.4.2. Method 2

A second set of experiments was performed in order to keep the same amount of species as in the previous test; however, the final volume of the colloidal solution of AuNRs, in all cases, was the same ($\sim 8.0 \text{ mL}$). Table 4 summarises the reaction conditions adopted in this study. Fig. 7 shows the UV–vis absorption spectra and TEM images of the particles obtained 24 h after AuNR formation started.

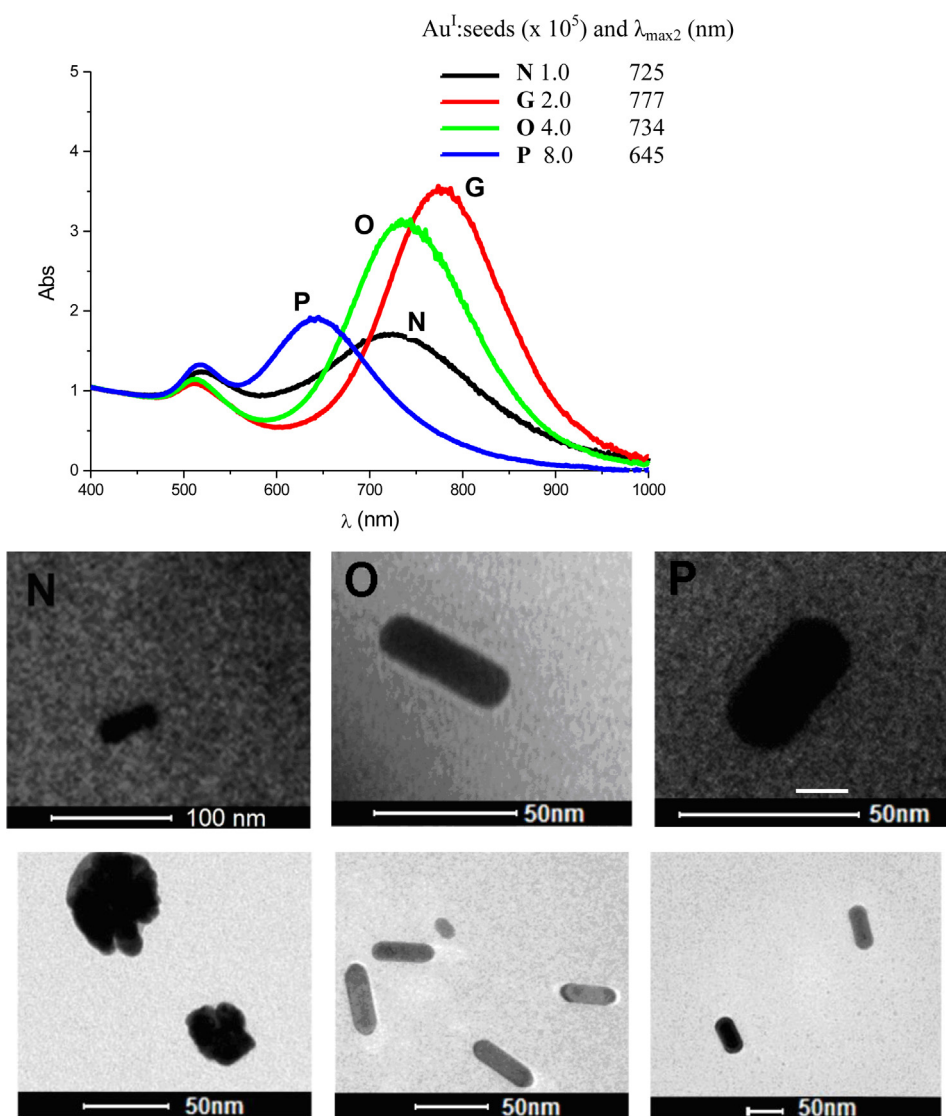


Fig. 7. Absorption spectra of the colloids containing gold nanorods prepared with different amounts “monomers” in the reaction medium. All spectra were obtained 24 h after rod formation. Samples N, G, O, and P were prepared from growth solutions with Au^{I} concentration of 0.32, 0.64, 1.28, and 2.56 mmol/L , respectively. TEM images of gold nanorods obtained from samples N, O, and P. Volume of seed solution added: $120 \mu\text{L}$.

Table 4

Reaction conditions^a for the preparation of gold nanorods in the presence of different amounts of reagents, but with the same final volume of the colloidal solution of gold nanorods (~8.0 mL), and characteristics of the particles obtained.

Sample	[Au ^{III}] (mmol/L)	[CTAB] (mmol/L)	[Ag ^I] (mmol/L)	[AA] (mmol/L)	Au ^I :seeds ^b × 10 ⁵	λ _{max1} (nm)	λ _{max2} (nm)	AuNR length (nm)	Aspect ratio
N^c	0.32	32	0.20	0.40	1.0	518	725	–	–
G^d	0.64	64	0.40	0.80	2.0	509	777	54 ± 4	3.6
O	1.28	128	0.80	1.6	4.0	512	734	50 ± 4	3.1
P	2.56	256	1.6	2.4	8.0	518	645	4 ± 5	1.8
Q^e	6.40	640	4.0	8.0	20	–	–	–	–

CTAB: Cetyltrimethylammonium bromide; AA: ascorbic acid; AuNRs: gold nanorods.

^a The final volume of the colloidal systems were ca. 8.0 mL; seed solution (120 μL); CTAB:Au molar ratio = 100.

^b Ratio of Au^I species and seed particles in the reaction medium.

^c Particles with different shapes, Fig. 7.

^d TEM images, Fig. 5.

^e There was total precipitation of the particles, leading to a clear solution.

In this study, we determined that the concentration of the solution employed is in fact important, since the particles are different if the concentrations are different. This demonstrates that diffusion effects play a role in the particle formation process. Overall, we observed that, at higher concentrations, the particles formed were generally larger and with a lower aspect ratio. This is a curious result. We expected that, having the same number of particles formed, since the same amount of seed was added, we should expect that particles formed with a greater should have a reduced width; however, this is not the case. To explain such an incongruence, two events are possible: (i) at higher concentrations, some seed particles do not develop or (ii) in diluted conditions, part of the “monomers” do not have access to the surface of the growing particles. We are carrying out additional experiments to get more information in order to understand such tendencies. However, we suggest that at higher concentrations, some seed particles are blocked by the high concentration of CTAB in the medium, thus, prohibiting the development of some seed particles into AuNRs. This results in more “monomers” available to those seed that do develop, leading to larger particles.

4. Conclusion

Although the synthesis of AuNRs is already considered a consolidated subject, some aspects of their preparation still generate discussion. In this work, we verified that the synthesis of anisotropic AuNPs via the seed-mediated method is quite susceptible to the reaction conditions adopted. Several variables, such as reagent concentrations and the molar ratios between them are important aspects to be considered to tune the synthesis of the desired particles. Different results are obtained with reactions with the same molar ratio between the reagents, but under different concentrations. With the method of synthesis employed here, the desired particles were formed between 2 and 4 h and were stable for around 2 days, where after Ostwald ripening began to govern the growth process. To obtain good quality AuNRs in good yields, without enrichment, we suggest keeping the growth-driving agent/gold molar ratio between 200 and 100 and the Au^I/seed particle ratio between 10.0×10^5 and 2.0×10^5 .

Nevertheless, one must take in account the concentration of the reagents in the final solution within specific ranges. For example, even keeping the Au^I/seed particle molar ratio at reasonable values, in relatively highly concentrated reaction solutions, some seed particles do not develop. However, in diluted conditions, some of the “monomers” do not have access to the surface of the growing particles, since the seed particles are blocked by the high concentration of CTAB in the medium.

Acknowledgments

The authors thank CNPq, CAPES, and FAPEAL for partial financial support and for their research fellowships.

References

- [1] G. Schmid (Ed.), *Nanoparticles: From Theory to Application*, Wiley, Weinheim, 2004.
- [2] M.A. El-Sayed, R. Narayanan, X. Chen, C. Burda, *Chem. Rev.* 105 (2005) 1025.
- [3] M.C. Daniel, D. Astruc, *Chem. Rev.* 104 (2004) 293.
- [4] F. Viñes, C. Loschen, F. Illas, K.M. Neyman, *J. Catal.* 266 (2009) 59.
- [5] J.H. He, Y.Q. Wan, L. Xu, *Chaos Solitons Fractals* 33 (2007) 26.
- [6] K.L. Kelly, E. Coronado, L.L. Zhao, G.C. Schatz, *J. Phys. Chem. B* 107 (2003) 668.
- [7] P.K. Jain, I.H. El-Sayed, M.A. El-Sayed, *Nano Today* 2 (2007) 18.
- [8] G. Mie, *Ann. Phys.* 25 (1908) 377.
- [9] U. Kreibitz, M. Vollmer (Eds.), *Optical Properties of Metal Clusters*, Springer-Verlag, Berlin, Heidelberg, New York, 1995.
- [10] E.C. da Silva, M.G.A. da Silva, S.M.P. Meneghetti, G. Machado, M.A.R.C. Alencar, J.M. Hickmann, M.R. Meneghetti, *J. Nanopart. Res.* 10 (Supp. 1) (2008) 201.
- [11] H.E. Toma, L.S. Bonifácio, F.J. Anaissi, *Quim. Nova* 28 (2005) 897.
- [12] L.M. Liz-Marzan, *Materials Today* 7 (2004) 26.
- [13] X. Huang, S. Neretina, M.A. El-Sayed, *Adv. Mater.* 21 (2009) 4880.
- [14] T.H. Ha, H.J. Koo, B.H. Chung, *J. Phys. Chem. C* 11 (2007) 2451.
- [15] X. Kou, S. Zhang, C.K. Tsung, Z. Yang, M.H. Yeung, G.D. Stucky, L. Sun, J. Wang, C. Yan, *Chem. Eur. J.* 13 (2007) 2929.
- [16] L. Wang, Y. Liu, W. Li, X. Jiang, Y. Ji, X. Wu, L. Xu, Y. Qiu, K. Zhao, T. Wei, Y. Li, Y. Zhao, C. Chen, *Nano Lett.* 11 (2011) 772.
- [17] I. Mannelli, M.P. Marco, *Anal. Bioanal. Chem.* 398 (2010) 2451.
- [18] H. Wender, L.F. de Oliveira, A.F. Feil, E. Lissner, P. Migowski, M.R. Meneghetti, S.R. Teixeira, J. Dupont, *Chem. Commun.* 46 (2010) 7019.
- [19] X. Xu, M.B. Corti, *Adv. Funct. Mat.* 16 (2006) 2170.
- [20] M. Law, D.J. Sibuly, J.C. Johnson, J. Goldberger, R.J. Saykally, P. Yang, *Science* 305 (2004) 1269.
- [21] R.F. Souza, M.A.R.C. Alencar, E.C. da Silva, M.R. Meneghetti, J.M. Hickmann, *Appl. Phys. Lett.* 92 (2008) 201902.
- [22] J. Gong, C.B. Mullins, *Acc. Chem. Res.* 42 (2009) 1063.
- [23] E. Katz, I. Willner, *Angew. Chem. Int. Ed. Engl.* 43 (2004) 6042.

- [24] K. Sokolov, M.F. Aaron, I. Pavlova, A. Malpica, R. Lotan, R.R. Kortum, *Cancer Res.* 63 (2003) 1999.
- [25] R.A. Sperl, P.R. Gil, F. Zhang, M. Zanella, W.J. Parak, *Chem. Soc. Rev.* 37 (2008) 1896.
- [26] G. Maltzahn, A. Centrone, J. Park, R. Ramanathan, M.J. Sailor, T.A. Hatton, S.N. Bhatia, *Adv. Mater.* 21 (2009) 3175.
- [27] M. Choi, K.J. Stanton-Maxey, J.K. Stanley, C.S. Levin, R. Bardhan, D. Akin, S. Badve, J. Sturgis, J.P. Robinson, R. Bashir, N.J. Halas, S.E. Clare, *Nano Lett.* 7 (2007) 3759.
- [28] S. Zimmermann, H.M. Urbassek, *Int. J. Mass Spectrom.* 272 (2008) 91.
- [29] M. Nie, K. Sun, D. Meng, *J. Appl. Phys.* 106 (2009) 054314.
- [30] Y. Mizukoshi, R. Oshima, Y. Maeda, Y. Nagata, *Langmuir* 15 (1999) 2733.
- [31] G.A. Ozin, *Adv. Mater.* 4 (1992) 612.
- [32] W. Wang, R. Stoltenberg, S. Liu, Z. Bao, *ACS Nano* 2 (2008) 2135.
- [33] D. Zanchet, B.D. Hall, D. Ugarte, *J. Phys. Chem. B* 104 (2000) 11013.
- [34] D. Zanchet, M.S. Moreno, D. Ugarte, *Phys. Rev. Lett.* 82 (1999) 5277.
- [35] X. Peng, *Adv. Mater.* 15 (2003) 459.
- [36] X. Peng, *Chem. Eur. J.* 8 (2002) 334.
- [37] D.J. Milliron, S.M. Hughes, Y. Cui, L. Manna, J. Li, L. Wang, A.P. Alivisatos, *Nature* 430 (2004) 190.
- [38] T.S. Ahmadi, Z.L. Wang, T.C. Green, A. Henglein, M.A. El-Sayed, *Science* 272 (1996) 1924.
- [39] R. Jin, Y. Cao, E. Hao, G.S. Metraux, G.C. Scharzt, C.A. Mirkin, *Nature* 425 (2003) 487.
- [40] X.C. Jiang, A. Brioude, M.P. Pileni, *Colloids Surf. A, Physicochem. Eng. Asp.* 277 (2006) 201.
- [41] J.L. Burt, J.L. Elechiguerra, J.G. Reyes, J.M.C. Montejano, M.J. Jose-Yacamán, *Cryst. Growth* 285 (2005) 681.
- [42] Y. Yin, R.M. Rioux, C.K. Erdonmez, S. Hughes, G.A. Somorjai, A.P. Alivisatos, *Science* 304 (2004) 711.
- [43] H. Wender, P. Migowski, A.F. Feil, L.F. de Oliveira, M.H.G. Precht, R. Leal, G. Machado, S.R. Teixeira, J. Dupont, *Phys. Chem. Chem. Phys.* 13 (2011) 13552.
- [44] C. Murphy, T. Sau, A. Gole, C. Orendorff, J. Gao, L. Gou, S. Hunyadi, T. Li, *J. Phys. Chem. B* 109 (2005) 13857.
- [45] A. Tao, P. Sinsermsuksakul, P. Yang, *Angew. Chem. Int. Ed.* 45 (2006) 4597.
- [46] L.Y. Cao, T. Zhu, Z.F. Liu, *J. Colloids Interface Sci.* 293 (2006) 69.
- [47] A. Gole, C.J. Murphy, *Chem. Mater.* 16 (2004) 3633.
- [48] N.R. Jana, L. Gearheart, C.J. Murphy, *Adv. Mater.* 13 (2001) 1389.
- [49] N.R. Jana, C.J. Murphy, *Adv. Mater.* 14 (2002) 80.
- [50] L.F. Gou, C.J. Murphy, *Chem. Mater.* 17 (2005) 3668.
- [51] A.V. Alekseeva, V.A. Bogatyrev, B.N. Khlebtsov, A.G. Mel'nikov, L.A. Dykman, N.G. Khlebtsov, *Colloid J.* 68 (2006) 661.
- [52] X.C. Jiang, M.P. Pileni, *Colloids Surf. A, Physicochem. Eng. Asp.* 295 (2007) 228.
- [53] Y. Takenaka, H. Kitahata, *Chem. Phys. Lett.* 467 (2009) 327.
- [54] T.K. Sau, C.J. Murphy, *Langmuir* 20 (2004) 6414.
- [55] X.H. Huang, I.H. El-Sayed, W. Qian, M.A. El-Sayed, *J. Am. Chem. Soc.* 128 (2006) 2115.
- [56] Y.Y. Yu, S.S. Chang, C.L. Lee, C.R.C. Wang, *J. Phys. Chem. B* 101 (1997) 6661.
- [57] C.S. Ah, S.D. Hong, D.J. Jang, *J. Phys. Chem. B* 105 (2001) 7871.
- [58] F. Kim, J.H. Song, P. Yang, *J. Am. Chem. Soc.* 124 (2002) 14316.
- [59] Y.J. Zhu, X.L. Hu, *Chem. Lett.* 32 (2003) 1140.
- [60] J.P. Pérez-Juste, I.P. Santos, L.M. Liz-Marzán, P. Mulvaney, *Coord. Chem. Rev.* 249 (2005) 1870.
- [61] C.J. Murphy, L.B. Thompson, D.J. Chernak, J.A. Yang, S.T. Sivapalan, S.P. Boulos, J. Huang, A.M. Alkilany, P.N. Sisco, *Curr. Opin. Colloid In.* 16 (2011) 128.
- [62] B. Nikoobakht, M.A. El-Sayed, *Chem. Mater.* 15 (2003) 1957.
- [63] K.T. Yong, Y. Sahoo, M.T. Swihart, P.M. Schneeberger, P.N. Prasad, *Top. Catal.* 47 (2008) 49.
- [64] C. Johnson, E. Dujardin, S. Davis, C. Murphy, S. Mann, *J. Mater. Chem.* 12 (2002) 1765.
- [65] P. Mulvaney, M. Giersig, A. Henglein, *J. Phys. Chem.* 97 (1993) 7061.
- [66] N.R. Jana, L. Gearheart, C.J. Murphy, *J. Phys. Chem. B* 105 (2001) 4065.
- [67] J. Pérez-Juste, L.M. Liz-Marzán, S. Carnie, D.Y.C. Chan, P. Mulvaney, *Adv. Funct. Mater.* 14 (2004) 571.
- [68] M. Giersig, A. Henglein, *J. Phys. Chem.* 98 (1994) 6931.
- [69] Z. Wang, M. Mohamed, S. Link, M.A. El-Sayed, *Surf. Sci.* 440 (1999) L809.
- [70] R. Zou, Q. Zhang, Q. Zhao, F. Peng, H. Wang, H. Yu, J. Yang, *Colloids Surf. A, Physicochem. Eng. Asp.* 372 (2010) 177.
- [71] J. Gao, C.M. Bender, C.J. Murphy, *Langmuir* 19 (2003) 9065.
- [72] X. Peng, J. Wickham, A.P. Alivisatos, *J. Am. Chem. Soc.* 120 (1998) 5343.
- [73] F. Ratto, P. Matteini, F. Rossi, R. Pini, *J. Nanopart. Res.* 12 (2010) 2029.
- [74] X. Xu, M.B. Cortie, *Adv. Funct. Mater.* 16 (2006) 2170.

New and tunable hydroxylated driving agents for the production of tailor-made gold nanorods†‡

Cite this: *RSC Advances*, 2013, 3, 18292

Received 13th June 2013,

Accepted 30th July 2013

DOI: 10.1039/c3ra42949k

www.rsc.org/advances

Monique Gabriella Angelo da Silva,^{ab} Mario Roberto Meneghetti,^b
Audrey Denicourt-Nowicki^{*a} and Alain Roucoux^{*a}

Gold nanorods with a relevant aspect ratio were synthesized in high yields and good selectivities in the presence of ammonium surfactants bearing tunable hydroxyalkylated headgroups. The role of the OH function was demonstrated and the dynamics of the growth process were investigated through UV-vis measurements.

Among the various shapes of gold particles, nanorods (AuNRs) have attracted great interest¹ owing to their extremely attractive surface-plasmon based optical properties,² which render them pertinent candidates for numerous applications in optics,^{3–7} medicine,^{8–10} with a blossom in cancer diagnosis and photothermal therapy^{11–14} and more recently in catalysis according to their index facets.^{15,16} Their tunable properties are strongly dependent on the size, shape and aspect ratio (length/width) of the gold particles.¹⁷ Short AuNRs with an aspect ratio between 4 and 7 scattered blue/green and yellow light, providing many opportunities for sensing and imaging applications, whereas longer rods (aspect ratio around 10) preferentially scattered lower-energy orange/red light.^{18,19}

Several reliable methods for the synthesis of gold nanoparticles have been developed over the last half-century to achieve decent yields and sample monodispersity.²⁰ Among the various methodologies,²¹ the seed-mediated growth approach in aqueous solution^{7,22} is frequently used to produce AuNRs with diverse aspect ratios and dimensions,^{7,23,24} assisted almost exclusively by cetyltrimethylammonium bromide (CTAB) as growth driving agent. This ammonium salt seems to be of crucial importance for a well-controlled growth process by blocking the long axis crystal faces through the surfactant bilayer structure and thus promoting metal growth on the short-axis faces to produce

AuNRs.²⁵ Many works have been carried out to efficiently tune the aspect ratio, which could be affected by several synthetic parameters, such as the amount of the driving agent,^{26,27} the size of the crystal seeds used,²⁸ the effect of additives.¹⁸ The influence of the growth-driving agents is also of crucial importance in the AuNRs elongation, according to previous works by Murphy *et al.*⁷ Thus, binary mixtures were used, such as CTAB/BDAC (benzyltrimethyl ammonium chloride)²² with modest results in terms of selectivity or CTAB/OTAB (octyltrimethylammonium bromide) gelled mixed surfactant solution.²⁹ To our knowledge, only the cetylpyridinium chloride, possessing a larger and more anisotropic headgroup, has previously been investigated alone as directing agent to produce AuNRs, but unfortunately multi-shaped nanoparticles, such as nanospheres, triangles, pentagons, were observed.³⁰

Herein we describe a real alternative preparation of size and form-controlled gold NPs by the seed-mediated growth in aqueous media with high yields and selectivities, using an original library of easily tunable *N,N*-dimethyl-*N*-cetyl-*N*-(hydroxyalkyl)ammonium bromide salts (HAA16Br) as growth-driving agents (Fig. 1), instead of the usual CTAB. These growth-driving agents, bearing hydroxylated polar heads and possessing a high water-solubility as well as a good stability in a large range of pH, are easily synthesized in a one-step high-yielding quaternarization of the (*N,N*-dimethylamino)-1-alcohol with bromohexadecane (see ESI†).



Fig. 1 Chemical structure of HAA16Br surfactants investigated as gold NPs growth driving agents.

^aEcole Nationale Supérieure de Chimie de Rennes, CNRS, UMR 6226, 11 Allée de Beaulieu, CS 50837, 35708 Rennes Cedex 7, France. E-mail: alain.roucoux@ensc-rennes.fr

^bGrupo de Catálise e Reatividade Química GCaR, Instituto de Química e Biotecnologia da Universidade Federal de Alagoas, Av. Lourival de Melo Mota, s/n CEP 57072-970, Maceió, AL, Brazil

† Electronic supplementary information (ESI) available. See DOI: 10.1039/c3ra42949k

‡ Patricia Beauvier from UPMC is acknowledged for performing TEM analysis.

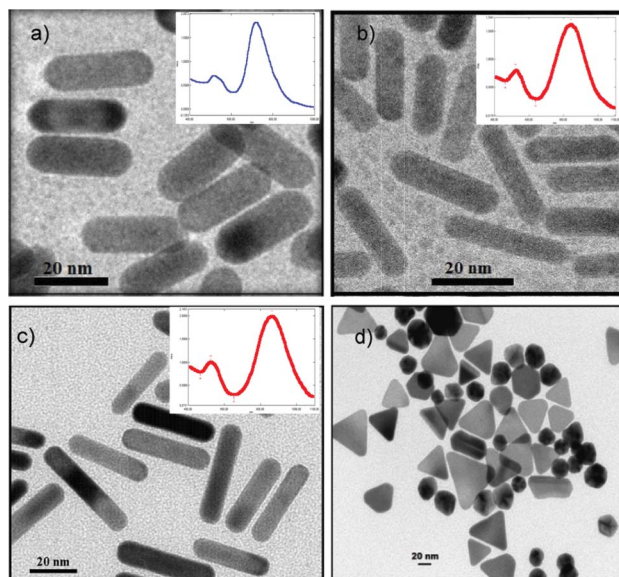


Fig. 2 UV-vis absorption spectra and TEM pictures of AuNRs (a) HEA16Br, (b) HPA16Br and (c) HBA16Br and comparison with a non-hydroxylated surfactant (d) PA16Br.

In comparison with CTAB, we interestingly demonstrated the influence of the hydroxylated headgroup on the surfactant in the controlled growth dynamics of AuNRs.

In a first set of experiments, the three surfactants possessing a different length on the hydroxylated polar head (Fig. 1), *i.e.* HEA16Br (HEA: hydroxyethylammonium), HPA16Br (HPA: hydroxypropylammonium) and HBA16Br (HBA: hydroxybutylammonium) were investigated as growth-driving agents of Au nanorods. The results were compared to those obtained with the classical cetyltrimethylammonium bromide (CTAB) under the same experimental conditions. In this study, only the initial step of the seed-mediated growth process was explored at constant pH (3.5) according to the preparation's conditions, since the second and third steps are only used for the elongation of the preformed nanocrystals.

Whatever the length of the hydroxylated polar head, the UV-vis absorption spectra of AuNRs prepared with the HAA16Br series as growth-driving agent present two typical absorption bands (Fig. 2). This result was confirmed by transmission electron microscopy (TEM) analyses, showing rod-like particles with various lengths and widths providing modulated aspect ratios (Table 1), with very narrow size distribution. Higher values were achieved when the hydroxylated alkyl chain increased (respectively, 4.2 and 4.4 for HPA16Br and HBA16Br *vs.* 3.0 for HEA16Br). For comparison, the aspect ratio of AuNRs obtained with CTAB by the same procedure is around 3.3 (40 × 12 nm), similar to the values reported by Murphy.¹⁹ The selectivity was determined on the crude solution without any centrifugation step, in opposition to the results usually reported in the literature (Table 1).

In order to determine the influence of the hydroxyl group of the polar head on the dynamics of rods' formation, the PA16Br surfactant (*N,N*-dimethyl-*N*-cetyl-*N*-propylammonium bromide, see

Table 1 Main characteristics of AuNPs obtained with various growth-driving agents^a

Driving agent	Length (nm)	Width (nm)	Aspect ratio ^b	Selectivity ^c
HEA16Br	30 ± 5.2	10 ± 1.3	3.0	88
HPA16Br	30 ± 3.0	7.2 ± 0.8	4.2	85
HBA16Br	39 ± 6.4	8.8 ± 1.2	4.4	82
CTAB	40 ± 4.8	12.4 ± 2.3	3.3	89
PA16Br	Spheres; prisms		—	<0.1

^a Conditions: 5 × 10⁻³ mmol HAuCl₄·H₂O (0.2 mL; 28 mmol L⁻¹); 6 × 10⁻⁴ mmol AgNO₃ (0.15 mL; 4 × 10⁻³ mol L⁻¹); 5.5 × 10⁻³ mmol ascorbic acid (0.07 mL; 0.0788 mol L⁻¹); 0.060 mL of seed.

^b Aspect ratio (Length/Width). ^c Selectivity = (Number of AuNRs/Number of AuNPs) × 100, determined after 500 counts and evaluated without centrifugation purification

ESI[†]) was also evaluated and the results have to be compared with those obtained with HEA16Br (Fig. 3). Here, we assimilated the steric hindrance of the methyl similar to the OH group to only compare their physicochemical supply.

TEM images showed the formation of prisms and spheres in the case of the non-hydroxylated PA16Br surfactant as driving agent (Fig. 2d), while nanorods were observed with the 2-hydroxyethylammonium HEA16Br, thus demonstrating the obvious role of the hydroxyl in the growth process. The favorable polar long chain packing through hydrogen bond, thus providing a better supramolecular organization and efficient protection of the lateral facets, could explain this phenomenon.

The polar heads have an influence on the structural parameters and also on the selectivity of AuNRs, thus allowing a control of the growth process and an easy modulation of the NRs features thanks to a judicious choice of the growth driving agent, higher aspect ratios being achieved with HBA16Br. Moreover, in contrast to CTAB, higher quality (narrow size distributions) of AuNRs, were obtained with hydroxylated ammonium surfactants (Table 1 and Fig. S1–S4, ESI[†]). Thus, using the three hydroxylated ammonium salts (HEA, HPA and HBA), highly homogeneous AuNRs were produced with high selectivities (higher than 88%, without any centrifugation step), and with various structural parameters (length and aspect ratio), thus opening interesting opportunities in terms of design and applications of AuNRs. Considering these preliminary results, we suggested that the functionalized chain may efficiently protect the lateral facets of the AuNRs in growth, improving the selective addition of the gold source onto the {111}



Fig. 3 Influence of the hydroxyl group – HEA16Br *vs.* PA16Br.

and {110} tip facets and thus providing a longitudinal growing along the {110} and {100} directions.¹⁶

To understand the growth mechanism, we carried out some kinetic studies to compare the rate of the particle formation, during the first 3 h, comparing AuNRs prepared in the presence of CTAB, HEA16Br, HPA16Br, or HBA16Br as surfactants (Fig. 4). Whatever the growth-driving agent is, the AuNRs growth seems to be attained after less than 1 h and the colloidal systems are stable at least for 3 days, without any change based on UV-vis intensities (Fig. S5, ESI†). Moreover, as described for CTAB, a bathochromic effect is observed followed by a hypsochromic effect for the surfactants in the following order: CTAB (14 min.) \approx HEA16Br (12 min.) < HPA16Br (23 min.). This classical and well-known behaviour proves that the aspect ratio of the particle in formation decreases during its growth owing to a less efficient protection of the lateral facets. In the case of HBA16Br, only a bathochromic shift was observed, which is unusual in the literature.

From the UV-vis spectra, we analyzed the rate in which the intensity of the second band increases in the first 60 min. after the beginning of the NRs' formation (Fig. 5). On the first 20 min, we observed that with CTAB and HEA16Br, the NRs grow rapidly and heterogeneously. Moreover, the redistribution in size seems to be less efficient in the case of CTAB, which could be correlated with a broad size histogram (see width and length size distributions of AuNR@CTAB, ESI†). With HBA, the very slow growth leads to a better organization, suggesting that a more hindered polar head hampers the access of the gold source on the lateral facets of the AuNRs in development, thus achieving higher aspect ratios owing to the polar chain packing. The HPA16Br surfactant possesses an intermediate behaviour between HEA16Br and HBA16Br, with a fast growth process but a good control. With CTAB, HEA16Br and HPA16Br, the colloidal stability tends to be attained in around 20 min, but the size control seems more efficient with HPA16Br. This could be correlated to a higher interaction of the polar head with the particle's surface. A similar but more pronounced tendency was observed with HBA16Br, but in that case, the colloidal stability was attained in a longer time (\sim 60 min.), probably due to an enhanced steric hindrance.

In summary, various ammonium surfactants bearing original hydroxylalkylated headgroups were used as a new library of versatile growth-driving agents for AuNRs in high yields and with good selectivities, allowing an efficient control of the growth process. The easy modulation of these ammonium salts could lead to the formation of nanorods possessing various aspect ratios and dimensions, according to the desired application. The novelty concerns the presence of the hydroxylated group, which proves to be essential to increase the steric hindrance on the particle surface, thus leading to the formation of rods-like particles of modulated aspect ratios. Further investigations on the interaction of the driving agent within the facets of AuNRs will constitute a breakthrough to better understand the influence of the hydroxyl group in the growth process. The dynamics of the NRs growth were studied through UV-vis measurements to understand the differences in size and aspect ratio observed between the various surfactants. These promising results open new perspectives in the design of original growth driving agents to produce anisotropic

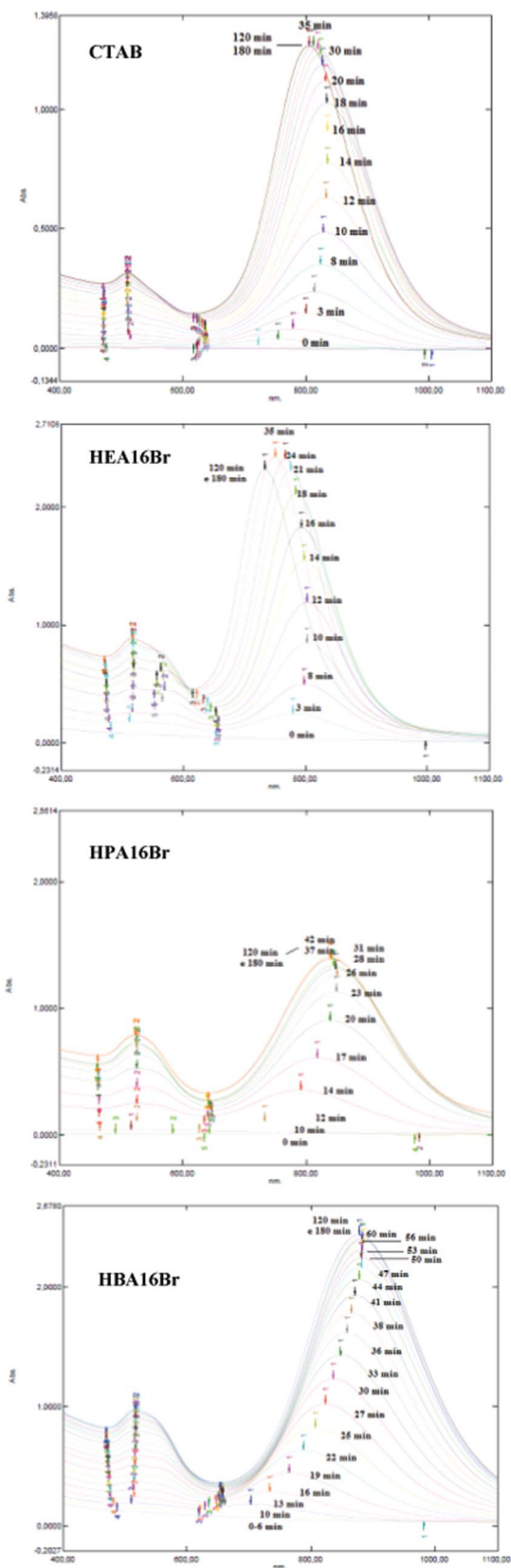


Fig. 4 UV-vis spectra of the colloids obtained from various growth-driving agents, collected during the first 3 h of the NPs formation.

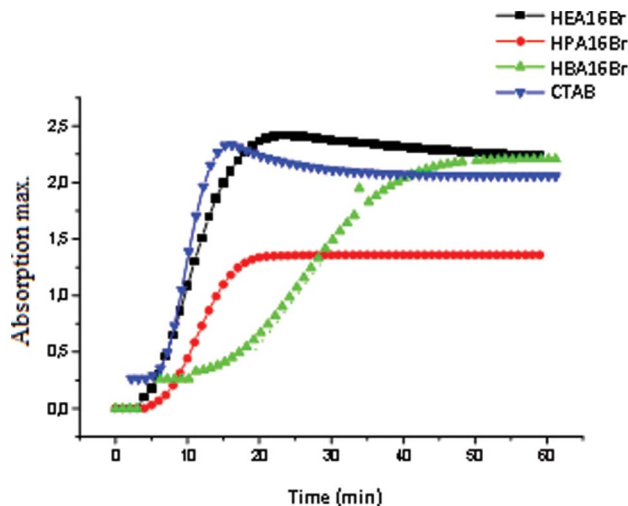


Fig. 5 Absorption maximum of the wavelength of the second band in function of time from 0 to 60 min, using four various growth-driving agents.

gold nanoparticles with well-controlled dimensions. According to the tunable surface morphology of AuNRs, their use and investigation for new selectivities in chemical applications such as catalysis are under way.

The CAPES-COFEUCB programs N°965/09 and N° Ph695/10 is gratefully acknowledged for the PhD grant of M. G. Angelo da Silva and financial support.

Notes and references

- C. L. John, S. Xu, Y. Jin, S. L. Strating and J. X. Zhao, *Synthesis and Applications of Gold Nanorods in Trace Analysis with Nanomaterials*, Wiley-VCH Verlag GmbH & Co. KGaA, 2010, pp. 359–381.
- H. Chen, L. Shao, Q. Li and J. Wang, *Chem. Soc. Rev.*, 2013, **42**, 2679–2724.
- B. Saute, R. Premasiri, L. Ziegler and R. Narayanan, *Analyst*, 2012, **137**, 5082–5087.
- M. A. El-Sayed, *Acc. Chem. Res.*, 2001, **34**, 257–264.
- M.-C. Daniel and D. Astruc, *Chem. Rev.*, 2004, **104**, 293–346.
- S. Eustis and M. A. El-Sayed, *Chem. Soc. Rev.*, 2006, **35**, 209–217.
- C. J. Murphy, T. K. Sau, A. M. Gole, C. J. Orendorff, J. Gao, L. Gou, S. E. Hunyadi and T. Li, *J. Phys. Chem. B*, 2005, **109**, 13857–13870.
- X. Huang, S. Neretina and M. A. El-Sayed, *Adv. Mater.*, 2009, **21**, 4880–4910.
- D. A. Giljohann, D. S. Seferos, W. L. Daniel, M. D. Massich, P. C. Patel and C. A. Mirkin, *Angew. Chem., Int. Ed.*, 2010, **49**, 3280–3294.
- C. J. Murphy, A. M. Gole, J. W. Stone, P. N. Sisco, A. M. Alkilany, E. C. Goldsmith and S. C. Baxter, *Acc. Chem. Res.*, 2008, **41**, 1721–1730.
- X. Huang, I. H. El-Sayed, W. Qian and M. A. El-Sayed, *J. Am. Chem. Soc.*, 2006, **128**, 2115–2120.
- R. S. Norman, J. W. Stone, A. Gole, C. J. Murphy and T. L. Sabo-Attwood, *Nano Lett.*, 2008, **8**, 302–306.
- W.-S. Kuo, C.-N. Chang, Y.-T. Chang, M.-H. Yang, Y.-H. Chien, S.-J. Chen and C.-S. Yeh, *Angew. Chem., Int. Ed.*, 2010, **49**, 2711–2715.
- K. Hayashi, M. Nakamura, H. Miki, S. Ozaki, M. Abe, T. Matsumoto and K. Ishimura, *Chem. Commun.*, 2013, **49**, 5334–5336.
- S. Hebie, L. Cornu, T. Napporn, J. Rousseau and B. Kokoh, *J. Phys. Chem. C*, 2013, **117**(19), 9872–9880.
- M. Eo, J. Baek, H. D. Song, S. Lee and J. Yi, *Chem. Commun.*, 2013, **49**, 5204–5206.
- V. Sharma, K. Park and M. Srinivasarao, *Mater. Sci. Eng., R*, 2009, **65**, 1–38.
- K.-T. Yong, Y. Sahoo, M. Swihart, P. Schneeberger and P. Prasad, *Top. Catal.*, 2008, **47**, 49–60.
- T. K. Sau and C. J. Murphy, *Langmuir*, 2004, **20**, 6414–6420.
- J. Pérez-Juste, I. Pastoriza-Santos, L. M. Liz-Marzán and P. Mulvaney, *Coord. Chem. Rev.*, 2005, **249**, 1870–1901.
- L. Vigdeman, B. P. Khanal and E. R. Zubarev, *Adv. Mater.*, 2012, **24**, 4811–4841.
- B. Nikoobakht and M. A. El-Sayed, *Chem. Mater.*, 2003, **15**, 1957–1962.
- L. Gou and C. J. Murphy, *Chem. Mater.*, 2005, **17**, 3668–3672.
- J. Zhang, H. Liu, Z. Wang and N. Ming, *Adv. Funct. Mater.*, 2007, **17**, 3295–3303.
- C. J. Murphy and N. R. Jana, *Adv. Mater.*, 2002, **14**, 80–82.
- A. R. Ferhan, L. Guo and D.-H. Kim, *Langmuir*, 2010, **26**, 12433–12442.
- M. G. Angelo da Silva, A. M. Nunes, S. M. P. Meneghetti and M. R. Meneghetti, *C. R. Chim.*, 2013, **16**, 640–650.
- A. Gole and C. J. Murphy, *Chem. Mater.*, 2004, **16**, 3633–3640.
- Y. Takenaka and H. Kitahata, *Chem. Phys. Lett.*, 2009, **467**, 327–330.
- J. Gao, C. M. Bender and C. J. Murphy, *Langmuir*, 2003, **19**, 9065–9070.

COMMUNICATION

Tunable hydroxylated surfactants: an efficient toolbox towards anisotropic gold nanoparticles†

Cite this: *RSC Adv.*, 2014, 4, 25875Monique Gabriella Angelo da Silva,^{ab} Mario Roberto Meneghetti,^b Audrey Denicourt-Nowicki^{*a} and Alain Roucoux^{*a}Received 18th April 2014
Accepted 2nd June 2014

DOI: 10.1039/c4ra03550j

www.rsc.org/advances

Easily tunable *N,N*-dimethyl-*N*-alkyl-*N*-(hydroxyalkyl)ammonium salts have been synthesized and used as capping agents to produce size- and shape-controlled anisotropic gold nanoparticles. The influence of the lipophilic chain length and the counter-ion of this original library of hydroxylated surfactants has been evaluated. From this study, various shapes (spheres, rods, prisms) have been achieved.

Anisotropic gold nanoparticles (AuNPs) have received widespread attention in the last decades, owing to their unusual shape- and size-dependent physical and chemical properties, including optical and electronic responses^{1–4} or catalytic activity.^{5,6} For example, spherical AuNPs present one plasmon absorbance of similar energies whatever the size. On the contrary, one of the most outstanding features of gold nanorods (AuNRs) remains the presence of two plasmon bands in the UV-vis-NIR absorption spectrum, and more especially the longitudinal plasmon which is strongly dependent of the aspect ratio.^{7,8} These nanomaterials, possessing shape- and size-dependent properties, have found numerous applications in sensing,^{9,10} diagnostics,¹¹ photothermal therapy for cancer.^{12,13} For catalytic applications, anisotropic nanoparticles could provide a promising tool to tune the catalytic activity through the availability of high index facets that could facilitate adsorption and surface reactions.^{14–17} In that context, the optimization of the AuNPs performances for a given application relies on the production of AuNPs with precisely designed physico-chemical properties, and a rigorous control of the shape (aspect ratio) and the dimensions (length and diameter).^{18–21} Among the various synthetic approaches,²² the seeded-growth methodology proved

to be the most versatile to produce AuNPs with quite decent yields and sample monodispersity,^{23,24} given rise to a vast library of nanostructures ranging from octahedra or cubes,^{24,25} to prisms^{26,27} or to original nanostructures with high index facets.^{28–30} Various surfactants, and more particularly quaternary ammonium salts, have been used as capping agents to achieve a good shape control over the nucleation and growth of AuNPs, owing to their dual role. First, these compounds are efficient capping agents, adsorbing on gold surface in a bilayer fashion and thus avoiding undesirable agglomeration. Secondly, they could promote specific interactions within the particle facet, thus influencing the growth kinetics and thereby the morphology of nanospecies.¹⁷ Until now, cetyltrimethylammonium bromide (CTAB) remains the most widely used and the influence of several structural parameters,³¹ such as the hydrophobic chain length,^{32,33} the counter-ion^{33,34} and the impurity ions present in the cationic surfactants,²⁷ have been studied. To our knowledge, only a few works have been reported to the potential impact of the surfactant head group and their functionalisation. In 2006, Wang *et al.*^{35,36} have explored the effect of the surfactant headgroup size on the growth of gold nanostructures, comparing various cetyltrialkylammonium bromides. More recently, our group reported a new family of easily tunable *N,N*-dimethyl-*N*-cetyl-*N*-(hydroxyalkyl)ammonium bromide salt (HAA16Br), bearing an hydroxylated polar head with various lengths from ethoxy (HEA) to butoxy (HBA) groups, as efficient driving agents.³⁷ We have demonstrated that the presence of the hydroxyl group was beneficial to promote headgroup packing at the metal surface, thus leading to the formation of rod-like particles of tunable aspect ratios.

Herein, we extend the library of hydroxylated ammonium salts for the production of size and shape-controlled gold NPs in high yields and selectivities. New *N,N*-dimethyl-*N*-alkyl-*N*-(hydroxyalkyl) ammonium salts (HAAX) were investigated as capping agents in anisotropic gold nanoparticle synthesis by the seed-mediated growth in aqueous media (Fig. 1).

In addition to the length of the polar head,³⁷ several structural parameters have been studied, such as the length of the

^aEcole Nationale Supérieure de Chimie de Rennes, CNRS, UMR 6226, 11 Allée de Beaulieu, CS 50837, 35708 Rennes Cedex 7, France. E-mail: alain.roucoux@ensc-rennes.fr; audrey.denicourt@ensc-rennes.fr

^bGrupo de Catalise e Reactividade Quimica GCaR, Instituto de Química e Biotecnologia da Universidade Federal de Alagoas, Av. Lourival de Melo Mota, s/n CEP 57072-970, Maceió, Brazil

† Electronic supplementary information (ESI) available. See DOI: 10.1039/c4ra03550j

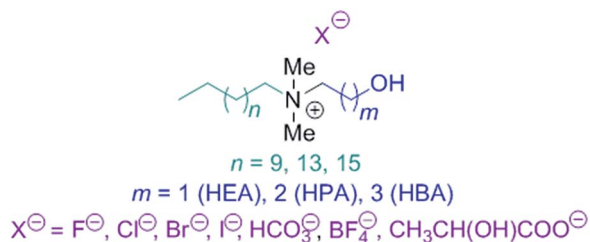


Fig. 1 General chemical structure of *N,N*-dimethyl-*N*-alkyl-*N*-(hydroxyalkyl) ammonium salts (HAAX) as NPs growth-driving agents.

lipophilic chain (C12, C16, C18),³⁸ (ii) the nature of the counterion through an anionic metathesis reaction ($X^- = F^-, Cl^-, Br^-, I^-, BF_4^-, HCO_3^-$ and lactate).^{39,40} Based on several sets of experiments, we report in this manuscript how to produce anisotropic gold nanoparticles with well-controlled morphologies according to an easy chemical modification of the surfactant and not just as an addition of the corresponding salt in the mixture.

Results and discussion

In this study, AuNPs were synthesized by the seeded-growth methodology in aqueous media, using *N,N*-dimethyl-*N*-alkyl-*N*-(hydroxyethyl)ammonium salts (HEAX), bearing a 2-hydroxyethyl polar head, various lengths for the lipophilic chain (C12 to C18) and counter-ions ($X^- = F^-, Cl^-, Br^-, I^-, BF_4^-, HCO_3^-$ and lactate), as capping agents. The syntheses were performed in the presence of silver nitrate $AgNO_3$. The selectivity was determined, without centrifugation step, as the number of AuNPs in a well-defined shape over the number of NPs from Transmission Electron Microscopy (TEM).

In a first set of experiments, we investigated the influence of the length of the lipophilic chain (C12, C16, C18) on the particle morphology, considering a 2-hydroxyethylammonium (HEA) polar head and a bromide as counter ion. These surfactants were easily prepared by quaternarization of *N,N*-dimethylethanolamine with the appropriate bromoalkane (see ESI†). The results were compared to those obtained with the classical cetyltrimethylammonium bromide (CTAB) under the same preparation conditions. Fig. 2 shows the UV-vis absorption spectra and TEM images of AuNPs prepared by the seeded-growth method, as a function of the different chain lengths for *N,N*-dimethyl-*N*-alkyl-*N*-(hydroxyethyl)ammonium bromide salts (HEA n Br, with $n = 12, 16, 18$).

As already observed with various CTAB analogues of various lengths for the hydrocarbon tail, the lipophilic chain seems to influence the AuNPs morphology and higher aspect ratio nanorods were produced while increasing the chain length. With a small lipophilic chain (HEA12Br), the growth control seems not very efficient, leading to a mixture of spherical particles (~10 nm) and low aspect ratio (2.4) nanorods with selectivity about 78% (Fig. 2a). In the case of HEA16Br, as previously reported,³⁷ the UV-vis absorption spectrum of AuNPs presents two typical absorption bands with a good correlation,

suggesting the formation of nanorods (Fig. 2b). This result was confirmed by TEM analyses, showing rod-like particles with an aspect ratio of 3.0 (30×10 nm) with a high selectivity of 88%. This surfactant, possessing a higher water-solubility thanks to the hydroxylated polar head in comparison with CTAB derivatives, is easily synthesized in good yields and could be used in a large range of concentration if needed in nanoparticles synthesis. For comparison, the aspect ratio of AuNRs obtained with CTAB by the same procedure is around 3.3 (40×12 nm), similar to the values reported in the literature.^{37,41} The hydroxyalkylammonium bearing an alkylchain with 18 carbons (HEA18Br) was also evaluated as directing agent, but it is difficult to compare the result, owing to the use of less concentrated surfactant solution (see Experimental section). However, dog-bone shape particles, which could find promising applications, leading to a red-shift,⁴² were mainly produced (Fig. 2c), probably owing to an insufficient amount of capping agents. It is also worth mentioning that without a hydroxyethyl substituent on the nitrogen atom, only few anisotropic AuNPs are produced due to the low water solubility of the capping agent. Moreover, the aspect ratios are lower than those observed by Murphy *et al.* using CTAB analogues with different lipophilic chains,³² since only the initial step of the seed-mediated growth process was explored in this study. To resume, the highly water-soluble HEA16Br salt seems to be a good compromise to achieve pertinent aspect ratios, assuming an efficient binding of Au^{III} and Au^I ions into the cationic micelles present in solution,⁴³ as well as the van der Waals stabilization of the surfactant bilayer on gold surface owing to the interchain packing of the hydroxylated head group, which helps the underlying nanorod formation.³²

In a second set of experiments, the influence of the counterion on the particle formation was studied, considering the role of the counter-ions adlayers in the control over the shape development in the growth from a crystal seed.^{33,44} Various HEA16X ($X^- = F^-, Cl^-, Br^-, I^-, BF_4^-, HCO_3^-$ and lactate), bearing a lipophilic chain of 16 carbons and a 2-hydroxyethyl ammonium polar head, were easily synthesized by quaternarization of *N,N*-dimethylethanolamine with the appropriate halogenoalkane ($X^- = Cl^-, Br^-, I^-$),⁴⁵ or by anionic metathesis from HEA16Br.⁴⁰ They were evaluated as capping agents of AuNPs, in the presence of silver nitrate. First, although these counter-ions are original in gold nanoparticles synthesis, HEA16BF₄ and HEA16Lactate were not pertinent as capping agents, due to their quite low water-solubility and thus their aggregation even in more diluted concentrations. Secondly, the colloids prepared with HEA16F and HEA16Cl displayed only one absorption band in their respective UV-vis spectra (Fig. 3a and b), suggesting the formation of spherical particles, as assessed by Transmission Electron Microscopy pictures. The spherical AuNPs capped with HEA16F (8.5 nm) are smaller than those obtained by HEA16Cl (10 nm). Similar observations have already been reported by Kawasaki *et al.*,³³ with spherical AuNPs obtained by hydrazine reduction in the presence of CTAF and CTACl, and was attributed to a fast reduction rate promoting by the use of a fluoride salt. On the contrary, two absorption bands were observed in the UV-vis absorption spectra of colloids

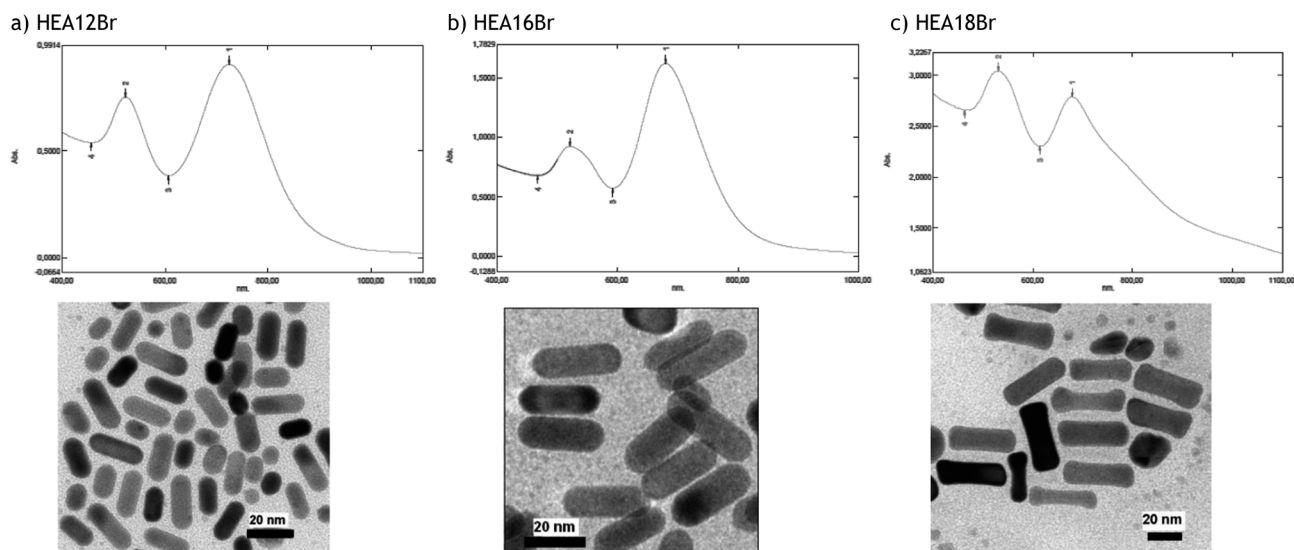


Fig. 2 UV-vis absorption spectra and TEM images of AuNRs obtained with (a) HEA12Br (19×8 nm, aspect ratio of 2.4, $\lambda_{\max} = 724$ nm), (b) HEA16Br (30×10 nm, aspect ratio of 3.0, $\lambda_{\max} = 679.50$ nm), (c) HEA18Br (45×14 nm, aspect ratio of 3.2, $\lambda_{\max} = 678$ nm). Size and aspect ratio were obtained after 500 counts for each sample. Scale bar = 20 nm.

synthesized from the newly HEA16HCO₃ salt (Fig. 3c) as well as HEA16Br (Fig. 2b), being consistent with the Au nanorods observed by TEM analyses. This shape tendency of AuNPs according to the counter-ion species may be attributed to the adsorption affinity of the surfactant anion on gold surface during the crystal growth.⁴⁶ A similar tendency has already been observed with CTAX salts, and was correlated with the decrease in the frequency shift of Quartz Crystal Microbalance (QCM) in the following order: Br⁻ > Cl⁻ > F⁻.^{33,46} Thus, the fluoride and chloride anions generate weak interactions within the particle surface, thus disfavoring the formation of a stable and compact double layer of the surfactant around the growing particle, while the high-affinity adsorption of Br⁻ onto Au surfaces

produces anisotropic gold nanoparticles. Moreover, in the synthetic method used, silver ions are also introduced into the reaction, and thus the influence of halides on crystal growth are more complex since the halides interact with the Au ions in solution and the gold surface, and also with the silver ions in solution. In fact, Mirkin *et al.*¹⁹ have found that in the presence of larger halides, the stability of the underpotentially deposited silver layer decreases, owing to the increasing strength of the Au-halide interaction relative to the Ag-Au and Ag-halide interaction.

In the particular case of HEA16HCO₃ salt, we could presume that, by analogy to carboxylate anions or polycarboxylates, such as citrate polyanions, the hydrogenocarbonate counter-ion

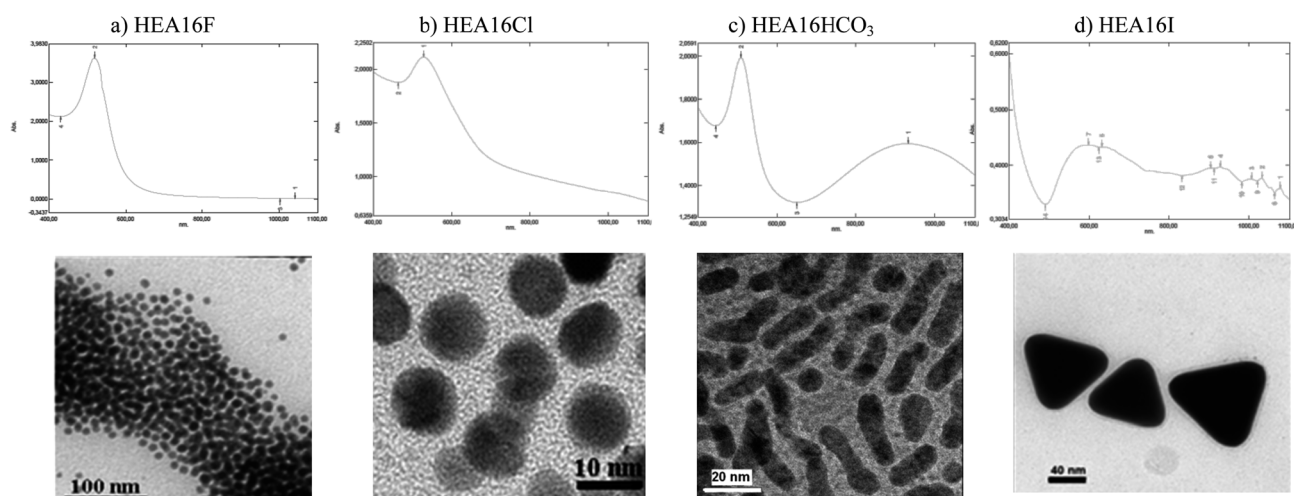


Fig. 3 Influence of the surfactant counter-ion on the morphology of AuNPs – UV-vis absorption spectra and TEM images of (a) HEA16F (spherical NPs, 8.5 nm, scale bar = 100 nm), (b) HEA16Cl (spherical NPs, 10 nm, scale bar = 10 nm), (c) HEA16HCO₃ (worm-like NPs, 29×7 nm, aspect ratio = 4.2, $\lambda_{\max} = 932$ nm, scale bar = 20 nm), (d) HEA16I (prisms NPs, scale bar = 40 nm). Size and aspect ratio were obtained after 500 counts for each sample.

provides an intermediate adsorption affinity at the growing NP surface, between the bromide and the chloride ones. However, a poor relationship between the two typical absorption bands was observed, which could be attributed to a less efficient control of the NPs growth, as confirmed by TEM images with the formation of peanut pod shape AuNPs (Fig. 3c).

Finally, the iodide counter-ion plays a critical role in the growth control of Au nanocrystals, with mainly the formation of well-formed nanoprisms (41%) as shown by TEM analyses (Fig. 3d) even if other morphologies (spheres, penta-twinned crystals) were observed (see ESI Fig. 7†). This counter-ion is known to promote the formation of nanoprisms by preferential binding to facet of gold nanocrystal with binding energies that follows the ion polarizability ($I^- > Br^- > Cl^-$) and crystal facet ($\{111\} > \{110\} > \{100\}$).⁴⁷ This effect of iodide on the shape of AuNPs have already been described with low concentrations (<3.0 ppm) of iodide impurities present in CTAB^{27,48} or with the deliberate addition of potassium iodide in the presence of CTAB.^{19,44} These gold triangular nanoprisms are promising materials with applications in optics and electronics,⁴⁹ and as biosensing platforms.⁵⁰

Conclusions

In summary, a novel library of easily tunable hydroxylated ammonium surfactants were synthesized and used as versatile growth driving agents of AuNPs. This original family provides more flexible shape templates than the CTAB, giving rise to AuNPs of various morphologies (rods, spheres, prisms...) and different sizes through the easy modulation of the capping agent (length of the lipophilic chain, or of the polar head, and the counter-ion), with good yields and selectivities without size/shape selection step. These promising results open new perspectives in the design of original growth driving agents to produce anisotropic gold nanoparticles with well-controlled morphologies and dimensions according to the desired application, in aqueous solution without any mixture with CTAB or addition of different additives as ions and solvents.

Experimental section

General

Tetrachloroauric acid hydrate, $HAuCl_4 \cdot H_2O$ (99.9%), sodium borohydride, (+)-L-ascorbic acid (99%), CTAB and $AgNO_3$ (99%) were used as purchased, without any purification. The *N,N*-dimethyl-*N*-alkyl-*N*-(hydroxyalkyl)ammonium salts (HAAX) were synthesized and characterized by Mass and NMR spectroscopy (data are presented in the ESI†).^{40,45} Distilled water was used to prepare all solutions. UV-Vis/near-IR spectra were recorded on a Shimadzu UV-vis 1800 spectrophotometer, using optical glass cells with length of 1 cm. The set-up was configured to fix the baseline of distilled water absorption band from 400 to 1000 nm. TEM analyses were performed on a JEOL TEM 100CXII electron microscope at an accelerating voltage of 100 kV. The samples were prepared by the addition of a drop of the gold colloidal solution on a copper grid coated with a porous carbon film. TEM images and determined selectivity were obtained

from the produced gold suspension of particles without treatment such as centrifugation.

Seed-mediated growth synthesis

AuNPs prepared in this study were produced by a seeded-growth method, adapted from the protocols developed by Murphy⁷ and El Sayed.²³ The method consists in preparing two solutions: (i) the seed solution and (ii) the growth solution.

Seed solution. In a 25 mL flask, 0.1 mL of an aqueous solution of $HAuCl_4 \cdot 3H_2O$ (0.025 mol L^{-1} , 0.0025 mmol) was added to a 7.4 mL aqueous solution of surfactant ($0.0676 \text{ mol L}^{-1}$, 0.5 mmol) (in the case of HEA18Br, a 7.4 mL aqueous solution of surfactant ($0.0337 \text{ mol L}^{-1}$, 0.25 mmol) was used). Then, under stirring, 0.6 mL of an ice-cold aqueous solution of sodium borohydride (0.01 mol L^{-1} , 0.006 mmol) was added. The solution color immediately turned to brown. After 2 min, the system remains at least 2 h, without stirring before used.

Growth solution. In a 25 mL flask, 0.2 mL of an aqueous solution of $HAuCl_4 \cdot 3H_2O$ (0.025 mol L^{-1} , 0.005 mmol) was added to a 7.3 mL aqueous solution of surfactant ($0.0685 \text{ mol L}^{-1}$, 0.5 mmol) (except for HEA18Br, a 7.3 mL aqueous solution of surfactant ($0.0342 \text{ mol L}^{-1}$, 0.25 mmol) was used). Then, 0.15 mL of an aqueous solution of silver nitrate ($4 \times 10^{-3} \text{ mol L}^{-1}$) was added under stirring, followed by ascorbic acid (0.070 mL, 0.0788 M). The system turned to colorless, proving the reduction of Au^{3+} to Au^+ .

Growing process. 0.060 mL of seed particles were added to the freshly prepared growth solution. The solution is kept under stirring for just 10 s and then allowed to stand for 4 h without stirring prior to characterization to ensure the system stability.

Acknowledgements

This work was supported by the CAPES-COFECUB program Ph/650-10 (PhD grant of M. G. Angelo da Silva and financial support). We thank Patricia Beaunier from Université Pierre et Marie Curie for performing TEM analyses.

Notes and references

- 1 S. Eustis and M. A. El-Sayed, *Chem. Soc. Rev.*, 2006, **35**, 209–217.
- 2 S.-F. Lai, C.-C. Chien, W.-C. Chen, Y.-Y. Chen, C.-H. Wang, Y. Hwu, C. S. Yang and G. Margaritondo, *RSC Adv.*, 2012, **2**, 6185–6191.
- 3 S. Kumar and T. Nann, *Small*, 2006, **2**, 316–329.
- 4 R. Sardar, A. M. Funston, P. Mulvaney and R. W. Murray, *Langmuir*, 2009, **25**, 13840–13851.
- 5 K. Rahme, M. T. Nolan, T. Doody, G. P. McGlacken, M. A. Morris, C. O'Driscoll and J. D. Holmes, *RSC Adv.*, 2013, **3**, 21016–21024.
- 6 B. Lim and Y. Xia, *Angew. Chem., Int. Ed.*, 2011, **50**, 76–85.
- 7 C. J. Murphy and N. R. Jana, *Adv. Mater.*, 2002, **14**, 80–82.
- 8 S. E. Lohse and C. J. Murphy, *Chem. Mater.*, 2013, **25**, 1250–1261.

- 9 K. Saha, S. S. Agasti, C. Kim, X. Li and V. M. Rotello, *Chem. Rev.*, 2012, **112**, 2739–2779.
- 10 K. Liu, H. Pang, J. Zhang, H. Huang, Q. Liu and Y. Chu, *RSC Adv.*, 2014, **4**, 8415–8420.
- 11 S. H. Radwan and H. M. E. Azzazy, *Expert Rev. Mol. Diagn.*, 2009, **9**, 511–524.
- 12 L. C. Kennedy, L. R. Bickford, N. A. Lewinski, A. J. Coughlin, Y. Hu, E. S. Day, J. L. West and R. A. Drezek, *Small*, 2011, **7**, 169–183.
- 13 A. M. Alkilany, L. B. Thompson, S. P. Boulos, P. N. Sisco and C. J. Murphy, *Adv. Drug Delivery Rev.*, 2012, **64**, 190–199.
- 14 M. Eo, J. Baek, H. D. Song, S. Lee and J. Yi, *Chem. Commun.*, 2013, **49**, 5204–5206.
- 15 S. Hebié, L. Cornu, T. W. Napporn, J. Rousseau and B. K. Kokoh, *J. Phys. Chem. C*, 2013, **117**, 9872–9880.
- 16 L.-F. Zhang and C.-Y. Zhang, *Nanoscale*, 2013, **5**, 5794–5800.
- 17 J. Xiao and L. Qi, *Nanoscale*, 2011, **3**, 1383–1396.
- 18 A. R. Tao, S. Habas and P. Yang, *Small*, 2008, **4**, 310–325.
- 19 M. R. Langille, M. L. Personick, J. Zhang and C. A. Mirkin, *J. Am. Chem. Soc.*, 2012, **134**, 14542–14554.
- 20 Y. Xia, Y. Xiong, B. Lim and S. E. Skrabalak, *Angew. Chem., Int. Ed.*, 2009, **48**, 60–103.
- 21 M. Grzelczak, J. Perez-Juste, P. Mulvaney and L. M. Liz-Marzan, *Chem. Soc. Rev.*, 2008, **37**, 1783–1791.
- 22 V. R. Dugyala, S. V. Daware and M. G. Basavaraj, *Soft Matter*, 2013, **9**, 6711–6725.
- 23 B. Nikoobakht and M. A. El-Sayed, *Chem. Mater.*, 2003, **15**, 1957–1962.
- 24 T. K. Sau and C. J. Murphy, *J. Am. Chem. Soc.*, 2004, **126**, 8648–8649.
- 25 Y. Xiang, X. Wu, D. Liu, L. Feng, K. Zhang, W. Chu, W. Zhou and S. Xie, *J. Phys. Chem. C*, 2008, **112**, 3203–3208.
- 26 J. E. Millstone, G. S. Métraux and C. A. Mirkin, *Adv. Funct. Mater.*, 2006, **16**, 1209–1214.
- 27 J. E. Millstone, W. Wei, M. R. Jones, H. Yoo and C. A. Mirkin, *Nano Lett.*, 2008, **8**, 2526–2529.
- 28 T. Ming, W. Feng, Q. Tang, F. Wang, L. Sun, J. Wang and C. Yan, *J. Am. Chem. Soc.*, 2009, **131**, 16350–16351.
- 29 J. Zhang, M. R. Langille, M. L. Personick, K. Zhang, S. Li and C. A. Mirkin, *J. Am. Chem. Soc.*, 2010, **132**, 14012–14014.
- 30 Y. Yu, Q. Zhang, X. Lu and J. Y. Lee, *J. Phys. Chem. C*, 2010, **114**, 11119–11126.
- 31 M. G. A. da Silva, Á. M. Nunes, S. M. P. Meneghetti and M. R. Meneghetti, *C. R. Chim.*, 2013, **16**, 640–650.
- 32 J. Gao, C. M. Bender and C. J. Murphy, *Langmuir*, 2003, **19**, 9065–9070.
- 33 H. Kawasaki, K. Nishimura and R. Arakawa, *J. Phys. Chem. C*, 2007, **111**, 2683–2690.
- 34 S. E. Lohse, N. D. Burrows, L. Scarabelli, L. M. Liz-Marzán and C. J. Murphy, *Chem. Mater.*, 2014, **26**, 34–43.
- 35 X. Kou, S. Zhang, C.-K. Tsung, M. H. Yeung, Q. Shi, G. D. Stucky, L. Sun, J. Wang and C. Yan, *J. Phys. Chem. B*, 2006, **110**, 16377–16383.
- 36 X. Kou, S. Zhang, C.-K. Tsung, Z. Yang, M. H. Yeung, G. D. Stucky, L. Sun, J. Wang and C. Yan, *Chem.–Eur. J.*, 2007, **13**, 2929–2936.
- 37 M. G. A. da Silva, M. R. Meneghetti, A. Denicourt-Nowicki and A. Roucoux, *RSC Adv.*, 2013, **3**, 18292–18295.
- 38 J. Schulz, A. Roucoux and H. Patin, *Chem.–Eur. J.*, 2000, **6**, 618–624.
- 39 A. Roucoux, J. Schulz and H. Patin, *Adv. Synth. Catal.*, 2003, **345**, 222–229.
- 40 E. Guyonnet Bile, R. Sassine, A. Denicourt-Nowicki, F. Launay and A. Roucoux, *Dalton Trans.*, 2011, **40**, 6524–6531.
- 41 T. K. Sau and C. J. Murphy, *Langmuir*, 2004, **20**, 6414–6420.
- 42 X. Xu and M. B. Cortie, *Adv. Funct. Mater.*, 2006, **16**, 2170–2176.
- 43 J. Pérez-Juste, L. M. Liz-Marzán, S. Carnie, D. Y. C. Chan and P. Mulvaney, *Adv. Funct. Mater.*, 2004, **14**, 571–579.
- 44 T. H. Ha, H.-J. Koo and B. H. Chung, *J. Phys. Chem. C*, 2007, **111**, 1123–1130.
- 45 G. Cerichelli, L. Luchetti, G. Mancini and G. Savelli, *Tetrahedron*, 1995, **51**, 10281–10288.
- 46 V. Sharma, K. Park and M. Srinivasarao, *Mater. Sci. Eng., R*, 2009, **65**, 1–38.
- 47 O. M. Magnussen, *Chem. Rev.*, 2002, **102**, 679–725.
- 48 D. K. Smith, N. R. Miller and B. A. Korgel, *Langmuir*, 2009, **25**, 9518–9524.
- 49 D. Lee, S. Hong and S. Park, *Bull. Korean Chem. Soc.*, 2011, **32**, 3575–3580.
- 50 Z. Guo, X. Fan, L. Liu, Z. Bian, C. Gu, Y. Zhang, N. Gu, D. Yang and J. Zhang, *J. Colloid Interface Sci.*, 2010, **348**, 29–36.

